Series in instrumentation technology and applications

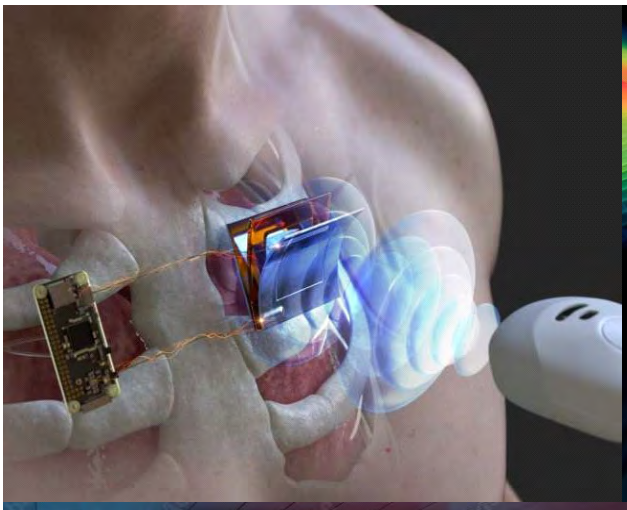
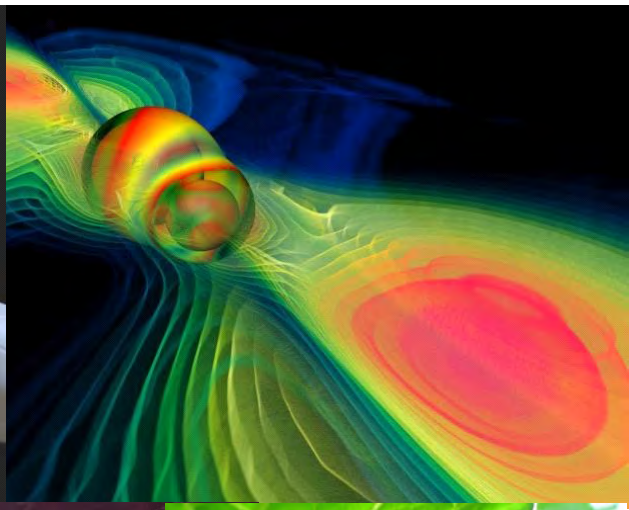

Applied Instrumentation

Student works

2023-2024 academic year

Editors: Trinitat Pradell
José E. García
Oscar Casas

ÍNDEX

“Els humans tenim una relació d’amor-odi amb la nostra tecnologia. Amem cada un dels avanços però odiem quan ràpid estan canviant el nostre món”

Daniel H Wilson (Enginyer i escriptor. 1978-)

Pròleg

La intel·ligència artificial acapara l'interès d'empreses i institucions, monopolitza els titulars dels mitjans de comunicació i fins i tot suscita els recels del gran públic. No obstant això, aquesta tecnologia, fonamental en la quarta i la cinquena revolucions industrials, a penes hauria pogut progressar sense la matèria primera més preuada en l'actualitat: les dades. Però no qualsevol dada serveix. Aquestes han de tenir una exactitud prou bona perquè siguin fiables les conclusions que se n'extreguin. I es que mesurar en certs àmbits pot ser relativament fàcil, però fer-ho amb exactitud i sobre tot amb consciencia de les seves limitacions, ja no ho és tant. En aquest context s' ha fet necessària l' existència d' un nou tipus de professional: científics i enginyers que estiguin al dia dels límits tecnològics de cadascuna de les disciplines que són necessàries per l’obtenció d’aquestes dades. Som conscients que en aquesta assignatura només hem ficat la primera pedra de la muntanya de coneixements necessaris per poder treballar en aquesta àmbit de recerca i desenvolupament. Però esperem que hagi estat un primera pedra molt engrescadora.

Aquest llibre recull els treballs realitzats pels alumnes d'Enginyeria Física de la Universitat Politècnica de Catalunya dins l'assignatura d'Instrumentació en el curs acadèmic 2023-2024, i presenten l'ús de modernes tècniques instrumentals en molt diferents àmbits d'aplicació. Van des de la instrumentació nuclearhospitalària, o les ones gravitacionals, fins a les ones elèctriques en plantes o els moderns sistemes de monitorització de les persones amb pàrkinson. Esperem que la seva lectura sigui una motivació per continuar estudiant i treballats amb aquest àmbit en el que encara queden moltíssimes tècniques instrumentals que imaginar i crear.

Barcelona, Juny de 2024

Trinitat Pradell

José E. García

Oscar Casas

Professors de l’assignatura d’Instrumentació

Present and Future of Gravitational Wave Astronomy

Pau Blancafort, Guerau Dasca, Aitor da Rocha, Gonzalo Martín, Jonathan Rodríguez and Laia Solé
Instrumentació. Grau en Enginyeria Física. Universitat Politècnica de Catalunya.
(Dated: May 20, 2024)

Gravitational waves, predicted by Einstein's theory of general relativity in 1916 and directly observed in 2015, are disturbances in spacetime caused by the movement of mass. Despite their weak interaction with matter, GW have immense significance in astrophysics, and detecting them requires extreme precision due to their minuscule effects on space. This article discusses their detection highlighting the importance of minimizing the noise sources and how to tackle them. Looking to the future, different projects aim to enhance sensitivity and broaden the observation band, promising significant advancements in gravitational wave detection technology.

Keywords: Gravitational waves, detection, interferometer, noise.

I. INTRODUCTION

Before delving into the main subject matter of this article, the measurement of gravitational waves, it is necessary, however, to offer a brief and cursory review of what gravitational waves are and their origins.

A gravitational wave is a perturbation of spacetime produced by the motion of mass, propagating through space at the speed of light. Although gravitational waves were not directly observed until September 14, 2015 (by LIGO and Virgo), their existence had already been theorized in 1916 by Einstein as a result of his theory of general relativity, as a reason of the fact that changes in the gravitational field could not occur instantaneously at all points in space, but had to propagate.

Gravitational waves are generated by accelerated masses, where larger masses result in higher amplitude GW, implying that black holes, supernova explosions or collisions of binary neutron stars are important sources of GW [1]. However, GW interact very weakly with matter (unlike electromagnetic waves), making their scattering and absorption complex. What we can assume is that when these wave interact with matter, stretching occurs in objects in the transverse direction of wave propagation, with a magnitude that is proportional to the length of the object under study and the amplitude of the GW. Therefore, the aim for detection of such waves is to measure these distances changes, which turn out to be on the order of:

$$\delta L = L|h| \approx 10^{-19} m$$

Where we have supposed an object of longitude $L \approx 10^3 m$, such as the length of an interferometer arm; and a common value for the amplitude of the GW of $|h| \approx 10^{-22}$, that are always extremely small values of this order of magnitude[2].

This highlights the true challenge of measuring and detecting GW, and the advancement represented by their direct discovery in 2015. It is therefore a truly complex field of detection, demanding the use of the state-of-the-art and cutting-edge technology, with the primary challenge being the issue of noise in the measurements.

II. GRAVITATIONAL WAVES DETECTORS

As said before, the objective is to detect small deformations of space. For this task, the most successful method is to use a Michelson interferometer[3]. As can be seen in Figure 1, the idea is to split a light beam in two different directions, two "arms", make each of them travel a certain distance and then merge the two beams again before sending the resulting beam to a detector. Gravitational waves change the total length each beam travels, thus affecting the interference and providing observable measures.

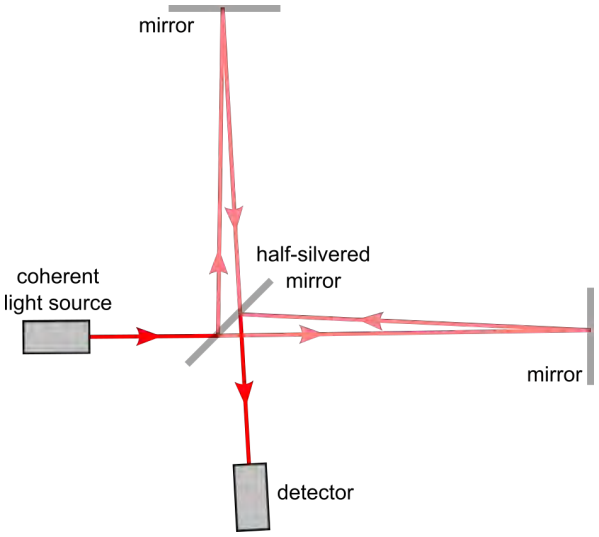

FIG. 1. Michelson interferometer.

The power measured by the Michelson interferometer can be expressed in the following form:

$$P_{out} \propto P_{in} \sin^2[k(L_y - L_x)] = P_{in} \sin^2(\delta\theta)$$

where P_{in} is the power of the original beam, L_x and L_y the traveled distances by each of the split beams and k is the wave number, defined as $k = 2\pi/\lambda$ with λ the wavelength of the beam. From this, is obvious that we

will want to use high frequency light beams in order to make the phase difference $\delta\theta$ bigger and easier to detect.

The order of magnitude of the space deformations is, as said before, $10^{-22}L$, where L is the size of the region of study. That is, gravitational waves shrink or expand space uniformly, so the bigger the region of space we are studying is, the bigger the total deformation [3]. Note, however, that even with a detector of 1km, the expected perturbation is of the order of $10^{-19}m$, three orders of magnitude smaller than the radius of a proton [4].

One example of this kind of detector is LIGO [5]. The basic idea is the same, but it has some optimizations to ease the detection. For example, it has a pair of mirrors in each arm, making the beams go back and forth around 300 times. The arms are only 4km long, but with this method the effective travel length reaches a few thousand kilometers.

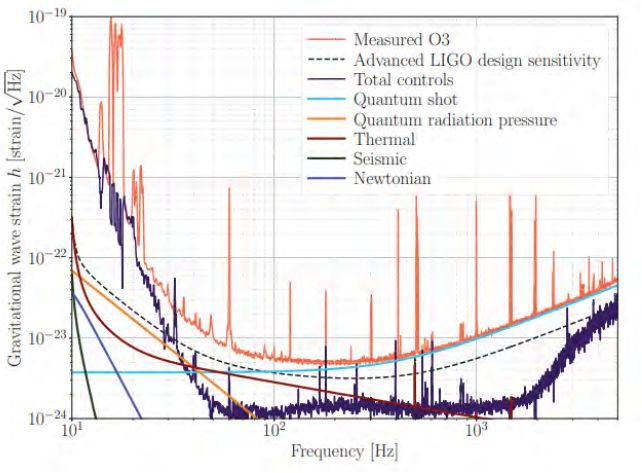

FIG. 2. O3 LIGO Hanford gravitational wave noise budget from [6]

III. NOISE SOURCES IN GRAVITATIONAL WAVE DETECTORS

Since the distance fluctuation due to the passage of a GW is very small, there are other reasons for which the detector can experience a power change. Therefore, to increase the sensitivity of the system it is necessary to study the sources of noise at a very small scale. We can divide the noise into fundamental noise (that includes quantum, thermal, seismic and Newtonian noise) and technical noise. The first one is due to the physical principles behind the design of the detector, while the second one is not intrinsic to the design but can limit its performance.

As said, there are other factors than the GW that can vary the distance of the mirrors, the so called noises. To distinguish these sources of noises from the gravitational signal, we define the amplitude spectral sensitivity for each noise as:

$$h_i(f) = \frac{\sqrt{\tilde{x}^2(f)}}{L} \tag{1}$$

where L is the length of the arm and $\tilde{x}^2(f)$ is the power spectral density of the displacement due to the noise source. Then, the sensitivity of the GM detector is defined as:

$$h(f) = \sqrt{\sum_{i=1}^{n} h_i^2(f)} \tag{2}$$

where n is the total number of noises. The sensitivity curve represents the minimum intensity of the gravitational signal detectable by an interferometer.

A. Quantum Noise

The quantum nature of light is the cause of two undesired phenomenon related with the fluctuations of the photon flux due to Heisenberg's uncertainty principle: radiation pressure noise and shot noise. The radiation pressure is the force by unit area exerted on a surface due to the of the momentum of the photons when there is light reflection. Then, fluctuations of this pressure cause the suspended mirrors to recoil, changing the length of the arms of the interferometer and adding radiation pressure noise to the measured signal at low frequencies. Shot noise is a high frequency noise due to the Poisson fluctuations of the photons at the detection, whilst the radiation pressure is more present at lower frequencies.

Shot noise is, in fact, a white noise due to the randomness of the photons arriving to the detector. This noise has an amplitude spectral density inversely proportional to the beam power. Therefore, it is possible to reduce the shot noise by increasing the laser power. However, the radiation pressure amplitude spectral density is directly proportional to the same quantity, and therefore one cannot reduce both noises at the same time. Then, the decision of what power to use depends in the working range of frequencies that we want to work with. Figure 2 illustrates this.

With some calculations, we can obtain the optimal power for each frequency that reduces the total quantum noise. It has the following form:

$$P_{opt} = \frac{\pi^3 c\lambda M f^2}{16F^2}\left[1 + \left(\frac{f}{f_p}\right)^2\right] \tag{3}$$

Another technique is to use squeezed states of light as an extra input for the laser detectors, as explained in [3]. This is useful to narrow the shot noise and hence leaving only the radiation pressure noise to be treated.

B. Thermal Noise

The displacement of the mirrors and their suspension system due to thermal fluctuation in its atoms is also a source of noise. In general it is related to mechanical losses in the materials, as described by the fluctuation-dissipation theorem.

Therefore, a first approach to reduce this kind of noise is to use low-mechanical-loss materials for the mirrors and their suspensions. Also, a newer idea is to lower the temperature of the mirrors using cryocoolers and other strategies to reach cryogenic temperatures, as mentioned in [7].

In fact, this noise has two main contributions, the suspension thermal noise which is due to dissipation in the wires, and the mirror thermal noise due to dissipation processes inside the mirrors themselves. Each contribution is more or less significant depending on the frequency range.

To reduce the suspension thermal noise, predominant at frequencies lower than 50Hz, fused silica can be used as the mirror's material, as explained in [3]. For higher frequencies (between 50 to 150HZ), the mirror's thermal noise is more important and can be minimized by reducing the coating thickness or by increasing the laser beam size.

C. Seismic and Newtonian Noise

Seismic noise is due to the earth geological activity physically shaking the suspended mirrors. This noise limits the sensitivity for frequencies below 5 Hz. The earth's surface vibrates 1μm, 10 order of magnitudes larger than the signal found in the detector. To reduce this noise, the mirrors are suspended by a system of pendulums in cascade and other mechanical isolation structures that separate the movement of the mirrors to the ground's motion. This can be used together with inertial sensors to improve their performance.

Another solution found to this problem is to locate the detectors underground, where the seismic motion is far less noticeable. For example, this is implemented in [7], where they constructed a detector inside a mountain as it's base acts as cushion and mitigates the vibrations.

Newtonian noise is also due to seismic activity but in this case it doesn't propagate through the motion of the ground, but through changes on the local Earth's gravitational field. Therefore, its not possible to mitigate its effects using a better mechanical isolation. A solution is to measure it and actively substract it's contribution to the signal found.

D. Technical Noise Sources

Technical noises are caused by imperfections in all the system. There is a wide variety of technical noise sources, including: length and angular control noise, laser frequency and intensity noise, scattered light and other sources, all of which carefully discussed in [8].

Control noises are the main contribution to technical noise, and they are associated to the alignment sensing and control system that holds the interferometer optics on resonance.

Normally, the magnitude of these noises is difficult to predict or detect, but for a large range of frequencies these noises are irrelevant compared to rest of the noises discussed before, as can be seen in Figure 2 (Total Controls curve).

IV. FUTURE OF THE GRAVITATIONAL WAVE DETECTORS

The main goals of the future gravitational wave detectors are increasing the sensitivity, improving the signal-to-noise ratio and eliminate the disturbances that can be mistaken for astrophysical signals. The actual detectors have been upgraded, but they are still not good enough to further develop this field. For comparison, figure 3 compares the sensitivity of the actual detectors and the projection of the future ones. Bearing that in mind, two of the most promising, third-generation projects will be presented: the Einstein Telescope (European project) and the Cosmic Explorer (American project). Some other projects are also being developed, such as the LISA and DECIGO space located detectors [1], which should have a much better signal-to-noise ratio than any earth based detectors, but they are still in early stages.

A. Einstein Telescope

The idea behind the Einstein Telescope is to improve sensitivity by constructing longer arm detectors and therefore be able to move the observation band below 10Hz [10] (Nowadays, the bandwidth starts at 30Hz). The project, which will be underground, owing to the fact that there the seismic noise is reduced [11] and will include six interferometers with an arm length of 10 km. This improvements will make distinguishing between primordial black holes (those created at the beginning of the universe) and star-formed black holes (the ones created from a collapsing star) possible. Moreover, the improved sensitivity will lead to a better understanding of the formation of binary star systems and the factors that can favor their formation, as well as a more accurate calculation of their intrinsic parameters, such as their Love numbers, which include information on the star's inner structure, could be calculated with an accuracy improvement of about an order of magnitude. This will also enable a greater degree of certainty when the consistency between the assumptions made and the experiments done is checked [11].

This could also lead to the detection of some types of gravitational waves that can't be detected with the

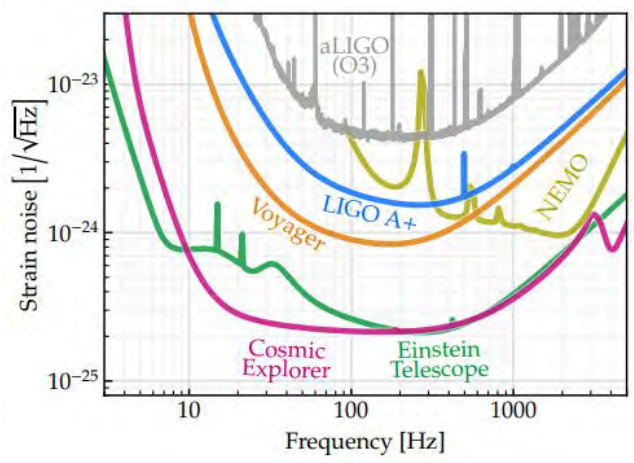

FIG. 3. Sensitivity comparison between different detectors from [10]

current detectors, but we know that are a GW source, such as pulsars and non-axisymmetric neutron stars.

B. Cosmic Explorer

The Cosmic Explorer is aimed to be a larger "version" of the Einstein Telescope, as it is going to be a single 40 km surface detector. The sensitivity that this detector is aiming to have is of the order of $\frac{10^{-25}}{\sqrt{Hz}}$ in the audio band. In the present days, such sensitivity has not yet been achieved, but it is thought that it will be possible by the 2030s. Other characteristics that this detector will feature are fused silica test masses and suspensions (used to improve sensitivity), a 1064 nm laser and improved vibration isolation and mirror coatings [10]. The fields in which the Cosmic Explorer will contribute include the study of the first stars, formation of galaxies and compact binary star systems, structure and formation of neutron stars, the chemical evolution of the universe and dark matter and dark energy. We can see that most fields overlap with the ones described for the Einstein Telescope.

V. CONCLUSION

The detection of gravitational waves has revolutionized our understanding of the universe, providing a new way to observe and study cosmic events. The journey from Einstein's theoretical prediction to the direct detection by LIGO in 2015 marks a significant milestone in physics and astronomy. The ability to measure these minute perturbations in spacetime, caused by massive astrophysical events, relies on advanced technology and sophisticated instruments.

Moreover, the ongoing efforts to improve detector sensitivity and mitigate noise are crucial for future discoveries. The planned advancements with projects such as the Einstein Telescope and Cosmic Explorer promise even greater capabilities, allowing us to explore new realms of the universe.

In conclusion, the study of gravitational waves not only validates a fundamental aspect of general relativity but also opens up a new observational window into the cosmos. The continuous improvement of detection techniques and technologies will undoubtedly lead to further breakthroughs, deepening our understanding of the universe and its myriad phenomena. As we look forward, the future of gravitational wave astronomy holds immense potential for expanding our knowledge and uncovering the secrets of the universe.

[1] G. Vajente, Present and future of gravitational wave astronomy, Galaxies **10**, 91 (2022).

[2] C. Moreno, R. García-Salcedo, A. Lara, and J. Ramírez, Introducción a las ondas gravitacionales, Lat. Am. J. Phys. Educ. **2**, 311 (2008), published in Latin American Journal of Physics Education.

[3] I. Nardecchia, Detecting gravitational waves with advanced virgo, Galaxies **10**, 10.3390/galaxies10010028 (2022).

[4] A. Antognini, F. Nez, K. Schuhmann, *et al.*, Proton structure from the measurement of 2s-2p transition frequencies of muonic hydrogen, Science **339**, 417 (2013), https://www.science.org/doi/pdf/10.1126/science.1230016.

[5] B. P. Abbott, R. Abbott, R. Adhikari, *et al.*, Ligo: the laser interferometer gravitational-wave observatory, Reports on Progress in Physics **72**, 076901 (2009).

[6] C. Cahillane and G. Mansell, Review of the advanced ligo gravitational wave observatories leading to observing run four, Galaxies 2022 **10** (2022).

[7] H. Abe, T. Akutsu, M. Ando, A. Araya, N. Aritomi, H. Asada, Y. Aso, S. Bae, M. Jackson, R. Bajpai, K. Cannon, and et. al., The current status and future prospects of kagra, the large-scale cryogenic gravitational wave telescope built in the kamioka underground, Galaxies 2022 **10** (2022).

[8] A. Buikema, C. Cahillane, G. L. Mansell, C. D. Blair, R. Abbott, C. Adams, R. X. Adhikari, A. Ananyeva, S. Appert, K. Arai, *et al.*, Sensitivity and performance of the advanced ligo detectors in the third observing run, Phys. Rev. D **102**, 062003 (2020).

[9] W. Commons, Interferometer (2007), file: `Interferometer.svg`.

[10] G. Vajente, Present and future of gravitational wave astronomycosmic explorer: A next-generation ground-based gravitational-wave observatory, Galaxies **10** (2022).

[11] S. D. P. et.al., Research facilities for europe's next generation gravitational-wave detector einstein telescope, Galaxies **10** (2022).

Electrical signals and their physiological significance in plants

Aina Creus, Álvaro De Irizar, Ferran Illa, Andrea Quesada, and Nika Zaloznik
Instrumentation. Degree in engineering physics. Universitat Politècnica de Catalunya. Campus Nord, 08034 Barcelona

Electrical impulses in plants play a crucial role in their capability to rapidly react to changes in their environment. Action Potentials (AP) and Variation Potentials (VP) transmitted through vascular bundles have been related to key processes in plants, such as photosynthesis or nutrient transport. In this review we provide a comprehensive introduction to classical measurement sensors and techniques, as well as insights of novel sensors and current fields of research.

Keywords: Action potential (AP), Extracellular recording, Intracellular recording, Plant Electrophysiology, Variation potential (VP).

I. INTRODUCTION

The transmission of nervous impulses has classically been associated with animals, who need to respond quickly to external stimuli to survive. However, the detection of electrical signals in plant cells suggested that there are other organisms capable of using electricity as a rapid communication channel over long and short distances.

Today we know that, indeed, many plant species can efficiently transmit Action Potentials, as well as long-distance Variation Potentials propagated through vascular bundles. This ability probably arises from the need to react quickly to external stimuli, complementing chemical signals, such as hormones, which are slower but longer lasting. These signals have been related to numerous physiological processes such as cellular respiration, photosynthesis, pollination, nutrient transport and defense.

The great environmental importance of plants at all levels justifies their study from a physical and technological point of view. Advances in methods of measuring electrical signals in plants could help improve selective breeding techniques and thus increase agricultural production. Current fields of study focus on the development of a new class of flexible sensors compatible with the curved and variable surfaces of the plant cell, since classic sensors are too rigid to adapt to the delicate cellular structure of plants.

II. ELECTRICAL SIGNALS AND TRANSMISSION

Action potentials (AP)

Well known in animals, AP are rapid, self-propagating electrical messages. They are transmitted at constant speed and amplitude and have an all-or-nothing character, that is, they are only transmitted once the stimulus that generates them reaches a certain threshold that depolarizes the cell membrane, but additional increases in the strength of the stimulus do not change the amplitude or shape of the transmitted wave.

The ionic mechanism of APs in plants is somewhat different from that of axons in neurons, which is based on Na^+ and K^+ channels; instead Ca^{2+}, Cl^- and K^+ voltage-gated channels (VGC) are used. These ion channels respond to changes in membrane potential, so excited membranes induce depolarization in adjacent non-excited regions, allowing the signal to passively self-propagate. Signals can be transmitted locally through plasmodesmata, small microscopic tubes in cell walls that connect the cytoplasm of groups of adjacent cells. When information needs to be transmitted to distant parts of the plant, electrical signals are conveyed through the phloem.

However, the speed at which these signals are transmitted is noticeably slower than in animals. For example, *Mimosa pudica* is a tropical plant known for its ability to retract its leaves quickly in response to mechanical impulses. The AP associated with this reaction is transmitted at a speed of about 20-30 mm/s,

a speed similar to the AP of an *Anodonta* clam (45 mm/s) but well below those of the nerves of mammals (100 m/s). In addition, they have associated refractory periods in which new impulses cannot be transmitted that vary, depending on the species, between about 50 seconds and 5 hours. In contrast, in mammalian nerves the absolute refractory periods last 0.0005 s and the relative refractory periods last 0.001 s to 0.01 s.

APs have been documented in plants in response to numerous non-damaging stimuli, such as electrical and mechanical stimuli, light transitions, pollination, cooling or irrigation, each with an associated physiological response.

Variation potentials (VP)

VPs are slower signals whose amplitude and speed decrease with distance from the origin. They are not self-propagating, but instead consist of local changes in the membrane potential generated by the transmission of another type of signal (mechanical or chemical).

Transmission is thought to occur through the dead xylem tissue. There are two possible methods of wave propagation: loss of xylem tension and pressure or hydraulic transport of chemical substances. These signals activate mechanosensitive channels (MSC) in the first case or ligand-activated channels (LAC) in the second, triggering membrane depolarizations as they pass. They do not, however, activate VGCs, as these are associated with APs.

Variation potentials are generally associated with damaging stimuli, such as wounds, organ removal, heating or burning.

III. MEASUREMENT TECHNIQUES

Extracellular recordings

Extracellular measurements offer a notable advantage, as they can capture electrical potential variances over prolonged periods (i.e. during several days), thus allowing to detect slow changes in the potential. These recordings provide us with information regarding the bioelectrical activity of large groups of cells. Two principal techniques stand out: surface recordings and measurements inserting metal electrodes.

Surface recordings are less harmful, given their non-invasive nature. Therefore, it is possible to measure the bioelectrical potential (BEP) with less probability of damaging the plant's tissues, and hence not leading to changes in the object of study. They use electrodes consisting of either $Ag/AgCl$ cotton-wrapped wires, or $Ag/AgCl$ pelleted electrodes connected by means of an aqueous conductive gel. They are placed on the plant's surface, together with a reference ground electrode, usually introduced in the soil. All electrodes are connected to a high-input impedance electrometer for data logging. A brief measure scheme is shown in *Figure 1.*

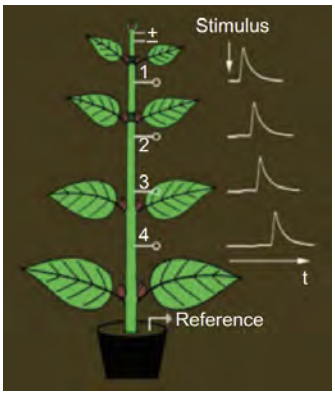

FIG. 1: Extracellular measurement with four channels and a reference electrode connected to the soil.

On the other hand, measurements involving inserted metal electrodes are invasive, given that the insertion may cause wound reactions. Consequently, the electrodes consist of thin metal wires, such as $Ag/AgCl$ wires of $0.4 - 1.0$ mm in diameter. Nevertheless, they provide better contact and access to deeper areas of the plant. The experimental setting is analogous to that of surface recordings.

Intracellular recordings

Unlike extracellular measurements, intracellular recordings only provide short-term measures, as they lose reliability after 1-2 h. Nevertheless, they offer superior precision, as the electrical signals are measured from specific cells, rather than a large group of them.

Hereafter, three distinct approaches for these measurements are highlighted.

i. *Measurement of membrane potential by implanting a single electrode*:

Born in the early 1900's, this method performs measurements of membrane potential (V_m). Examining V_m in distinct circumstances has been crucial in the field, specially for comprehending membrane selective permeability, electrogenic processes and action potentials. In fact, the existence of cation channels in plant cell membranes was predicted thanks to these studies.

ii. *Two-electrode voltage-clamp technique*:

This technique measures the amount of ionic current crossing a membrane at any given time, while maintaining V_m through an operational amplifier circuit. This method is not highly invasive as it does not damage cellular structures, yet is not widely used for the analysis of cation channels in higher plants due to its inconveniences, which include, for instance, limitations when using small cells.

iii. *Patch-clamp technique*:

Developed in the 1970s, patch-clamp technique received the Nobel Prize in 1991. It involves using a fine glass pipette with a large diameter at the tip. (i.e. $> 1\,\mu m$) to create a seal with a cell membrane, allowing for the measurement of its electrical activity (just one electrode monitors voltage and delivers current to maintain the voltage at a constant level).

Despite the many strengths of the patch-clamp technique, it still has certain disadvantages, including negative effects in native channels and their regulatory functions when treating plant cells with cellulytic enzymes, or the exchange of the native cytosolic solution for an artificial solution in whole cell mode.

IV. FLEXIBLE WEARABLES

Traditional rigid sensors are not suitable for continuous monitoring of plant physiology, this has motivated the development of new kinds of sensors with high adaptability to the shape changes of curvilinear surfaces. These sensors are known as flexible sensors, and have already been used in other fields such as healthcare or soft robotics, not just allowing for reliable contact under surface movement or modification, but also serving as multi-functional devices, capable of monitoring multiple variables.

When developing flexible sensors, the materials used can be divided into three categories:

i. Substrate materials: used to support the functional circuit. They provide ductile and bending capacities and, in some cases, some other specific properties (like air permeability or moisture absorption).

E.g.: Natural or synthetic polymers such as silk substrate, gelatin, or cellulose.

ii. Functional materials: crucial for the sensor to work. These materials include conductive materials and semiconductors.

E.g.: Metal films, flexible liquid metals, graphene, or nanowires.

iii. Packaging materials: Providing the shielding of the sensor. They must be flexible and malleable, sometimes allowing light transmission or electromagnetic shielding.

E.g.: Polyimide or polydimethylsiloxane.

Plant wearables used for electrical signal monitoring require electrodes with thorough contact with the plant surface to minimize signal interference. We can use adhesive flexible elements such as thin PET films when the surface is smooth and sticky and, for hairy plants, ionic electrodes based on thermo-gel have been developed.

Consistent energy supply is key for long-term monitoring. Solar cells could be a fitting solution, but they are susceptible to many factors,

such as light or weather conditions. Other solutions are triboelectric nanogenerators (TENG), converting mechanical energy into electrical energy through the friction-generation effect, providing long-lasting and self-sufficient energy. Unfortunately, they are still in a development stage, with complex manufacturing processes.

Plant Tattoo Sensor Array

Many flexible sensors are currently being tested, seeking versatile, multi-sensing devices. This particular experimental plant wearable adheres directly to the leaf surface without the need of any additional structure, providing both short and long term monitoring iwthout loss of reliability.

Made of gold and PET thin-film patterns, the tattoo sensor is composed by three sensors that are attached to its respective instrument through small alligators:

FIG. 2: Tattoo Sensor Arrays attached to a leave.

i. Biopotential electrode: Attached to an Arduino microcontroller (for voltage measurement) and to a metal electrode (clipped to the root of the plant).

ii. Temperature sensor: Operates as a thermistor that changes its resistance with temperature, it has a serpentine structure. It is connected to a multimeter that measures changes in the electrical resistance.

iii. Relative water content sensor: A circular pad electrode (1 mm diameter) and a thin ring electrode provide electrical impedance measurements. Together with a non-contact infrared surface thermometer, and a relative humidity sensor placed near the leaf (2 cm away).

V. CONCLUSION

This project aimed at introducing and reviewing theoretical and experimental approaches to understand electrical impulses in plants, and linking such knowledge with both historical and novel sensors in the field. Nevertheless, this paper has only discussed a handful of mainstream sensors and techniques, as a general approach has been thought to be more suitable for reviewing and introductory purposes.

In practice, every plant class and species introduce their own variables, and sensors need to be modified accordingly. Minimally invasive devices that suit multiple surfaces and work under a broad range of environmental conditions are currently needed to deepen our understanding of the role of electrical signals in plants, working towards breakthroughs in agriculture and selective breeding.

[1] Jörg Fromm and Silke Lautner. Electrical signals and their physiological significance in plants. *Plant, cell & environment*, 30(3):249–257, 2007.

[2] TE Kuleshova, Anna Vladimirovna Bushlyakova, and Nikolay Rostislavovich Gall'. Noninvasive measurement of bioelectric potentials of plants. *Technical Physics Letters*, 45:190–192, 2019.

[3] Chun-Chun Qu, Xu-Yang Sun, Wen-Xiu Sun, Ling-Xiao Cao, Xi-Qing Wang, and Zhi-Zhu He. Flexible wearables for plants. *Small*, 2021.

[4] Liang Dong Shihao Yin. Plant tattoo sensor array for leaf relative water content, surface temperature, and bioelectric potential monitoring. *Advanced Materials Technologies*, 2024.

[5] Alexander G Volkov. *Plant electrophysiology*. Springer, 2006.

Wireless and Powerless Sensor Systems

Miguel Ausejo Montserrat Ferré Eudald Puy Andreu Solà

Instrumentation. Degree in Physics EngineeringUniversitat Politècnica de Catalunya.
Campus Nord, 08034 Barcelona
Email: montserrat.ferre@estudiantat.upc.edu

Abstract

The challenges posed by limited battery life in sensor nodes, such as the labor-intensity that battery replacement methods constitute, have prompted the exploration of wireless and powerless sensor systems as a solution. This kind of systems offer the promise of eliminating the need for frequent battery replacement and extending the lifespan of sensor nodes. This paper provides an overview of wireless and powerless sensor systems, reviews the technology of these devices, presents their most important applications, as well as their implementation in sensor networks. The paper concludes by outlining future research directions and challenges in this field.

Keywords: wireless, powerless, sensors, WPT, WPSN, Internet of Things (IoT)

1 Introduction

Wireless sensors refer to those sensors comprising compact and embedded devices which communicate wireless in an specific arrangement. These sensors continuously monitor physical conditions, such as pressure or temperature, generating data in real-time and then sending it to sinks, where this data will be collected and processed. Usually the sinks can communicate this information to end-users via various channels, including direct connections, the Internet, or even satellites.

Achieving this connectivity entails ensuring that continuous power is provided to the wireless nodes to operate without interruptions. However, maintaining this continuous power flow is one of the main difficulties that these devices face to achieve an adequate functioning.

The conventional approach to supply these sensors are wiring the sensors to a power source or supplying them with batteries. In the first case, these types of system require the same number of power and ground cables as there is sensor units, yielding a complicated wiring system. These cable assemblies may also be damaged, lowering the reliability of the monitoring system. In the case of batteries, its the limited lifespan and the need of recharge presents also a significant drawback.

2 Technology

As the number of wireless devices grows, maintaining uninterrupted power supply becomes challenging, particularly due to the associated higher maintenance costs compared to the traditional charging methods. As an alternative, energy harvesting (also known as power harvesting or energy scavenging) offers a different solution by capturing and converting ambient energies, such as solar, thermal, and kinetic, into usable electrical energy. This allows the sensors to operate without the need to run wires or make frequent visits to replace batteries.

For example, photovoltaic cells are semiconductor devices that convert sunlight into electricity absorbing photons by the cells of semiconductor material. This absorption leads to release electrons that, at the end, generate the corresponding electricity. As a result, this eliminates the need to use external batteries as a power source. However, these power sources are usually unstable or uncertain and, therefore, unreliable.

To mitigate the issue of interrupted power supply, wireless power transfer (WPT) technologies offer a promising solution by ensuring uninterrupted operation of the wireless sensor devices, thereby enhancing sensor lifetime and throughput. Several physical mechanisms have been proposed:

WPT technology is not without its constraints, which vary based on the specific power transfer mechanism. A review of the potential of each mechanism is shown in Figure 2. Notice that numerical values are omitted as they are heavily reliant on the particular setup. Most widely used mechanisms are capacitive/inductive and radiofrequency (RF).

With an inductive or capacitive link it is possible to achieve high efficiencies, even with high power systems. The main limitation is the short charging distance which is in the range of cm.

Therefore, the transmitter (TX) and the receiver (RX) are placed in close proximity. The link efficiency is largely

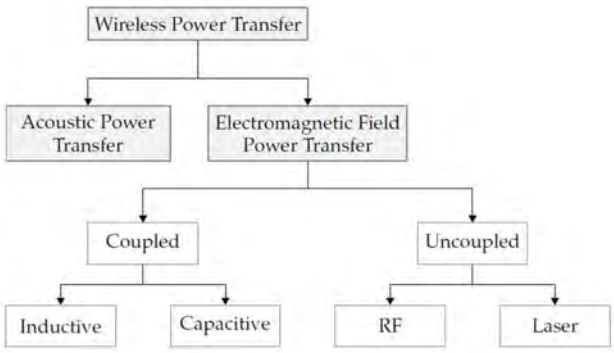

Figure 1: Wireless Power Transfer mechanisms [7]

determined by the coupling factor between TX and RX, depending on several design parameters such as the frequency. Figure 3 shows the system diagram of the most common approach.

First, a power supply in combination with a transmitter circuit provides an amplified sine wave that can be controlled in both frequency and amplitude. For this purpose, a pre-regulator, power inverter, and wave generator are required. The transmitter antenna is coupled with the receiver antenna by means of electric or magnetic fields. Thirdly, the receiver circuit consists of an AC/DC conversion by means of a rectifier, smoothing capacitors, and a switched-mode power supply (SMPS) to generate a stable DC voltage. A simpler variant is presented in [2]. A wireless and powerless temperature measurement system was implemented using the resonant frequency changes depending on the temperature of the SAW Sensor by reflection wave characters using bi-directional coupler.

On the other side, RF power transmission has recently received significant interest because radio waves offer the advantage of being ubiquitous and hence energy can be obtained over a large area, even in places with difficult access [6]. RF power can be harvested from ambient sources such as TV towers, Wi-Fi, and cellular communication systems. However, the power density available is extremely low. Dedicated sources can also be used, in practice the levels are often limited by regulations and safety levels. Consequently, multiple frequency bands are normally exploited to increase the harvested power.

Therefore, the sensor nodes are formed by integrating a traditional sensor device with a RF power receiver. Figure 4 shows the system diagram:

Therefore, the sensor node includes a receiving antenna, a unit for managing power and a rectifier to convert the radiofrequency power to DC. Usually, this kind of nodes, especially if they a part of a sensor network, integrates the sensing element and a microcontroller.

3 Applications

In the past decade, remarkable advancements in wireless technology have paved the way for diverse applications rooted in the Internet of Things (IoT), profoundly impacting our daily routines. These applications span various domains such as healthcare, smart home or industria (including communication, and transportation), highlighting their integral role in modern society's fabric as shown in Figure 5.

Security and safety considerations are paramount in these applications, underscoring the necessity of uninterrupted connectivity among the nodes. Some interesting applications include the following examples:

3.1 Power Supply for other devices

An important application of WPT consists of becoming the power supply for other devices. These devices can vary from widespread and rather simple such as laptops or smartphones, to very concrete and complex satellites, where a continuous supply with a reliable performance is key in order to ensure the correct functioning.

3.2 Healthcare

WPT can play a critical role in implantable medical devices by eliminating the need for patients to undergo surgery to replace batteries for pacemakers, hearing aids, or insulin pumps. For these applications, finding ways to harvest energy is crucial because of issues like battery life, voltage problems, and potential complications [8]. When comparing inductive power transfer and radiative power transfer, recent studies indicate that radio-frequency can greatly improve performance over its competitor. While some research shows successful use in heart and eye sensors, other studies highlight concerns about efficiency, safety, and effectiveness. However, advancements in optimizing how energy is transmitted and making devices smaller are expected to solve these problems over time. Furthermore, WPT will revolutionize the healthcare industry by facilitating a more convenient, efficient, and cost-effective means of powering medical devices and infrastructure, having the potential to participate in many healthcare applications,

3.3 Civil Engineering

During construction, it's important to constantly monitor larger structures in order to prevent unexpected problems. Even after construction, ongoing monitoring is needed to detect any weaknesses in the structure. Usually, wired sensors are used for this, but they are complicated to set up. Another major issue is replacing the batteries in these sensors over time. To address this, Wireless Power Transfer (WPT) method embedded within concrete was introduced.

WPT Technology		Power Transfer	Range	Frequency	Efficiency	Biological Impact
Inductive	IPT	W to MW	cm	kHz to MHz	high	minor
Capacitive	CPT	W to kW	mm/cm	kHz to MHz	high	minor
Laser	LPT	W/kW	m/km	> THz	medium	medium/significant
Radio frequency	RFPT	mW/kW	m/km	MHz to GHz	low	medium/significant
Acoustic	APT	mW/kW	m/cm	kHz to MHz	medium	significant/medium

Figure 2: Wireless Power Transfer characteristics [7]

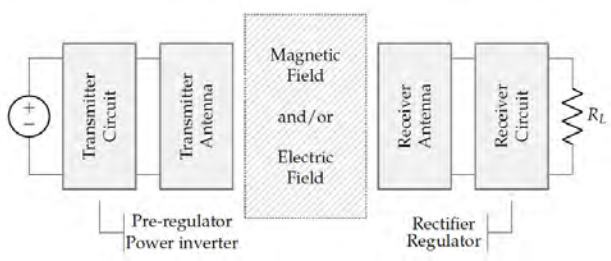

Figure 3: System diagram of a coupled WPT system [7]

Figure 4: System diagram of a RF WPT system [7]

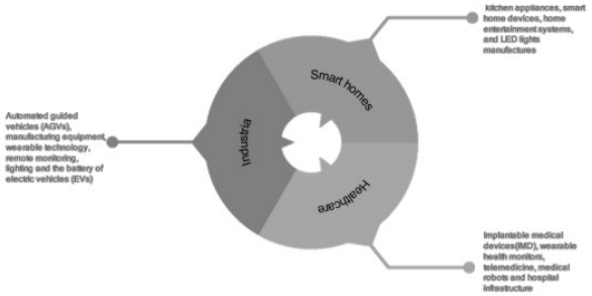

Figure 5: Applications of WPT [8]

They created a system where nearby steel bars, called rebars, act as a magneto-inductive field. The research [8] shows that sensors can be powered from almost 1 meter away and still maintain an adequate functioning.

3.4 Wearable Technology

In the industrial environment, wearable technology, such as smart helmets and safety vests, can improve worker safety and efficiency. The wireless charging of these devices, with WPT, eliminates the need for cumbersome battery packs and increases mobility [8].

4 Wireless powered sensor networks

One of the most promising and straightforward uses of wireless and powerless sensor are wireless sensor networks. Wireless sensor networks support several applications, including continuous environmental monitoring, surveillance, tracking, and so on. In this cases, the sensor nodes are very numerous and are spatially distributed with random locations.

Therefore, RF WPT can be used to prolong the network lifetime by providing sustainable energy supply to the distributed sensor nodes through Em waves. This concept is called wireless powered sensor networks (WPSN). The general concept of the WPSN is presented in Figure 6.

Therefore, WPSN require an energy transmitter or power beacon broadcasting power to the sensor nodes located in the beacon's coverage. A power beacon is a device that generates and emits energy in the form of electromagnetic waves. An antenna array is integrated with the power beacons to enable the power beacon to transmit power through the microwave beam. Hence, WPSN can be classified into two main types:[6]

1. Omnidirectional WPT: RF power is broadcast equally by the power beacon in all directions independently of the locations of the sensors
2. Directional WPT: the radiated energy from the power beacons is directed in the locations of the sensors through an energy beam-forming. This introduces additional complexity since, in general, it will be required that the microwave beam can be adaptively

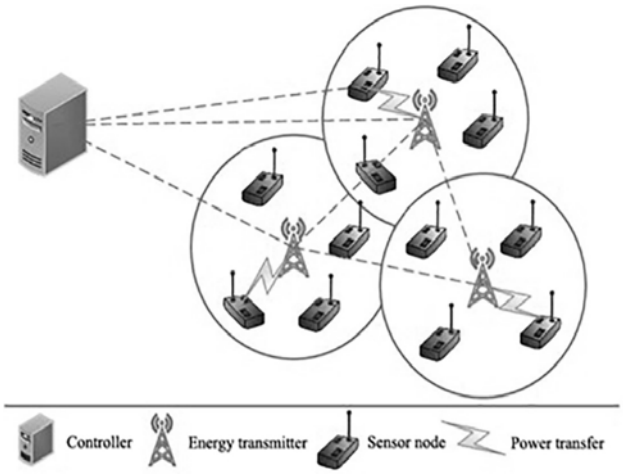

Figure 6: Architecture of a WPSN

steered in case some of the sensor changes its location.

Another important parameter of WSPN is the capability for for simultaneous wireless information and power transfer (SWIPT) [5]. SWIPT uses downlink communication facilitating the simultaneous transfer of information and energy. This requires two different circuit receivers to perform both information decoding and power supply, because it is impossible to accommodate power supply and information decoding on the same received signal, owing to the possibility that the information content of the signal is affected by the power supply [1].

5 Current challenges and areas for further research

5.1 Powering multiple nodes

Most research focuses on powering one sensor node with one beacon. Powering multiple nodes with one beacon is very complex as the beacon must allocate and direct energy at multiple sensors ensuring all are still powered. Different approaches are being researched, each with their own challenges: beam-splitting and time allocation.

Beam splitting splits a microwave beam to send directed energy to each sensor. This requires continuously locating the nodes and redirecting every beam to each of them. Additionally, energy must be evenly split between the beams for optimal performance. This two requirements are very hard to implement in practice. Despite this, this approach has succeeded in powering simple experimental systems.[4]

The other approach is time allocation. This means powering only one sensor for a given time cycling through all nodes. Unfortunately, in practice this is also very complicated: the beacon must ensure no node is depleted of energy. Each node has to communicate its energy level and the beacon must dynamically allocate charging time in response.[3]

5.2 Duplex broadcasts

A hybrid access point (H-AP) is a single beacon capable of broadcasting both energy and information with a distribution of nodes, as opposed to using a separate energy source and receiver. This considerably simplifies WPSNs. A H-AP can operate in duplex or half-duplex mode.

According to telecommunications terminology, we classify each communication channel according to its direction:

- Downlink (DL): energy from the H-AP to the nodes
- Uplink (UP): information from the nodes to the H-AP

In full-duplex mode, the H-AP sends energy in the DL simultaneously as information is received in the UP. The DL emission interferes with the UP reception so a self-interference cancellation (SIC) technique must be used to process the signal.

In half-duplex mode transmission must be either in the DL or UP, akin to a walkie-talkie. H-AP must allocate time between sending energy and receiving information in order to maximise energy and information throughput.

For multiple nodes, the H-AP must additionally allocate energy between the nodes in the DL as described in subsection 5.1.

Full-duplex has been shown to outperform half-duplex even with imperfect SIC techniques using a low-power H-AP with multiple nodes.[1] Current research is not conclusive and further investigation is needed to determine the optimal mode.

5.3 Energy efficiency

Current WPT implementations are very energy inefficient compared to wired power transfer. There is theoretical research and simulations to optimise the distribution of nodes and beacons, but experimentally measuring energy efficiency is challenging.

6 Summary

Wireless power sensor systems are already a proven solution for low-power applications and are finding real uses in the medical, industrial and engineering fields.

On the other hand, high-power WPTs capable of powering smartphones or wearable devices present difficult engineering problems. Research on this field is largely theo-

retical but there is steady progress and usable prototypes are expected in the next decade.

References

[1] Hyungsik Ju and Rui Zhang. "Optimal Resource Allocation in Full-Duplex Wireless-Powered Communication Network". In: *IEEE Transactions on Communications* 62.10 (Oct. 2014), pp. 3528–3540. ISSN: 1558-0857. DOI: 10.1109/TCOMM.2014.2359878. URL: https://ieeexplore.ieee.org/document/6907966 (visited on 05/20/2024).

[2] Soon-Young Hong et al. "Wireless Temperature Measurement System with RF Transceiver and Powerless Sensor". In: June 1, 2015, pp. 2602–2607. DOI: 10.1109/ICPE.2015.7168140.

[3] Kae Won Choi et al. "Wireless-Powered Sensor Networks: How to Realize". In: *IEEE Transactions on Wireless Communications* 16.1 (Jan. 2017), pp. 221–234. ISSN: 1558-2248. DOI: 10.1109/TWC.2016.2621766. URL: https://ieeexplore.ieee.org/document/7707470 (visited on 05/20/2024).

[4] Kae Won Choi et al. "Theory and Experiment for Wireless-Powered Sensor Networks: How to Keep Sensors Alive". In: *IEEE Transactions on Wireless Communications* 17.1 (Jan. 2018), pp. 430–444. ISSN: 1558-2248. DOI: 10.1109/TWC.2017.2767579. URL: https://ieeexplore.ieee.org/document/8094989 (visited on 05/20/2024).

[5] S. M. Asiful Huda, Muhammad Yeasir Arafat, and Sangman Moh. "Wireless Power Transfer in Wirelessly Powered Sensor Networks: A Review of Recent Progress". In: *Sensors* 22.8 (8 Jan. 2022), p. 2952. ISSN: 1424-8220. DOI: 10.3390/s22082952. URL: https://www.mdpi.com/1424-8220/22/8/2952 (visited on 05/20/2024).

[6] Gerald K Ijemaru, Kenneth Li-Minn Ang, and Jasmine KP Seng. "Wireless Power Transfer and Energy Harvesting in Distributed Sensor Networks: Survey, Opportunities, and Challenges". In: *International Journal of Distributed Sensor Networks* 18.3 (Mar. 1, 2022), p. 15501477211067740. ISSN: 1550-1329. DOI: 10.1177/15501477211067740. URL: https://doi.org/10.1177/15501477211067740 (visited on 05/20/2024).

[7] Jarne Van Mulders et al. "Wireless Power Transfer: Systems, Circuits, Standards, and Use Cases". In: *Sensors* 22.15 (15 Jan. 2022), p. 5573. ISSN: 1424-8220. DOI: 10.3390/s22155573. URL: https://www.mdpi.com/1424-8220/22/15/5573 (visited on 05/20/2024).

[8] Aisha Alabsi et al. "Wireless Power Transfer Technologies, Applications, and Future Trends: A Review". In: *IEEE Transactions on Sustainable Computing* PP (Mar. 1, 2024), pp. 1–18. DOI: 10.1109/TSUSC.2024.3380607.

Modern applications of Ultrasound Imaging

Leonardo Costa, Aniol Anglada, Maurici Bataller, Gabriel Badia, David Lecumberri, Alejandro Cortés
Instrumentació. Grau en Enginyeria Física. Universitat Politècnica de Catalunya.

I. GENERALITIES

Nowadays, in the field of medical imaging, significant advancements have been carried out. One of these consists of the use of ultrasound technology. This technology transmits sound waves in the body, detects and interprets the echoes, allowing for the creation of images of internal organs, tissue mapping, and other medical data. More specifically, ultrasound is a high-frequency sonar system that detects small echoes of sound waves as they travel through the body in order to get access to "what is happening inside a body". Progress in microelectronics has led to portable and highly efficient instrumentation that is supposing great improvements in our lives.

In our case, ultrasound is a diagnostic imaging technique that uses sound waves to create three-dimensional (3D) and real-time four-dimensional (4D) images of (as said) a developing fetus, organs, or other structures within the body. It provides more detailed and lifelike images compared to traditional 2D ultrasound, allowing for better visualization and assessment of anatomical structures.

How does it work?

A high voltage pulse stimulates a crystal (the piezoelectric transducer), causing a corresponding mechanical compression (an inverse piezoelectric effect), and thus creating the ultrasound wave that passes through the body (Figure 1).

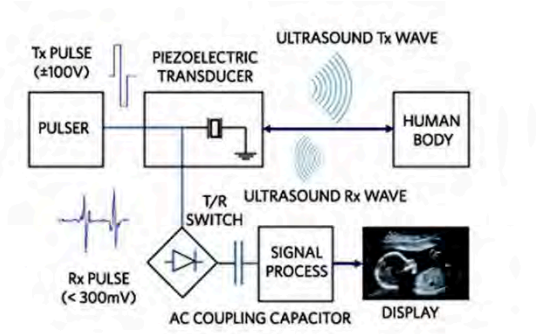

FIG. 1 Block diagram of an ultrasound system. [Source: Maxim Integrated, https://www.eetimes.com/high-performance-design-for-ultrasound-imaging]

A part of the wave is reflected at the interface between different tissues, and these reflected signals are also detected by the transducer, which generates an electric signal in response (piezoelectric effect).

The wave generated by the transducer is focused and directed by phased array techniques. It is important to remark that depending on the substances the wave encounters (such as soft tissues, bones, fat, and blood), the intensity characteristics of the reflection signal will vary.

There are some important issues that need to be taken into account for good performance:

- Synchronization of the transmission and reception circuits is essential, as these systems work at high frequencies.
- The phase noise (frequency-domain) or jitter (time-domain) is a crucial factor that can affect the quality of an ultrasound image. Phase noise is a result of a deviation of the clock signal's phase from its ideal position. It can lead to inaccurate measurements, so accuracy of the clock is of utmost importance.
- In order to avoid switching effects (coupling with the ultrasound signal), higher frequencies require additional measures whereas circuits for lower frequencies ultrasound have simpler designs and lower electromagnetic interference.

Another important aspect is the amplification. The transmitted sound pulse propagates through the body as a wave in the frequency range between 1 MHz and 15 MHz. However, it is important to remember that sound waves lose intensity as they travel through the human body. That is, as the signal travels it loses some of its energy and when it is reflected and comes back to the transducer it arrives with only a fraction of its original intensity. Most of the weak signals that happen long after the transmission begins are reflections. The signal that is reflected is analyzed and shown as an image on a screen. For this purpose, many microelectronic solutions have been created, which all include some amplification. Not all types of reflection need the same treatment. While the reflections from shallow focal points need little or no enhancement, the ones from deep focal points require larger amplification.

Most receivers must be able to adapt in both conditions, without saturating or distorting the signal, thus introducing a minimum noise.

The amplifier of ultrasound systems is simple. There are 2 main elements:

- A highly linear low-noise amplifier (LNA) with digitally programmable gain and impedance.
- A variable gain amplifier (VGA) to provide a better signal-to-noise radio (SNR) and phase noise for the path

Naturally, the signal is then digitized by the analog-to-digital convertor (ADC).

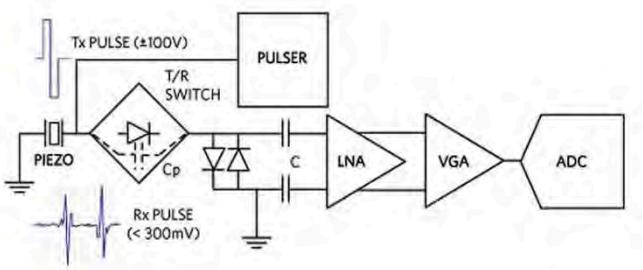

FIG. 2 Block diagram of the reception system for the ultrasound system. The transmit/receive (T/R) switch isolates the receiver during high voltage bursts in transmission. [Source: Maxim Integrated]

When designing these kind of systems:

1. Selecting a reception front-end circuit with strong overload recovery capabilities is crucial as overload scenarios may arise during transmission, hindering the processing of reflection signals and obscuring smaller signals among larger ones or causing the loss of the reflected signal altogether.
2. The LNA and VGA stages, as well as the ADC, should be designed in such a way that they all recover quickly from an overload condition
3. Choosing a high-quality ultrasound transceiver can simplify hardware and software development, minimize troubleshooting problems, speed up time-to-market, and improve image quality.

In this way, ultrasound imaging provides a diagnostic technique that helps in overall assessment of the patient's condition.

We will now discuss some interesting applications to exemplify the usefulness of Ultrasound technology.

II. SAM

Scanning Acoustic Microscopy (SAM) is a type of microscopy which is characterized by being non-destructive to the sample examined. Its main application is in the field of quality control, inspection and failure analysis in microelectronic components and materials although in recent times its application in medicine has increased. The most important difference with widely-used ultrasound in medicine is that SAM operates with high frequencies at relatively short distances.

A Scanning Acoustic Microscope is composed of three principal components: a transducer, a mechanical scanner and an image processor. The transducer takes on the same role as in any ultrasound device, emitting waves and measuring the reflections through the piezoelectric and inverse piezoelectric effect. Once the acoustic signal is generated, it travels through a sapphire (Al_2O_3) cylinder to the lens. There, refraction occurs in order to have a flat wavefront that focuses directly to the sample which is under the transducer. It is essential to place a water medium between the transducer's lens and the sample, so that the efficiency of acoustic waves transmission in the material is increased.

The ultrasonic pulses are transmitted or reflected depending on the variation of the acoustic impedance of the different interfaces of the material examined. This leads to echos (reflected waves) of different characteristics (intensity, frequency, etc) depending on when and where the reflection has occurred. Finally the echos are picked up in the transducer where the mechanical scanner transforms them into an electrical signal which is amplified and digitized by the image processor.

The acoustic impedance (Z) is defined as the product of the density (ρ) and the velocity of the sound in the material (c):

$$Z=\rho \cdot c \tag{1}$$

It expresses the resistance an acoustic wave receives from the medium it is on. Since Z is proportional to ρ and c, if one of these magnitudes increases, the acoustic impedance also increases.

The imaging of the sample is produced after the analysis of two different parameters: amplitude attenuation and time-of-flight.

While doing the scanning of the sample with the SAM, if an acoustic wave collides with an interface with normal incidence, some of the energy is reflected and the other gets transmitted. It is obvious that the amplitude of the echos depend on the difference of Z between the medium and the interface. Since the intensity of a wave is directly proportional to the square of its amplitude, the amplitude's attenuation implies also an attenuation on the intensity. This leads to define the reflection coefficient R as the following:

$$R = \frac{I_{Reflected}}{I_0} = \frac{(Z_{surface} - Z_{medium})^2}{(Z_{surface} + Z_{medium})^2} \tag{2}$$

Using this parameter it is possible to know the value of $Z_{surface}$ and consequently figure out the surface's material.

The time-of-flight parameter provides the depth information of each surface of the sample. If this time is small, it means that the reflection has occurred early, and consequently if the time is large the reflection has taken more time to happen.

Combining these two terms it is possible to make an image of the sample since it is known how the different surfaces and mediums are and in which depth they are located.

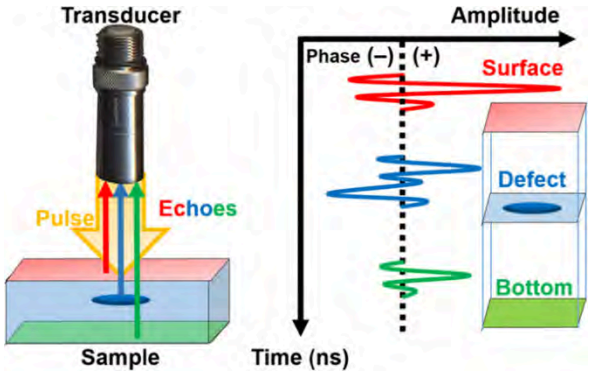

FIG.3 Diagram of the reflection of SAM pulses (left) and histogram of how the amplitude of the reflection pulses changes (right). [Source: NIH, https://www.ncbi.nlm.nih.gov/pmc/articles/PMC7818342/]

SAM has plenty of applications. In medicine it has been used to image gastric tumors, characterize infarcted myocardium and to observe the properties of a dialyzed kidney. The endothelial cells of the human umbilical vein were viewed using acoustic microscopy and it is also often used to observe the mechanical properties of the human bone.

Another use of this method of observation is in material characterization. It has been implemented to observe the growth of cracks in ceramics and it plays a role in the determination of the elastic constant.

In dentistry it has many applications, it can monitor the two-dimensional color distributions of human molars without any caries. It is also used for observing carious lesions as well as to image human teeth.

The fact that SAM can image the interior of optically opaque objects and that it can observe elastic properties of the studied body at cellular level without causing any damage to its natural structure is what makes the microscope a unique tool.

After a long period of research, SAM is being considered superior in resolution when compared to the conventional optical microscope. Acoustic microscopy has been gaining repeated attention from various medical and industrial sectors as well as from the commercial sector.

III. 4D FUNCTIONAL ULTRASOUND IMAGING OF WHOLE-BRAIN ACTIVITY IN RODENTS

Finally, we want to talk about the recent advances in ultrasound applied to the field of neuroscience, in particular to the study of the brain from the perspective of a dynamic global network of interacting regions.

The characteristics of this biological system require sharp observations of long duration and high sampling rate over a sufficiently large volume. In this respect, other neuroimaging modalities such as magnetic resonance imaging (MRI), electroencephalogram, or magnetoencephalography offer a large image at the cost of lower sensitivity and spatio-temporal resolution, while optical techniques or electrophysiology offer a prolonged image of high quality but only of a small region. On the other hand, photoacoustic tomography does meet all of the above requirements, but its application is limited as it is quite invasive. In the search for whole-brain high-resolution non-invasive imaging techniques, ultrasound is a promising candidate.

The underlying principle of functional ultrasound (fUS) is neurovascular coupling, a complex mechanism that increases the supply of oxygen and nutrients to the region where neuronal activity takes place. Thus, by measuring cerebral blood volume (CBV), we indirectly detect brain activity. The measurement of CBV is done by detecting the frequency of reflected waves, which will be lower or higher depending on the relative speed of the blood the waves reflected off of. The transmission of plane waves together with the implementation of an elaborate parallel electronic system endows this technique with ultra-fast frame sampling and ultra-sensitive Doppler imaging. However, this technology is currently limited to 2D regions, so a group of researchers at PSL University (Rabut et al., [2]) have developed an innovative methodology to overcome this limitation, which we want to discuss in depth.

Along the same lines as the 2D case, the objective is to compute a power Doppler volume, which is proportional to the CBV. To do this, a signal transmission process is carried out through a transducer formed by a high-frequency two-dimensional matrix. The signals have been previously encoded using Hadamard coefficients, which subsequently allow the information received for each pixel to be decoded at different depth levels. This way, multiple 2D images are obtained which, when combined, form the desired three-dimensional image. Finally, a spatiotemporal clutter filter is performed to separate the blood flow from the tissue movements.

That is, at a rate of thousands of frames per second, snapshots are taken from a flat screen with the difference that instead of capturing an optical response, it picks up the

ultrasound echoes emitted from each pixel of the screen itself. A mathematical process then separates the information into layers, reconstructs the three-dimensional image and distinguishes the blood from the tissues, in order to see where changes in blood flow occur and analyze the brain's response under different circumstances.

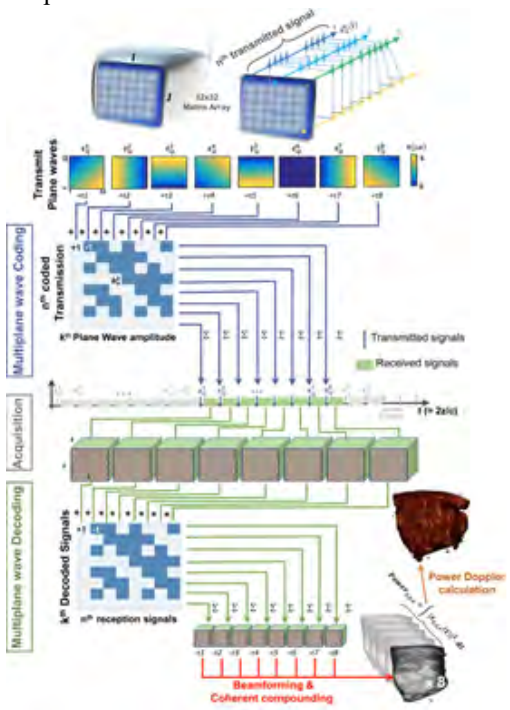

FIG. 4 Sketch of the signal processing method. [Source: Rabut et al. [2]]

To test the researcher's prototype, three experiments were carried out with rats (after performing a craniotomy to ensure a higher resolution). We will talk about the first two, as they showed the effectiveness of this proof of concept:

The first experiment involved measuring activation of sensory regions of the brain while the rats received stimuli (the light of a LED and a caress to the whiskers). As expected, fUS detected higher CBV levels in the visual and whiskers, respectively, sensory regions when the rats received the stimulus than when they did not, thus confirming the effectiveness of this prototype in measuring the activation of specific areas of the brain.

The last experiment involved the analysis of the propagation of transient epileptiform events through the brain. For this purpose, epileptiform events were induced by injecting 4AP into the cerebral cortex of 3 rats and mapping CBV variations and the spreading of cortical depression waves. The latter term refers to brain electrical activity silences that spread in a waveform, like when you drop a stone on water and isolation waves appear concentrically. From the fUS imaging obtained, the propagation speed could be measured and found to be consistent with that obtained previously in other studies in rabbits and rats. This demonstrated for the first time that 4D fUS imaging could be used for dynamic whole-brain functional imaging in rodents.

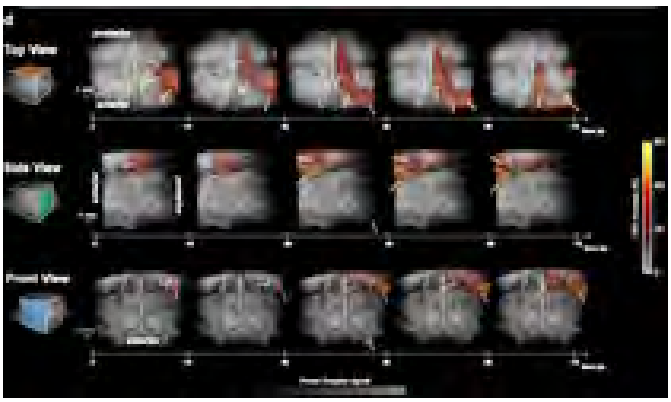

FIG. 5 Epileptiform events experiment results, from three different perspectives. The color corresponds to CBV level. [Source: Rabut et al. [2]]

Even though 4D fUS shows great promise, it still has relevant limitations. It only measures CBV, whose changes are delayed with respect to the changes in brain activity. It is also blind to other sources of brain activity information, such as calcium/voltage; and it can't detect almost horizontal capillaries. Additionally, the spatial resolution is still worse than that of 2D fUS and, for the setup used by the researchers, the subject's head must be fixed and a craniotomy needs to be performed, limiting its clinical applications, hopefully only for now.

[1] Huang, Q., & Zeng, Z. (2017). "A Review on Real-Time 3D Ultrasound Imaging Technology". BioMed research international.
[2] Rabut, C. et al. (2019) 4D functional ultrasound imaging of whole-brain activity in rodents. Nat Methods.
[3] Roman Gr. Maev (2008). "Acoustic Microscopy: Fundamentals and Applications". Wiley VCH, 1st ed.
[4] Roman Gr. Maev. (2014) "Advances in acoustic microscopy and high resolution ultrasonic imaging: from principles to new applications". Proceedings of the SPIE.
[5] https://wpo-altertechnology.com/how-it-works-scanning-acoustic-microscopy-c-sam/, last checked on 20th May, 2024.
[6] Hyunung Yu. (2020) "Scanning acoustic microscopy for material evaluation". Applied Microscopy.
[7] Karishma Desai et al. (2020) "Scanning Acoustic Microscope (SAM)- A Review". European Journal of Molecular & Clinical Medicine.
[8] K.G. Hampel et al. (2019) ¨Desafíos diagnósticos en epilepsia¨. Revista de Neurología.
[9] https://arturogoicoechea.com/2012/02/20/onda-de-depresion-cortical-propagada-2/, last checked on 20th May, 2024.
[10] https://my.clevelandclinic.org/health/diagnostics/4995-ultrasound, last checked on 20th May, 2024

Sensors Systems for Space Applications

Aniol de Ribot, Àlex Navarro, Marc Pliego, Martí Raurich, Marc Ruiz
Instrumentació. Grau en Enginyeria Física. Universitat Politècnica de Catalunya. Campus Nord, 08034 Barcelona

This study has been carried out with the aim of analyzing and getting an idea of how and for what reasons sensors are used in space applications. The machinery used to conduct explorations in outer space is subject to many threats that can put missions at risk, that is why sensors play a key role in both spacecraft maintenance and data acquisition and analysis.

Keywords: Sensors, Space Applications, Smart Sensors.

I. INTRODUCTION

The purpose of this article is to explore the subject of sensor systems for space applications.

In the realm of modern technology, sensors play a pivotal role in a multitude of applications, particularly within the field of space exploration. Sensors provide critical data supplying vital information that drives progress in a variety of fields.

Their importance in space exploration is immeasurable. Impressive accomplishments in this field have been made possible by sensors. They have made it easier to investigate the surface and atmosphere of Mars, find exoplanets in far-off star systems, and observe cosmic phenomena like neutron stars and black holes.

Spacecrafts require sensors, which fall into two categories: payload and platform components. The instruments and equipment created especially to carry out scientific studies and collect information about space are referred to as payload elements.

On the other side, platform elements are the systems that facilitate spaceship operation, guaranteeing proper functioning and safe space navigation. There are two categories of platform sensors: on-board and remote.

The purpose of remote sensors is to observe and gather data from a distance. Typically, they are used to measure atmospheric conditions, detect electromagnetic radiation, etc. On-board sensors, on the other hand, are built right into the spacecraft to provide real-time environmental analysis and condition monitoring. By continuously reporting on variables including temperature, pressure, radiation levels, and structural integrity, they are essential to preserve the spacecraft's health and functionality.

Further on the article will deal with the technical requirements for these types of sensors, knowing that several of these requirements are critical for space missions. High reliability is essential, often requiring a 99.99% reliability rate due to the high costs and rarity of repairs in space. Moreover, space sensors face significant radiation and work in vacuum, so they must be prepared for space conditions. Consequently, space sensors need special protection against environmental factors.

The discussion also touches upon the technical requirements and challenges of deploying sensors in space, the potential and limitations of smart sensors, and the various applications of these advanced technologies in space missions. By examining these aspects, one can gain insight into the integral role sensors play in the exploration and utilization of outer space.

II. TYPES OF SENSORS

Sensors are wildly used nowadays for infinite different purposes and have become a key aspect when it comes to developing technology. In the context of space applications, the elements of the spacecraft are divided into two groups: the payload and the platform. The payload consists of all the elements needed for the main purpose of the mission. The platform, on the other hand, refers to everything needed for the payload to function properly. Consequently, sensors can also be divided into these two groups, being able to distinguish between remote and on-board sensors. Basically, the on-board sensors analyze data from the immediate vicinity of the spacecraft or lander, whilst remote sensors gather information from a distance, with the use of electromagnetic techniques. These sensors can be categorized by the electromagnetic spectrum they operate in.

As said before, sensors are used to obtain data, which can be a purpose itself, for investigation, or simply used for the spacecraft to run. In this section, multiple types of sensors used for space applications will be discussed.

To begin with, the most used sensors of all, temperature sensors. Some common temperature sensors are thermocouples, Resistance Temperature Detectors (RTDs), Thermistors, Fiber Optic Sensors, and Pyrometers, which use different technologies and materials to measure temperature. However, they can be separated into ground

temperature sensors (GTS), those being designed to measure the temperature of the ground, and air temperature sensors (ATS), which measure the temperature of the surrounding air. Regarding their functioning, it may well vary on the unit carrying it. For instance, on the Mars Rover Environmental Monitoring Station (REMS) the GTS integrates the IR energy emitted by the ground. Aiming to avoid local temperature effects, the area studied is large enough so that after computing the mean temperature over it, the value obtained is close to the real one. ATS, on the other hand, use RTD thermistors type Pt1000 Class A.

Wind sensors are often needed as well. The data they provide helps with spacecraft navigation (since wind can affect its trajectory), space weather monitoring, and scientific research, amongst others. A few methods these use to measure wind are doppler velocimetry, ion wind sensors, star trackers, and thermal anemometry. This last one is the one used in the REMS mentioned before, which uses a set of 4 dice to measure.

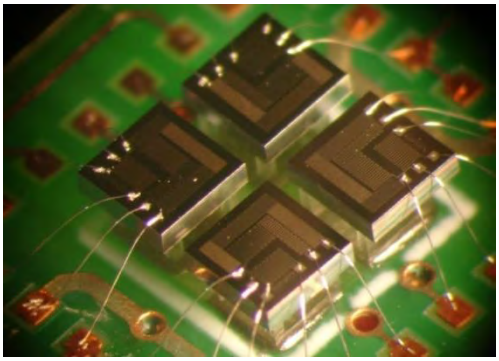

Figure 1:Detailed picture of the dice in the first prototype of the wind sensor of REMS

Relative Humidity sensors are used mainly to ensure the crew health and comfort (as the unit contains people inside), for equipment performance, and lastly for environmental monitoring. Commonly used methods to assess the relative humidity are capacitive sensors, resistive sensors, thermal conductivity sensors, and optical sensors.

Another essential are the Ultraviolet (UV) sensors. Some of their applications are studying solar radiation, space weather monitoring, and protecting the spacecraft and astronauts from harmful UV light. The most used techniques to detect and measure UV light are photodiodes, phototransistors, photoconductors, and photomultiplier tubes.

Coming in last position, pressure sensors must be considered as well. These have multiple purposes, such as monitoring spacecraft propulsion (e.g. regulating the tank's pressure), maintaining a habitable environment for astronauts, and space weather monitoring. Some methods used to measure pressure for space applications are piezoresistive sensors, capacitive sensors, resonant sensors, and optical sensors.

As previously stated, the sensors described are just a fraction of the totality used in a spacecraft. In fact, a spacecraft can have hundreds of sensors, 50% of which are temperature sensors and 30% monitor the voltage and status of components. Other sensors used for space applications are visual cameras, infrared cameras, microwave radiometers, telescopes, radars, sounders, sun sensors, Earth horizon sensors, magnetometers, star sensors, gyroscopes, accelerometers, flow meters, proximity sensors, smoke detectors, etc.

All these different types of sensors, as seen, can gather information through different physics principles and techniques. There are a few important things to take into consideration when choosing a sensor: from its requirements, which can be defined as the ambient conditions compatible with it, to its placement (that is, where are they located on the unit).

III. TECHNICAL REQUIREMENTS

Although every year more steps forward are made, outer space remains one of the most unknown concepts for humans. Space missions to explore what is out there have their basis in collecting lots of information with sensors located in the spacecrafts. As seen before, a spacecraft can be divided into the payload (where the main task of the mission is performed), and the platform, which provides everything the payload needs. In consequence, there are "payload sensors" and "platform sensors".

As lots of functions are dispensed by the satellite platform (such as thermal control, power supply, etc.), a big amount of sensors are needed in the spacecraft: half of them are temperature sensors, another big part control the voltage and how some components are working, and then there are, in a minor part, star sensors, Earth horizon sensors, Sun sensors, or even position and pressure sensors (to control the spacecraft's conditions), among others. It is common that some sensors do not work only on one function, but on lots of functions.

Talking now about requirements there are many things to highlight. To put a satellite or a spacecraft into an orbit is very expensive: around 1000$ into Low Earth Orbit (1kg), and 50000$ approximately into the Geostationary Orbit (also for 1kg); which means that it is very important to reduce mass as much as possible. Reliability is also fundamental, because it is not too frequent to repair something in space basically due to the very high costs. For this reason, it is very usual to have a reliability requirement of 99.99%.

In addition, satellites work generally in vacuum, and they are under big effects of radiation, which intensifies even more in the Allen Belts (regions around the Earth with very high energy). Radiation can also make the consequences even worse if a particle impacts the satellite/spacecraft and reduces the lifetime of the electronics. To deal with it, there are different approaches: the usage of shielding, the usage of radiation resistant technology and radiation tolerant system

architectures or carrying out extensive testing and selection from mass market electronic equipment.

Finally, it is also important to comment that as space sensors need special environmental protection, their use in terms of terrestrial applications is limited. To solve this, researchers have tried to make its hardware compatible with the space environment by performing additional verification testing or by making some modifications (adding "more things" to the design of it). This has led to some successful results, but nevertheless still causes a certain barrier to the new technological advances.

IV. SMART SENSORS: POTENTIAL AND LIMITATIONS

Before discussing the application of smart sensors in space, it is useful to define what constitutes a smart sensor. A smart sensor cannot be uniquely defined but can be considered an evolution of existing sensors. In the space field, a smart sensor is one that offers better performance or functionality than an ordinary sensor, or the same performance and functionality at a lower cost. Consequently, incorporating smart sensors on satellites presents two key opportunities. First, they enable the same signal sensing as current sensors but with improved performance and/or reduced mass, power, volume, and costs. Second, they facilitate new types of measurements, expanding the system's capabilities. Miniaturization is crucial for spaceborne smart sensors, allowing for more functions to be integrated into a unit without increasing mass and power requirements or achieving the same measurements with a smaller system impact.

To achieve cost reductions, it's important to recognize that overall costs are driven not by the sensor's direct procurement costs, but by the impact of the sensor on the system. Therefore, minimizing the sensor's mass and power requirements is essential. Additionally, the integration and testing costs of the entire satellite are significantly influenced by the number of sensors, representing a substantial portion of the total costs.

Besides lower mass and power requirements, some additional characteristics are highlighted: real-time and adaptive capabilities, which enhance system capabilities, and reduced data rate and post-sensing computation, which can either lessen accommodation requirements or boost system capabilities.

The effective use of smart sensor technology on satellites depends on various system trades, which are only partially influenced by the technology itself. These trades mainly involve the degree of spacecraft autonomy and the satellite's data handling system architecture. Understanding these trades is crucial, as the goal should be to optimize the entire satellite system, not just a sensor or sensor subsystem. A key example is the allocation of processing tasks, linked to both satellite autonomy and data handling architecture. Sensor information processing can occur in the sensor processor, the central processor of the data handling system, or on the ground after raw data transmission. A sensor with integrated processing capability is beneficial only if space processing of sensor information is needed.

However, satellite autonomy is influenced by factors such as mission objectives, real-time operation needs, satellite costs, complexity, and communication link availability. Simple satellites tend to be more autonomous due to the prohibitive costs of ground operations, while very complex systems require real-time operations.

V. APPLICATIONS

Smart sensors offer a brand-new technology to benefit from, however, they are not very present in spatial systems nowadays because they are still equipped with conventional sensors. The European Space Agency (ESA) has been making considerable efforts to introduce smart sensors in future projects and systems. To highlight the new possibilities that smart sensors can implement on spatial science and technology and to give a little insight on how they work, two real examples are provided below: visual monitoring cameras and solid-state micro-gyroscopes.

Smart sensors in monitoring applications

The purpose of external spacecraft monitoring is to analyze the state of the spacecraft during mechanical processes such as the deployment of antennas or solar panels. As space stations and spacecrafts grow larger, the installation of conventional sensors becomes impractical due to dimensional and power requirements. By using smart sensor technology, the implementation of visual monitoring can have a minimal impact on the spacecraft design. Ongoing developments are trying to produce single-chip smart cameras which may be also suitable for planetary rovers, where size and power consumption needs to be minimized. Cameras for space applications are based on the CMOS (Complementary Metal-Oxide-Semiconductor) Active Pixel Sensor (APS) technology. Each pixel sensor unit cell has a photodetector (typically a pinned photodiode) which generates a charge when it is struck by light. Then, amplifiers convert this photo-generated charge to a voltage and CMOS transistors amplify the signal to make the digital conversion easier. However, the overall system and camera dimensions are often large and have a negative impact on the design of the spacecraft. This is where smart sensors become important. Several projects have tried to solve the problem being the creation of the IRIS (Integrated Radiation-tolerant Imaging System) models one of the most promising. The utilization of these chips will allow taking images and directly communicate with the spacecraft while maintaining the optimal dimensions and power requirements. The first applications may consist in including IRIS sensors in visual

monitoring cameras to provide visual feedback of mechanical processes in spacecrafts.

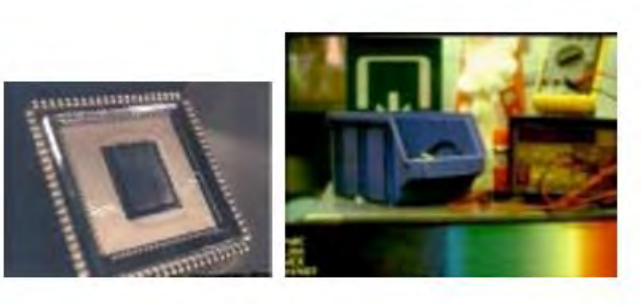

Figure 2: IRIS-1 sensor and Image captured with IRIS-1 sensor.

Solid State Micro-Gyroscopes

Solid state micro-gyroscopes are currently used in the automotive market but their applications in space are being studied. They may not be better than traditional mechanical gyroscopes, but they will provide a more accurate fault-tolerance and reliability technology. The difference between both models is that mechanical gyroscopes measure rotation using a spinning wheel or disc while solid-state ones use microelectronic components and sensors to do so.
Attitude angular rate, which tells how quickly an object turns, is a fundamental parameter for a satellite. However, mechanical gyroscopes do not currently allow systematic, continuous measurements of this parameter, which can prevent the detection of attitude anomalies (caused by system failures). Therefore, the utilization of these smart sensors would be useful to identify and correct earlier this type of errors.

VI. CONCLUSIONS

In conclusion, sensors are crucial in modern technology, and especially in space exploration. Throughout this article, different categories of sensors have been analyzed each type of them has been discussed.

Further on, the technical requirements for space sensors have also been pointed out, focusing on the extreme precision that these sensors must have and the special treatment they need because of where they work; essentially outer space.

Finally, the importance of smart sensors and their applications has been remarked. To achieve more effective, dependable, and extensive space exploration and usage, improved sensor technologies must ultimately be implemented in space missions. Smart sensors have the potential to significantly impact the future of space technology, as demonstrated by the continuous research and initiatives, especially from organizations such as the European Space Agency.

To sum up, space sensors are essential to the smooth functioning of spacecraft since they allow accurate data gathering for tasks that are crucial to the mission and system upkeep. Improved performance, lower costs, and greater measurement capabilities are possible with smart sensor technology, opening the door to more creative and effective space exploration and study.

VII. REFERENCES

[1] REMS: The Environmental Sensor Suite for the Mars Science Laboratory Rover. http://cab.inta-csic.es/rems//wp-content/uploads/2013/04/REMS.-Space-Science-Reviews-2012.pdf

[2] Mars mission timeline - NASA Science. (s. f.). https://science.nasa.gov/planetary-science/programs/mars-exploration/mission-timeline/

[3] Cordis, C. (2012, 23 octubre). New sensor technology to enable future space exploration missions and on-orbit satellite servicing. CORDIS | European Commission. https://cordis.europa.eu/article/id/89633-new-sensor-technology-to-enable-future-space-exploration-missions-and-onorbit-satellite-servic

[4] Space applications for smart sensors. https://amstel.estec.esa.int/tecedm/website/docs_generic/SmartSensor.pdf

[5] REMS - Centro de Astrobiología. cab.inta-csic.es/rems/es

[6] REMS Instrument Overview – MSL – Mars Science Laboratory. (s. f.). https://spaceflight101.com/msl/rems-instrument-overview/

Sensor Technologies for Caring People with Parkinson's disease

Anna Gravenhorst, Lua Cardell, Maria Alcover, Marta Llabrés
Instrumentació. Grau en Enginyeria Física. Universitat Politècnica de Catalunya.
Campus Nord, 08034 Barcelona

Parkinson's disease is a neurodegenerative disorder that causes unintended or uncontrollable movements. With its growing presence in society, sensors have been introduced to help monitor and diagnose the disorder. In this article, we look at a variety of sensors that stand out because of their innovative, accessible, and non-invasive nature when monitoring motor and non-motor symptoms of Parkinson's disease.

Keywords: Parkinson's disease, sensor, disabilities, symptom, tremor

I. INTRODUCTION

With an increasingly aging population, neuro-degenerative diseases become more present in society. Among them, Parkinson's Disease (PD) is the one with the fastest growing ratio, expected to affect around 12-17 million people by 2040 [1]. It is a condition caused by a lack of dopamine, primarily manifesting with motor symptoms -such as tremor, rigidity postural instability or bradykinesia- but with many other life altering complications that can vary from depression and dementia to sensory dysfunctions. These symptoms can appear to different extents in each patient and tend to fluctuate their intensity over time, which -added to the fact that there's a low availability of expert neurologists and caregivers- make PD a difficult condition to diagnose and monitor.

There are no existing objective tests or biomarkers to diagnose PD, but as of now, the Unified Parkinson's Disease Rating Scale (UPDRS) is the most used scale to assess PD symptoms (both motor and non-motor) and study its progression. It involves the patient performing different tasks, and the neurologist assigning ratings according to the UPDRS requirements. Although it was revised and upgraded in 2007 by the Movement Disorder Society, it is still flawed. The results are semi-subjective, (with a rate of misdiagnosis of around 25% [2]), and clinical trials must extend over several years to reliably observe changes in MDS-UPDRS results, increasing expenses and lowering advances. Therefore, improving the monitoring of a patient's everyday symptoms, especially between medical appointments, is crucial in PD management and diagnosis. In recent years, sensors have been introduced to achieve this goal, and to improve overall assessment of PD patients. In this article, several sensors both for diagnosing and monitoring PD will be revised and commented on.

II. MOTOR SYMPTOMS

Motor symptoms in PD significantly impact in daily activities and quality of life. These symptoms include tremor, bradykinesia (slowness of movement), rigidity and postural instability, among others. To facilitate the diagnosis and personalization of treatment, it is advantageous to track changes in patients' symptoms, which is challenging because it cannot be done in a single clinical visit and requires an extensive evaluation of the patient's condition. To conduct this examination, wearable sensors, worn by the patients for a period of time, can be a great tool.

There exists a conformable sensor to monitor motor symptoms in PD called the NIMBLE wearable sensor patch. This is a flexible and conformable device containing an accelerometer and electrography sensor. The accelerometer in the NIMBLE device measures and records patterns in movement by detecting changes in acceleration, allowing it to track the body's motion and orientation. On the other hand, the electromyography (EMG) sensor detects muscle activity by recording the electrical signals produced by muscle contractions. By combining the data from the accelerometer and EMG sensor, the NIMBLE device captures comprehensive information on both body movements and muscle activity. The patch is attached to the skin using an adhesive sticker and wirelessly transmits the data to a smartphone and cloud service for analysis. It allows for continuous and objective measurement of motor symptoms, including tremor and postural instability, both during wakefulness and sleep. The technology shows promise in providing accurate and real-time tracking of motor symptoms, potentially leading to improved patient engagement, communication with healthcare providers, and

overall quality of life for individuals with PD. [3]

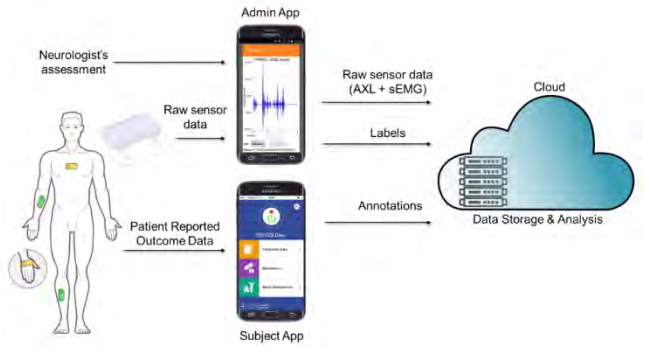

Figure 1. (Color online) Data transfer pathways from NIMBLE devices located at multiple body positions to smartphones and to a cloud server. [3]

Tremor -usually the first noticeable symptom of PD- has been proven in several studies to be one of the most troubling symptoms of PD, both in early and advanced stages of the disease [4]. To monitor its evolution and fluctuations continuously and in an objective manner the use of two wireless accelerometer nodes was proven useful [5]. The first one was set statically as a control and the second one placed on the dorsum of the hand by a glove designed to simulate PD hand tremor. Each node (G-Link® Wireless Accelerometer Node) weighs 46 grams and can sample data at multiple rates -in this case it is set to 512 Hz-. The node can send the resulting data of each trial wireless to a local PC which allows to calculate the magnitude of the acceleration and subsequently the acceleration waveform of the tremor. The results confirmed the capability of the sensor for quantifying simulated hand tremors with a 98% of accuracy, therefore proving it to be a useful tool for monitoring this symptom.

Gait disturbance represents another of the characteristic symptoms of PD. The most common alterations in gait are a reduction in velocity, the length and duration of the step, as well as an increase in the duration of the stance and double support phases [6]. The study of these alterations serves a dual purpose: it enables medical personnel to monitor the stage of the disease and its progression, and it facilitates the diagnosis of the disease itself [7].
A useful tool to find any walk anomalies is GAITRite®: an electronic walkway which uses pressure sensors to measure temporal and spatial gait parameters. The device is equipped with a horizontal grid of pressure sensors, each of which is separated by 12.7 mm from the others. These sensors are responsible for detecting the patient's gait when being walked over. The collected data is then transferred to a computer, where it is converted through software algorithms to gait parameters.
In the study of the parameters, it is important to consider that in the early stages of PD, gait analysis should focus on challenging motor control with imposed rhythms and velocities, as well as dual task paradigms. This is because slow and small-stepped walking patterns may be influenced by other factors or conditions other than PD. As the disease progresses, the gait alterations become more complex, which facilitates the diagnosis of PD through gait studies [8].

Another walking related difficulty of PD is the Freezing of Gait (FoG), characterized by the momentarily incapacitance or difficulty to move the feet forward despite the will to do so. It manifests during the latter stages of PD and happens on a regular basis to 47% of patients [9]. Although the cause of FoG has not yet been determined, its assessment and monitoring are essential since it may lead to falls and injuries, as it frequently happens when turning or obstacles are in the patients' path. To perform long-term monitoring of this difficulty and complement physicians' gait assessments, researchers have proposed the use of sensors in the lower extremities to collect data.
Zabaleta et al. [10] conducted research to determine whether FoG could be predicted using movement data collected from sensors placed on the lower extremities (precisely at the thighs, calves and ankles). The sensor used was Sparkfun Inertial Miniature Unit, into which a triple axis accelerometer (ADXL330) and a dual axis gyroscope (IDG300) are integrated. After asking the subjects to perform day to day movement tasks (walking forwards and backwards, avoiding obstacles) it was noted that an increase of the main frequency appeared before episodes of FoG, which corresponded to a brief fluttering of the patients' legs. It was also concluded that for best detecting this signal the sensor should be placed at the lower limbs or heels.
A similar study was carried by Ghassemi et al. [11], where patients were asked to turn 180-degree after straight walking 10 m at their own pace and speed. Sensors were positioned at the ankle level and measured acceleration and angular velocity at a frequency of 102.4 Hz. Each unit consisted of a tri-axial accelerometer (range Shimmer 2R: ±6 g, Shimmer 3: ±8 g) and a tri-axial gyroscope (range Shimmer 2R: ±500/s, Shimmer 3: ± 1000/s).

DynaPort7 is another useful sensor for the diagnosis of PD. To use the device, the patient must wear it with an elastic strap at the lower back, like a belt. The sensor is a lightweight box with dimensions of 106.6 x 58 x 11.5mm and incorporates an integrated tri-axial accelerometer and tri-axial gyroscope; the battery has a lifespan of 5 days, and the memory can store data for up to 8 weeks. DynaPort7 can recognize several different activities, including lying, standing, sitting, climbing stairs, cycling, and shuffling, and samples data of each one of them. This is obtained through the analysis of trunk orientation and the pattern between activities. Additionally, the device is capable of measuring energy expenditure and movements during nocturnal periods. Data stored in the DynaPort7 can be transferred to a computer via any available connection: Wi-Fi, Bluetooth

or USB. A high number of sensor types are available for this purpose; however, the number of sensors needed, and the battery life vary between them, affecting the comfort levels for the patient.

It is also important to remark that motor complications can arise from PD's existing treatments. The most common one is levodopa, a drug that replenishes the dopamine levels of the patient, which has been proven to cause dyskinesia in the later stages of the disease, primarily peak-dose dyskinesia [12], associated with the moments following the oral intake of the drug. To mitigate these motor fluctuations, it was thought that a continuous administration of levodopa would be best, since the drug's concentration in blood would be more uniform. The method consisted of infusing a solution of the drug through a subcutaneous pump. A recent study [13] comparing both oral and subcutaneous treatments was conducted in different specialized PD centers around Europe and the USA concluded that this innovative method prolonged the treating effects of levodopa without causing related dyskinesia.

III. NON-MOTOR SYMTPOMS

Non-motor symptoms (NMS) in PD, which include sleep disorders, depression, constipation, and olfactory dysfunction among others, tend to be neglected. However, they can have a greater impact on PD patients than motor symptoms, especially at its later stages [14], so monitoring them could be crucial to lower their impact.

For example, sleep disorders like Rapid eye movement (REM), insomnia or restless leg syndrome affect up to 90% of PD patients [15]. Actigraphy is a non-invasive method of monitoring that consists of an actigraph (a watch-like device) that is usually worn on the non-dominant wrist. The actigraph consists of an accelerometer that generates a continuous electrical signal in response to motion, which is sampled with a specific frequency (usually of 10 Hz or 10 samples per second) and then processed in three different ways in order to obtain different information: Time Above Threshold (TAT) (duration), Proportional Integration Mode (PIM) (intensity), and Zero Crossing Mode (ZCM) (frequency) [16]. The latter one involves counting how many times per minute the transducer signal (i.e., voltage) crosses a preset threshold, typically set close to zero, and is the most widely used for sleep recognition. The extracted information is then digitized as data points at 1-min recording intervals, which accounts for around 1440 data points every 24 hours [17]. This data can also be downloaded to a personal computer, and through a specific algorithm it can offer information like time in bed, sleep efficiency or the total nocturnal moving time. Several studies show that actigraphy data and more subjective data like that of a sleep diary seem to be in accordance with PD patients [18], so a combination of the two would be best for monitoring nocturnal problems.

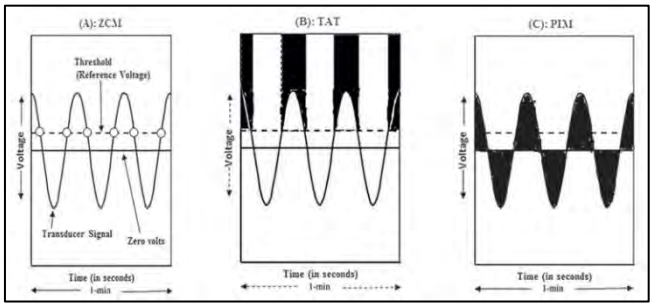

Figure 2. Diagrammatic representation of the three modes in which wrist movement data is digitized and stored by the Motionlogger Sleep Watch actigraph [17].

Moreover, other studies have tried to apply innovative wearable sensors that, unlike actigraphy, allow specific motor behaviors to be identified and monitored during sleep. Most relevant studies show that body rotations are reduced in frequency, velocity, and acceleration [19]. These results are consistent with the prevalence of nocturnal akinesia in PD patients, which involves lack of movement and difficulty to initiate it during nighttime. It is important to note the lack of research based on sensors around primary sleep disorders that affect PD patients, such as restless leg syndrome or periodic limb movement disorder.

Most sensor-based studies on NMS of PD are on sleep disorders. Some papers can be found regarding the use of wearable sensors for gastrointestinal problems as a symptom of PD, even though around 50% of patients experience constipation and 70% experience gastroparesis [20]). In 2019, van Wamelen et al. [21] used the Parkinson's KinetiGraph (PKG™) to correlate bradykinesia and constipation in PD patients. This device is worn on the wrist, weighs 35 grams and includes a rechargeable battery along with a 3-axis accelerometer configured to capture acceleration measurements digitally at 11 bits. The accelerometer operates within a range of ±4 g and samples data at a rate of 50 samples per second. These measurements are processed using a digital microcontroller, and the data is stored in flash memory [22].

PD is also known to affect breathing. The relation between PD and breathing was already noted by James Parkinson in 1817. The respiratory symptoms often manifest years before clinical motor symptoms, which indicates that they could be the key for an earlier diagnosis. In 2022, a team from MIT developed an artificial intelligence model that can detect PD just from analysing a person's nocturnal breathing patterns. This tool is a neural network, able to discern the severity of someone's PD and track the progression of their disease over time.

The MIT-developed device, with the appearance of a Wi-Fi router, can capture breathing signals using radio signals, therefore it can work in a completely contactless manner. The breathing signals are extracted from radio frequency (RF) signals that bounce off people's bodies. The RF data is collected using a multi-antenna frequency-modulated continuous waves (FMCW) radio, which is commonly used in passive health monitoring. The radio reflections are analysed to determine the subject's breathing pattern. Respiration signals extracted with this process are highly accurate, even when there is more than one person in the same bed. The nocturnal breathing signals can also be extracted from a breathing belt, although their datasets have only one or two nights per person and lack MDS-UPDRS scores. In contrast, the wireless datasets include longitudinal data for up to 1 year and MDS-UPDRS scores, allowing us to validate the model's predictions of PD severity and its progression. Lastly, the breathing patterns are sent to the neural network to assess PD in a passive manner. The AI model utilizes machine learning algorithms, including deep learning models, to examine the extracted breathing signals and recognize patterns that suggest the presence of PD. These algorithms are trained on a large dataset comprising individuals with and without PD to learn the distinguishing features of PD-related breathing patterns. These features may include variations in breathing rate, depth, or regularity, which can serve as biomarkers for detecting and tracking PD. Once trained, the AI model can predict the presence of PD, estimate disease severity, and track progression based on the analysed breathing signals. With this method there is zero effort needed from the patient and caregiver. [23]

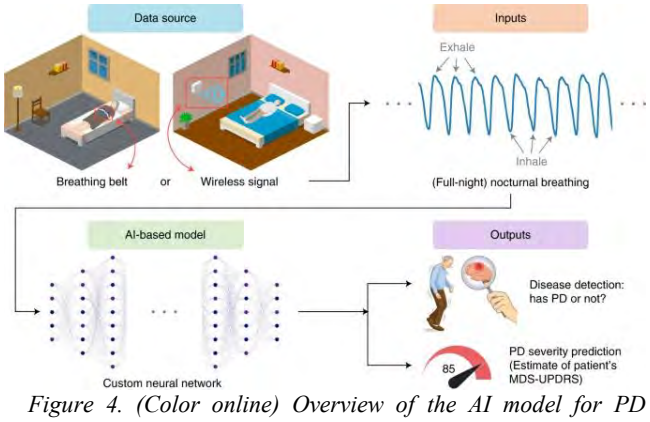

Figure 4. (Color online) Overview of the AI model for PD diagnosis and disease severity prediction from nocturnal breathing signals.[23]

IV. CONCLUSION

It's no secret that sensors have an endless number of applications in the scientific world, especially experimentally wise. However, their use can go beyond experimental sciences, since they also have many everyday uses that can make everyone's life easier. In this article, it has been shown that wearable sensors can be the key to overcome the difficulties that arise when monitoring and caring for PD patients. The Unified Parkinson's Disease Rating Scale has been criticized for being semi-biased and because of its sporadicity since a long time can pass between medical appointments. Wearable sensors decrease these issues; they can monitor the patient's symptoms on a day-to-day basis and offer objective data that can be obtained in a non-invasive manner.

Several sensors for monitoring motor and non-motor symptoms have been exposed, but there is still work to be done. Further research could consider the integration of these technologies on existing healthcare systems, and usability and accessibility of such sensors for elderly patients.

[1] E. Dorsey, T. Sherer, M. Okun and B. Bloem, "The Emerging Evidence of the Parkinson Pandemic," *Journal of Parkinson's Disease,* vol. 8, pp. 3-8, 2018.

[2] S. V. Perunal and R. Sankar, "Gait and tremor assessment for patients with Parkinson's disease usingwearable sensors," *ICT Express,* pp. 168-174, 2016.

[3] B. Boroojerdi, R. Ghaffari, N. Mahadevan, M. Markowitz, K. Melton, B. Morey, C. Otoul, S. Patel, J. Phillips, E. Sen-Gupta, O. Stumpp, D. Tatla and D. Terricabras, "Clinical feasibility of a wearable, conformable sensor patch to monitor motor symptoms in Parkinson's disease," *Parkinsonism & Related Disorders,* vol. 61, pp. 70-76, 2019.

[4] L. E. Heusinkveld, M. L. Hacker, M. Turchan, T. L. Davis and D. Charles, "Impact of Tremor on Patients With Early Stage Parkinson's Disease," *Frontiers in Neurology,* 2018.

[5] R. LeMoyne, T. Mastroianni and W. Grundfest, "Wireless accelerometer configuration for monitoring Parkinson's disease hand tremor," *Scientific Research Publishing,* 2013.

[6] A. Salarian, H. Russmann, F. Vingerhoets and Y. B. P. B. K. A. C. Dehollain, "Gait assessment in Parkinson's disease: toward an ambulatory system for long-term monitoring," *IEEE Transactions on Biomedical Engineering,* pp. 1434-1443, 2004.

[7] A. Muro-de-la-Herran, B. Garcia-Zapirain and A. Mendez-Zorrilla, "Gait Analysis Methods: An Overview of Wearable and Non-Wearable Systems, Highlighting Clinical Applications," *Sensors (Basel),* 2014.

[8] G. Ebersbach, C. Moreau, F. Gandor, L. Defebvre and D. Devos, "Clinical syndromes: Parkinsonian gait," *Movement Disorders ,* pp. 1552-1559, 2013.

[9] M. Macht, Y. Kaussner, J. Möller, K. Stiasny-Kolster, K. Eggert, H. Krüger and H. Ellgring, "Predictors of freezing in parkinson's disease: A survey of 6620 patients.," *Movement Disorders,* 2007.

[10] H. Zabaleta, T. Keller and E.Fimbel, "Gait analysis in frequency domain for freezing detection in patients with Parkinson's disease," *Gerontechnology,* 2008.

[11] N. H. Ghassemi, J. Hannink, N. Roth, H. Gaßner, F. Marxreiter, J. Klucken and B. Eskofier, "Turning Analysis during Standardized Test Using On-Shoe Wearable Sensors in Parkinson's Disease," *Sensors*

(Besel), 2019.

[12] D. Kwon, M. Kwatra, J. Wang and H. S. Ko, "Levodopa-Induced Dyskinesia in Parkinson's Disease: Pathogenesis and Emerging Treatment Strategies," *Cells,* 2022.

[13] A. J. Espay and e. al, "Safety and efficacy of continuous subcutaneous levodopa–carbidopa infusion (ND0612) for Parkinson's disease with motor fluctuations (BouNDless): a phase 3, randomised, double-blind, double-dummy, multicentre trial," *The Lancet. Neurology,* vol. 23, no. 5, pp. 465-476, 2024.

[14] H. M. Lee and S.-B. Koh, "Many Faces of Parkinson's Disease: Non-Motor Symptoms of Parkinson's Disease," *Journal of Movement Disorders,* vol. 8, no. 2, pp. 92-97, 2015.

[15] L. H. M. Keir and D. P. Breen, "New awakenings: current understanding of sleep dysfunction and its treatment in Parkinson's disease," *Journal of Neurology,* vol. 267, no. 1, pp. 288-294, 2019a.

[16] A. Zampogna, A. Manoni, F. Asci, C. Liguori, F. Irrera and A. Suppa, "Shedding Light on Nocturnal Movements in Parkinson's Disease: Evidence from Wearable Technologies," *Sensors,* vol. 20, 2020.

[17] D. Fekedulegn, M. E. Andrew, M. Shi, J. M. Violanti, S. Knox and K. E. Innes, "Actigraphy-Based Assessment of Sleep Parameters," *nnals of Work Exposures and Health,* vol. 20, no. 18, pp. 350-367, 2020.

[18] K. Stavitsky, J. L. Saurman, P. McNamara and A. Cronin-Golomb, "Sleep in Parkinson's disease: A comparison of actigraphy and subjective measures. Parkinsonism & Related Disorders," *Parkinsonism & Related Disorders,* vol. 16, no. 4, pp. 280-283, 2010.

[19] M. Yoneyama, Y. Kurihara, K. Watanabe and H. Mitoma, "Accelerometry-based gait analysis and its application to parkinson's disease assessment— part 2 : A new measure for quantifying walking behavior.," *IEEE Transactions on Neural Systems and Rehabilitation Engineering,* vol. 21, no. 6, pp. 999-1005, 2013.

[20] M. N. Han, D. I. Finkelstein, R. M. McQuade and S. Diwakarla, "Gastrointestinal dysfunction in parkinson's disease: Current and potential therapeutics," *Journal of Personalized Medicine,* vol. 12, no. 2, p. 144, 2022a.

[21] D. van Wamelen, V. Leta, A. Podlewska, D. Trivedi, Y. M. Wan, V. Metta, P. Odin, H. Reichmann and K. R. Chaudhuri, "Wearable sensor (parkinson's kinetigraph) and dopamine transporter imaging as potential biosignature for constipation in parkinson's," *Neurology,* vol. 92, no. 15, 2019.

[22] H. Khodakarami, L. Ricciardi, M. F. Contarino, R. Pahwa, K. E. Lyons, V. J. Geraedts, F. Morgante, A. Leake, D. Paviour, A. De Angelis and M. Horne, "Prediction of the Levodopa Challenge Test in Parkinson's Disease Using Data from a Wrist-Worn Sensor," *Sensors,* vol. 19, no. 23, 2019.

[23] Y. Yang, Y. Yuan, G. Zhang, H. Wang, Y.-C. Chen, Y. Liu, C. G. Tarolli, D. Crepeau, J. Bukartyk, M. R. Junna, A. Videnovic, T. D. Ellis, M. C. Lipford, R. Dorsey and D. Katabi, "Artificial intelligence-enabled detection and assessment of Parkinson's disease using nocturnal breathing signals," *Nature Medicine,* vol. 28, p. 2207–2215, 2022.

Ús i calibratge d'activímetres en medicina nuclear

Pau Feliu, Isaac Ibós, Marcelo Jiménez, Joan Llorente*, Hugo López, Oriol Sales
Instrumentació. Grau en Enginyeria Física. Universitat Politècnica de Catalunya.
Campus Nord, 08034 Barcelona
**e-mail: joan.llorente@estudiantat.upc.edu*

La medicina nuclear sorgeix de la necessitat d'observar l'activitat dels òrgans i el funcionament del cos humà amb mètodes no invasius. L'ús d'imatges detallades de l'interior del cos humà permet un diagnòstic eficient de malalties i el seguiment dels tractaments del pacient, i en molts casos requereix de l'ús de substàncies radioactives. Per a mesurar-les es fa servir un activímetre, ha de ser calibrat, i la qualitat de les seves mesures revisada periòdicament. Aquest treball es centra en com funciona l'activímetre i en com es duen a terme els diferents controls de precisió i exactitud de les mesures realitzades.

I. INTRODUCCIÓ

En medicina (especialment en diagnòstic per imatge) s'usen radiofàrmacs, unes substàncies que contenen isòtops radioactius que emeten raigs X (o gamma, en funció de les necessitats de la prova). Altes dosis d'aquests isòtops poden ser perjudicials pel pacient, és per això que s'empra el criteri ALARA (*As Low As Reasonably Achievable*: irradiar el mínim possible), però sense perdre la qualitat de la imatge. Per complir amb aquesta mesura de seguretat, cal determinar correctament les dosis de radiofàrmacs amb l'ajut d'una màquina: l'activímetre, que té la funció principal de detectar l'activitat radioactiva d'una mostra.

En aquest cas, per a "activitat" entendrem tant les partícules (partícules alfa i beta) com ones electromagnètiques (raigs X i gamma) emeses per un material. L'activitat es mesura en Becquerels (Bq), que correspon a 1 emissió / s (per tant, 1 Bq = 1 s^{-1} o Curies ($1\,Ci := 3{,}7 \cdot 10^{10} Bq$).

Altes dosis d'aquests isòtops poden ser perjudicials pel pacient i provocar tumors, és per això que s'empra el criteri ALARA (*As Low As Reasonably Achievable)* per irradiar el mínim possible i seguir tenint una bona qualitat d'imatge. Per complir amb aquesta mesura de seguretat, cal determinar correctament les dosis de radiofàrmacs amb l'ajut d'una màquina: l'activímetre, que té la funció principal de detectar l'activitat radioactiva d'una mostra.

Aquestes partícules i ones, en molts casos poden ionitzar la matèria, és a dir, extreure un electró d'un àtom i deixar-lo com un catió carregat positivament. L'activímetre aprofita aquest efecte per a detectar la radiació: conté dues malles metàl·liques coaxials, entre les quals es troba un gas (en el nostre cas, argó a 12 atm). Entre les dues malles s'estableix una diferència de potencials (15kV) (RadiaProt - Healthcare Radiation). Se situa la mostra dins del cilindre intern, de tal manera que la major part de la radiació emesa acaba entrant dins la cambra. Quan la radiació ionitza un àtom del gas, l'electró es veu immediatament atret per la malla positiva (i l'ió, per la negativa), de tal manera que es tanca el circuit i s'estableix un corrent entre els dos pols, que, en ser amplificat i enregistrat per l'electrònica de l'activímetre, ens donaria una indicació del nivell d'activitat de la mostra. Aquest muntatge s'anomena *cambra de ionització*.

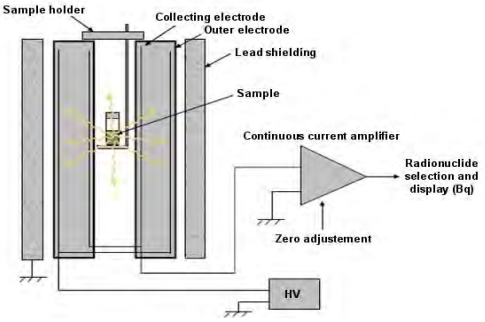

Figura 1: (Laboratoire National Henri Becquerel) *Esquema d'una cambra de ionització.*

Idealment, la intensitat rebuda hauria de ser proporcional amb l'activitat, de tal manera que tindríem una única constant "k" tal que I = k·A, i podríem trobar l'activitat amb facilitat. No obstant, ens trobem amb diversos problemes:

- No totes les emissions ionitzen de la mateixa manera; depèn del tipus (fotons, electrons, partícules alfa) i de la seva energia.
- No tots els isòtops emeten el mateix tipus de radiació: depèn de com són els seus nuclis (per exemple, tenim nuclis com el ^{18}F que emet per β+; o el ^{99m}Tc per captura electrònica), per tant, dos isòtops amb la mateixa activitat podrien generar ionitzacions molt diferents.
- El parell iònic generat també pot interaccionar amb altres partícules, generant alhora més interaccions i en conseqüència, més intensitat.
- La diferència de potencial també pot afectar a la intensitat: si és petita, molts electrons mai arribaran als elèctrodes i no seran enregistrats; si és massa gran,

aquests electrons tindran una energia cinètica molt elevada i interaccionaran amb altres àtoms del gas.
- Les parets internes de l'activímetre aturen part de la radiació, especialment les partícules alfa, i quasi tot el que es rep al gas seran fotons (siguin emesos directament per l'isòtop, o per aniquilació d'un positró emès per l'isòtop).
- Tot això destrueix la linealitat del sensor; i, fa que la corba característica serà diferent per a qualsevol isòtop. A la figura (2) es pot veure un exemple de corba sensibilitat-energia; és a dir, quina resposta en intensitat causa un fotó en funció de la seva energia:

No només no és constant (que és el que desitjaríem per a un model lineal: sensibilitat constant), sinó que a més presenta màxims i mínims. Per tant, no tenim més remei que escollir un rang petit de valors (en funció de l'ús que se li donarà) i calibrar l'activímetre per a cada isòtop concret. Un cop calibrat, s'han de realitzar diferents mesures periòdicament per a comprovar que l'activímetre no es desvia.

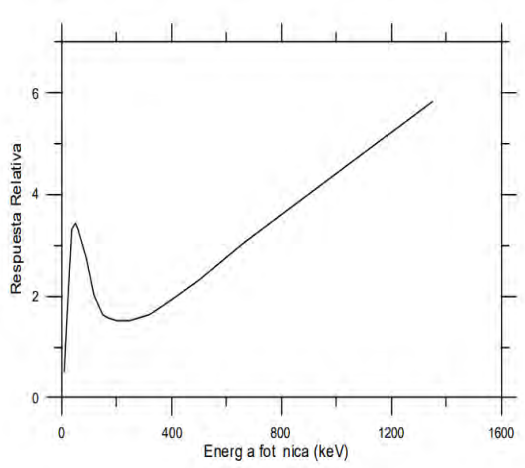

Figura (2): (Domínguez Montero, y otros) Aspecte típic de la corba característica.

II. RADIOFÀRMACS

Dins la física mèdica, la principal funcionalitat d'un activímetre és la de mesurar l'activitat d'un radiofàrmac que ha de ser administrat a un pacient.

Els radiofàrmacs són radioisòtops emissors de radiació (marcadors), units a una biomolècula (molècula transportadora, que tingui gran afinitat o capacitat d'adhesió als teixits, o certes propietats que la facin útil com a vehicle pel radioisòtop). Alguns radioisòtops no necessiten estar units a una biomolècula (Organismo Internacional de la Energía Atómica).

La seva aplicació clínica més usual és la visualització anatòmica d'un òrgan o sistema d'òrgans: el pacient pren (o se li injecta) el radiofàrmac, que es distribuirà a l'organisme. Mitjançant l'equipament adient, es poden obtenir imatges o mapes amb l'activitat a cada punt del cos del pacient. D'aquesta manera, es pot saber com s'ha distribuït el radiofàrmac, i un metge especialitzat pot avaluar si aquesta distribució és normal o bé correspon a una patologia. Per exemple, alguns tumors tenen activitats cel·lulars més altres del que correspondria a un teixit sa, i per tant absorbiran majors dosis del marcador i mostraran activitats anormalment altes.

II.1. Procediment de preparació i ús

Els radiofàrmacs poden arribar a ser molt diversos (de fet, el 2003 hi havia més de 250 productes autoritzats), i molts d'ells presentaran característiques diferents. No obstant, sí que hi ha certes característiques comuns en el seu procediment.

No qualsevol isòtop radioactiu és útil en medicina. Les vides mitges s'han de trobar en un rang al voltant d'hores, o com a poc, minuts: una vida mitja massa curta impediria que pogués ser preparat i administrat al pacient (tot el medicament es desintegraria abans que el pacient pogués ser examinat), però una vida mitja massa llarga farà que el pacient sigui una font de radiació durant dies, comportant un perill per al mateix pacient, el seus familiars i el públic general.

Els radioisòtops són subministrats als hospitals tant en preparats monodosi com en vials multidosi. Com l'activitat d'un isòtop radioactiu canvia amb el temps, la dosi necessària també ho farà, i per tant en molts casos les dosis exactes s'han de preparar poc abans del seu ús al mateix hospital. En aquests casos, el preparat s'haurà d'extreure del vial i separar en dosis individuals, procés que també pot implicar la seva dilució (és en aquests casos en què l'activímetre es fa més necessari, per a assegurar que l'activitat del preparat és l'adequada). Una activitat baixa impedirà que la imatge tingui bona qualitat, però una activitat elevada augmentarà el risc per al pacient i els treballadors.

El radiofàrmac es pot subministrar al pacient de diverses formes. Les més comuns són orals i intravenoses, però certs preparats es subministren per injecció subcutània o per inhalació (Cortés-Blanco & Esteban Gómez, 2003). Normalment, es deixa al pacient unes hores en repòs, perquè el medicament es pugui distribuir pel cos. Durant aquest període, el pacient ha de romandre en unes habitacions apantallades amb plom i s'ha de minimitzar l'exposició, especialment al personal hospitalari. Per a evitar que tot el marcador es concentri al cervell o als músculs els pacients hauran de restar en repòs, a les fosques, i sense llegir ni dormir. També hauran d'orinar abans que es prenguin les imatges.

Finalitzat aquest temps, ja es poden prendre les imatges pertinents. En funció del tipus de radiació emesa pel fàrmac,

serà mitjançant una gammacàmera (detecció de raigs gamma) o PET (detecció de positrons).

II.2. Radiofàrmacs comuns

El radioisòtops més usats en diagnòstic són el ^{18}F, ^{99m}Tc, el ^{123}I, i el ^{68}Ga (Cortés-Blanco & Esteban Gómez, 2003). Tots ells es poden unir a diferents molècules i formar diferents radiofàrmacs, però aquí només breument algunes presentacions a mode il·lustratiu.

- El ^{18}F, lligat a una molècula de glucosa, forma la fludesoxiglucosa (FDG), amb una vida mitjana de 109,77 minuts. Emet positrons, que ràpidament s'aniquilen generant dos fotons que són detectats per un PET. S'usa en oncologia, neurologia i cardiologia. Com la molècula transportadora és la glucosa, que totes les cèl·lules del cos necessiten per a funcionar, es concentrarà en els teixits més actius (com tumors o zones inflamades, però també al cervell) i a la bufeta (Cortés-Blanco, 2006).
- El ^{99m}Tc forma pentetat de tecneci (DTPA), que emet raigs gamma amb una semivida de 6 hores. Administrat de forma intravenosa, serveix per a l'estudi del sistema renal i del cervell; oral, de l'aparell digestiu; i inhalada, de la ventilació pulmonar, sempre mitjançant la gammacàmera. En el primer cas, es prenen les imatges 1h després de rebre la dosi, en els altres, immediatament després (Agencia Española del Medicamento y el Producto Sanitario).

III. PROVES DE QUALITAT DE LA MESURA

L'activímetre ha de passar diverses proves de forma periòdica per assegurar el seu correcte funcionament: principalment, les proves d'estabilitat, precisió i exactitud, amb periodicitats diària, la primera, i trimestrals les altres.

En tots els casos, sempre que es duu a terme una prova, s'ha de procedir de la mateixa manera: abans de començar, s'ha d'encendre l'activímetre i deixar-ho 30 minuts perquè l'equip s'estabilitzi. Aleshores s'haurà de fer una mesura del fons radioactiu, allunyant totes les possibles fonts del pou de l'activímetre, i esperant que la mesura s'estabilitzi.

Fet això, es podran prendre les mesures: s'introdueix dins del pou la mostra, esperem uns segons a què la lectura sigui estable, i anotem. Entre mesura i mesura convé esperar una estona a què la lectura torni a ser igual al fons, i canviar la configuració de l'equip, per a així assegurar-nos que totes les mesures siguin independents.

Com en un laboratori s'acostuma a utilitzar diversos isòtops, s'hauran de calibrar els diferents canals o modes de l'activímetre. Per a fer-ho, podríem o bé fer servir l'element corresponent a cada material (encara que això obligaria el laboratori a disposar d'una font certificada de cada tipus, amb el consegüent cost), o bé utilitzar la mateixa mostra per a tots els canals. És a dir, per no haver de disposar d'una font calibrada de Cesi, Iode, Tecneci…, en tenim una sola de Cesi i la farem servir per a calibrar tots els canals. Normalment, les lectures no tindran cap sentit (si mesurem l'activitat del cesi amb el canal de Iode, obtindrem un resultat incorrecte), però com el que sempre ens interessa és mesurar les desviacions relatives, és suficient fer-ho així.

III.1. Prova d'estabilitat

L'objectiu d'aquesta prova és comprovar que les mesures són estables, és a dir, que amb el pas dels dies l'activímetre no es desvia d'una mesura de referència donada.

Semestralment, s'ha d'establir una referència. En el nostre cas vam utilitzar el Cs^{137}. Un cop encès l'equip i mesurat el fons, es prenen 10 mesures de l'activitat de la font, i n'obtindrem la mitjana. Aquesta serà la referència durant tot el semestre. Diàriament, es pren una mesura a cada canal i es comprova que no s'hagi desviat més d'un 5% de la referència.

III.2. Prova d'exactitud

Tot comprovat que el nostre equip és estable, el següent serà cerciorar-nos que és exacte i precís. Abans de tot, definirem correctament aquests conceptes que usualment porten confusions.

- **Precisió:** La precisió fa referència a la dispersió del conjunt de mesures obtingudes d'una magnitud.
- **Exactitud:** L'exactitud es refereix a com de prop del valor real es troba el valor mesurat. Un resultat.

Aquestes dues magnituds són independents. Un conjunt de mesures pot ser tant precís com exacte sense tenir en compte l'altra magnitud.

Aquesta prova té com a objectiu comprovar que el nostre activímetre és exacte. Per fer-ho compararem les mesures de l'equip amb una font calibrada. Per fer aquesta prova utilitzarem la mateixa referència presa anteriorment, és a dir, la mitjana de les 10 mesures d'activitat de la font. L'exactitud serà la desviació relativa de les mesures respecte a una font calibrada, expressada en %.

$$\varepsilon_r = \frac{\underline{A} - A_c}{A_c}, \qquad \begin{cases} \underline{A}, \text{valor mitjà de les mesures preses} \\ A_c, \text{activitat de la referència} \end{cases}$$

Per a calcular A_c, cal tenir en compte el decaïment exponencial des de la data de calibratge de la mostra. El valor de ε_r ha de ser inferior al 10%.

III.3. Prova de precisió

Igual que en les altres dues proves, usarem com a referència la mitjana dels valorse de les 10 mesures de l'activitat de la font. La precisió serà el coeficient de variació dels resultats, en %.

$$CV = \frac{s(A_i)}{\underline{A}}, \qquad \begin{cases} \underline{A}, \text{valor mitjà de les mesures preses} \\ A_i, \text{conjunt de mesures preses} \\ s(A_i), \text{desviació típica de les mesures} \end{cases}$$

El valor absolut del CV ha d'estar per sota de l'1% (Sociedad Española de Física Médica, 2020).

IV. TAULA DE DADES

La taula exposa l'activitat mesurada d'una mostra de Cs-137, al canal del Cs-137, el dia 22 d'abril i el càlcul de la precisió i l'exactitud. El Cs-137 tenia una activitat de

245,68μCi el 7 de gener del 2008, i una vida mitja de 30,23 anys, per tant, el dia de la mostra, haurà de ser de $A_c = 168{,}92\mu Ci$.

Per tant, $\varepsilon_r = 2{,}85\%$ i $CV = 0{,}10\%$, dins dels llindars.

	Fons (μCi)	Activitat (μCi)
1	0,0	174.1
2	0,0	174,0
3	0,0	174,0
4	0,0	173,9
5	0,1	173,6
6	0,1	173,6
7	0,1	173,7
8	0,1	173,7
9	0,1	173,6
10	0,1	173,5
Valor mig	0,07	173,73
Desviació típica	0,04	0,18

V. CONCLUSIÓ

El calibratge periòdic de l'activímetre és l'única manera de garantir que l'equip funciona entre els límits acceptables i, per tant, que les seves mesures són prou exactes i precises. Un mal seguiment d'aquests protocols pot comportar una administració de dosis errònia, que pot alterar les imatges obtingudes o, fins i tot, posar en risc la salut dels pacients. Per això no només és necessari realitzar les proves dins dels terminis establerts, sinó que cal garantir una correcta manipulació de l'equip i dels radiofàrmacs per tal d'evitar generar contaminació externa que pugui alterar les mesures. L'activímetre estudiat en aquest cas ha superat amb èxit les proves de qualitat realitzades, així que es pot afirmar que es troba en molt bon estat i funciona correctament dins dels paràmetres recomanats.

VI. REFERÈNCIES

Agencia Española del Medicamento y el Producto Sanitario. (sense data). *Ficha Técnica DTPA Technescan.*

Cortés-Blanco, A. (2006). Especificaciones actuales de la ficha técnica de los radiofármacos compuestos de fludesoxiglucosa autorizados para comercialización en España. *Seguridad Nuclear*(40), 21-28. Recollit de https://www.aemps.gob.es/publicaciones/articulo/docs/fludesoxiglucosa_nov06.pdf

Cortés-Blanco, A., & Esteban Gómez, J. (2003). Radiofármacos de uso humano: marco legal e indicaciones clínicas autorizadas en España. *Seguridad Nuclear*(26), 5-15. Recollit de https://www.aemps.gob.es/publicaciones/articulo/docs/radiofarmacos_uso_humano.pdf

Domínguez Montero, P., Escalada, C., Ferrer, N., García-Toraño, E., Plaza, R., Rodríguez, C., . . . Rodríguez Zarauz, J. (sense data). *Protocolo para la calibración y uso de activímetros.* Madrid, Madrid, Espanya: CIEMAT. Consultat el 1 / maig / 2024, a https://rdgroups.ciemat.es/documents/1251782/0/Protocolo+para+la+calibraci%C3%B3n+de+Activ%C3%ADmetros/e503791e-7d1e-4686-95bd-733893d213ee

Laboratoire National Henri Becquerel. (sense data). *Ionization chambers - Figure.* Consultat el 1 / May / 2024, a Ionization chambers - Laboratoire National Henri Becquerel: http://www.lnhb.fr/home/presentation-en/ionization-chambers/

Organismo Internacional de la Energía Atómica. (sense data). *Radiofármacos de diagnóstico.* Consultat el 16 / May / 2024, a IAEA: https://www.iaea.org/es/temas/radiofarmacos-de-diagnostico

RadiaProt - Healthcare Radiation. (sense data). *Activímetro CRC(c)-55TR.* Recollit de https://radiaprot.com/wp-content/uploads/2022/04/Activimetro-CRC-55tR-en-espanol.pdf

Sociedad Española de Física Médica. (2020). *Protocolo de control de calidad de la instrumentación de medicina nuclear.* Recollit de https://sefm.es/wp-content/uploads/Protocolo-2020-final.pdf

VII. AGRAÏMENTS

Per a la realització d'aquest treball, es va dur a terme una pràctica la tarda del passat 22 d'abril amb el Sr. Antoni Castel Millán, cap del Servei de Protecció Radiològica dels hospitals de Quirónsalud Barcelon , en què a banda de prendre mesures també ens va explicar amb gran detall el mode de funcionament del servei, els radiofàrmacs, i els equipaments de què disposen. Agraïm enormement la seva col·laboració i atenció.

Control de qualitat d'un equip de tomografia per emissió de positrons (PET/CT)

Mar Artola, Jofre Bosch, Clàudia López i Eric Prat
Instrumentació. Grau en Enginyeria Física. Universitat Politècnica de Catalunya.
Campus Nord, 08034 Barcelona

1. Introducció

Des de la seva aparició, el principal objectiu de la medicina ha sigut identificar les anomalies bioquímiques en els organismes afectats per tal de poder actuar i reduir o eliminar aquestes anomalies mitjançant tractament tan aviat com sigui possible. Una de les tècniques de diagnòstic més implementades recentment és la tomografia axial computada, més coneguda com a TAC. Aquesta tècnica consisteix en una font de raig X que rota al voltant de l'organisme, mentre que al costat oposat hi ha un detector que rota sincrònicament amb la font i que la seva funció és detectar les variacions en l'absorció a mesura que travessa els teixits intermedis del pacient. El principal problema d'aquesta tècnica és que únicament és capaç de detectar aquelles anomalies que ja estiguin en un estat molt avançat.

A finals del segle XX, el 1998, es va utilitzar per primera vegada la tomografia per emissió de positrons (PET). Aquesta tècnica combina la precisió del TAC amb la detecció primerenca de les anomalies gràcies a la utilització d'un radiomarcador, és a dir, un isòtop radioactiu. Aquest radioisòtop, que s'injecta intravenosament a l'organisme, sol comportar-se com una glucosa perquè el cos l'assimili com a tal i això resulti en una major acumulació d'activitat radioactiva en aquelles zones que demanen més energia, que principalment és al cervell i a tumors. Després de ser absorbit, l'isòtop es desintegra emetent un positró, que quan xoca amb un electró s'anihilen quasi instantàniament emetent dos raigs gamma en sentits oposats. Aquests raigs penetren els teixits circumdants i són mesurats amb un conjunt circular de detectors. Finalment, s'aplica un algoritme matemàtic amb l'ajuda d'un ordinador que proporciona la distribució espacial de la radioactivitat en una pantalla de raigs catòdics. Per poder visualitzar millor aquesta distribució i la intensitat de cada punt sovint s'hi apliquen uns filtres per afegir colors en funció dels nivells d'activitat de radiació.

Un dels pocs problemes d'aquestes màquines tan sofisticades és la necessitat d'una calibració per assegurar el seu bon funcionament, com a mínim, anualment. Aquesta es fa mitjançant l'ús de fonts radioactives estandarditzades per tal de tenir unes condicions específiques d'activitat radioactiva en el moment de la prova i així assegurar un bon procés de calibratge.

2. Metodologia

2.1 Equipament

- Fantoma: Siemens Biograph de 9451 ml ple d'aigua destil·lada
- Activímetre
- Material radioactiu: ^{18}F fluorodesoxiglucosa (FDG)
- Quatre xeringues de 60 ml
- Xeringa amb agulla gran
- Agulla petita
- Guants de làtex

2.2 Procediment

2.2.1 Preparació de la dosi radioactiva

Per començar a fer el control de qualitat és necessari prèviament haver demanat una activitat suficient de ^{18}F-fluorodesoxiglucosa (FDG), de tal manera que hi hagi la dosi necessària per fer la calibració, que per especificacions del PET/CT utilitzat ha de ser d'1.6 mCi o 60 MBq en el moment d'inici de la prova. Un cop s'ha rebut la capsa amb el fluor s'ha d'extreure l'embolcall de plom que conté un vial amb l'activitat demanada. És important utilitzar guants de làtex per evitar el contacte amb qualsevol contaminació possible. Després d'extreure'n el vial del seu interior, aquest s'ha de portar a una càmera de plom amb només dues obertures per introduir els braços al seu interior i on poder extreure el ^{18}F evitant al màxim l'exposició a la radiació. Per fer aquesta extracció és necessari utilitzar ambdues agulles, la petita per trencar el buit del vial i la gran per extreure'n la dosi desitjada, que ha de ser prou gran com per assegurar que després de fer tota la resta de procediment previ al calibratge encara hi hagi una activitat superior a la necessària. En l'instant en què tenim la xeringa carregada és **molt important** anotar l'activitat que hi ha emmagatzemada i a quina hora s'ha pres aquesta mesura, ja que més endavant serà necessari tenir aquestes dades.

Figura 1: Extracció del ^{18}F del vial

2.2.2 Preparació del fantoma

Primer s'omple el fantoma amb aigua destil·lada fins a enrasar. És **important** que el fantoma sigui el que indica el fabricant, en el nostre cas el de Siemens de 9451 ml. A continuació, s'extreuen un total de 240 ml amb ajuda de les quatre xeringues i s'injecta la dosi de ^{18}F (s'anota l'hora de l'operació). És necessari obtenir una barreja totalment homogènia i per tal d'aconseguir-ho, fem rodolar el fantoma pel terra unes quantes vegades. Llavors afegim dues xeringues d'aigua i repetim el procés. Per acabar, introduïm l'aigua restant vigilant que no quedi cap bombolla d'aire i tornem a fer rodar el fantoma.

2.2.3 Càlcul de l'hora

És necessari calcular l'hora en què s'ha de fer la calibració per tal que l'activitat sigui 1,6 mCi (60 MBq) en el moment de realitzar-la. Per fer-ho es pot utilitzar un programa específic del PET Cross Calibration o es pot fer a través d'un full de càlcul. En el nostre cas hem creat un fitxer d'Excel on utilitzant la fórmula que descriu com decau l'activitat i les dades inicials: l'hora i l'activitat en aquella hora, podem calcular el moment exacte en què cal fer la calibració.

$$A(t)_{calc} = A_o \cdot e^{-ln(2)\cdot\frac{t}{\tau_{1/2}}}$$

$$A_o = 4{,}31\ mCi \quad \tau_{1/2} = 110\ min$$

Hora	**Temps** $t(min)$	**Activitat** $A_{calc}(mCi)$	
17:38	0	4.31	Extracció ^{18}F
18:12	34	4.478	Injecció fantoma
20:36	156.466	1.608	Moment calibració

A les 17:38 es van extreure 0.5 ml de ^{18}F amb una activitat de 4.31 mCi. Després, obtenim l'activitat a l'hora de la injecció. A continuació, aïllem el temps i obtenim l'hora en la qual hem de fer la calibració per tal que l'activitat sigui de 1.608 mCi.

2.2.4 Realització de la calibració

Abans de fer la calibració es demana que s'introdueixin una sèrie de dades a l'ordinador: dosi mesurada, temps en què s'ha mesurat, dosi residual, temps en què s'ha mesurat aquesta dosi residual i volum del fantoma.

Seguidament, utilitzant el suport pel fantoma, posicionem el fantoma de manera que quedi centrat. Ho fem amb l'ajuda dels làsers que proporciona l'aparell.

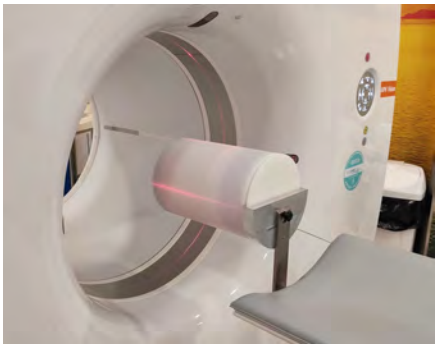

Figura 2: Fantoma col·locat per iniciar la calibració

Realitzem l'escaneig PET/CT utilitzant el protocol de Calibració Creuada amb 100 000 000 comptes.

2.2.5 Obtenció del CCCF(*Cross Calibration Correction Factor*)

L'objectiu final és el càlcul del CCCF. Tal com ens mostra l'expressió següent, aquest coeficient es calcula mitjançant la divisió de l'activitat específica calculada a l'inici de l'escaneig entre l'activitat específica mesurada a l'inici de l'escaneig.

$$CCCF = \frac{A_{calc}}{A_{measured}}$$

L'A_{calc} es calcula mitjançant l'expressió:

$$A_{calc} = \frac{A_o}{V_{phantom}} \cdot e^{-ln(2)\cdot\frac{t}{\tau_{1/2}}}$$

$$A_o = 160\ MBq\ (4{,}31\ mCi) \quad V_{phantom} = 9451\ ml$$

$$\tau_{1/2} = 110\ min$$

Per altra banda, l'$A_{measured}$ es calcula fent la mitjana de l'activitat mitjana (en Bq/ml) de 12 talls transversals de l'activitat registrada pel PET mitjançant l'eina ROI (*Region Of Interest*).

El valor obtingut del CCCF pot estar en tres zones que ajudaran a determinar l'estat de la màquina:

- CCCF $\in$ [0.9 , 1.1]. El valor es pren com a vàlid.
- CCCF $\in$ [0.8 , 0.9) $\cup$ (1.1 , 1.2]. El valor es pren com a vàlid, però s'ha de tenir present que és un valor atípic.
- CCCF $\notin$ [0.8 , 1.2]. El valor es pren com a erroni i s'ha de repetir la mesura per confirmar si és un error puntual o si és sistemàtic.

2.2.6 Normalització i calibració de l'escàner

Un cop obtingut el nou factor de calibració creuada s'ha de normalitzar i calibrar l'escàner per verificar que la calibració creuada ha estat exitosa.

En primer lloc, s'ha de verificar que el sistema estigui en un estat d'inactivitat de l'usuari. S'obre la finestra de **PET Quality Check** i es comprova que el CCCF aparegui en el camp de **Cross Calibration** i que el volum i totes les dades siguin correctes. Després, es normalitza el sistema executant el **PET Quality Check** i es mira el **computed ECF**(Efficiency calibration factor). Es registren el **Computed ECF** i el **Reviewed ECF** en el **PET Cross Calibration** tool que calcula el percentatge de la diferència entre el valor de ECF corregit i el revisat.

Llavors, mirant el manual de l'operador del PETsyngoVG7xx, podem veure que si aquest valor és menor que $\pm 5\,\%$, la calibració creuada del sistema pel calibrador de dosis ha estat exitosa.

3. Resultats

Els resultats que es detallaran a continuació no corresponen a les dades descrites anteriorment que van ser obtingudes per nosaltres el dia de la pràctica. Això és degut a un error extern que no ens va permetre obtenir els nostres propis resultats.
Les dades següents han estat proporcionades pel radiofísic Antoni Castel d'una altra calibració del mateix tipus.

Per tal de passar el control de qualitat les imatges obtingudes de cada tall amb el PET/CT estudiem l'uniformitat tomogràfica.

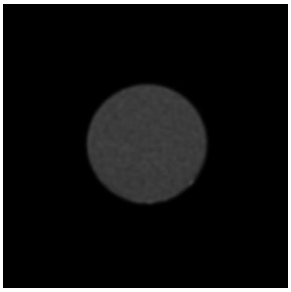

Figura 3: Imatge original tall 67

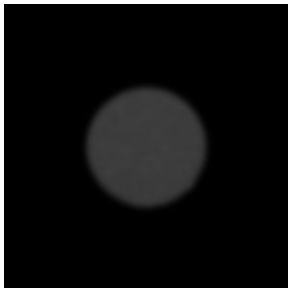

Figura 4: Tall 67 amb el Gaussian filter 5mm aplicat

En les figures 3 i 4 podem veure la imatge d'un tall transverstal que ens genera el PET/CT. La de l'esquerra és la orginal i a la de la dreta se li ha aplicat un filtre per tal de poder fer els estudis corresponents.
Per poder passar el control de qualitat primer s'analitzen els talls a simple vista. Per tal que la calibració sigui correcta no hi poden haver discontinuïtats brusques ens els perfiles transversals ni tampoc artefactes en forma d'anell en cada un dels talls. Al centre del sinograma s'ha d'observar uniformitat. Evidentment, tampoc hi poden haver bombolles d'aire en el fantoma ja que farien que l'aparell no superés el control de qualitat.

Per estudiar la uniformitat tomogràfica del PET es tracen 5 ROIs, que es poden observar a la Figura 5, en tres talls consecutius. A cada un dels ROIs es mesura el valor mitjà del SUV, la desviació estàndard (SD) i la diferència respecte el centre prenent una tolerància de $\leq 10\,\%$.

Figura 5: 5 ROIs en un dels talls

- Tall 67:

ROI	Valor mitjà SUV	SD	Diferència
Centre	3.09	0.11	
1	3.15	0.12	2.08 %
2	3.14	0.12	1.65 %
3	3.09	0.10	0.16 %
4	3.02	0.11	2.36 %

Valor màx: 3.15	Desviació màx: 2.36 %
Valor promig: 3.1	Desviació mitjana: 1.56 %

- Tall 65:

ROI	Valor mitjà SUV	SD	Diferència
Centre	3.12	0.13	
1	3.09	0.13	0.83 %
2	3.08	0.09	1.26 %
3	3.09	0.12	0.76 %
4	3.03	0.10	2.89 %

Valor màx: 3.09	Desviació màx: 2.89 %
Valor promig: 3.08	Desviació mitjana: 1.43 %

- Tall 69:

ROI	Valor mitjà SUV	SD	Diferència
Centre	3.13	0.16	
1	3.10	0.11	0.80 %
2	3.15	0.09	0.67 %
3	3.05	0.11	2.37 %
4	2.98	0.13	4.61 %

Valor màx: 3.15	Desviació màx: 4.61 %
Valor promig: 3.08	Desviació mitjana: 2.11 %

Amb aquests resultats obtenim que la màxima desviació entre talls és de 0.53 % i la màxima desviació observada en algun dels talls és de 4.61 %.
Amb tot això, concloem que la calibració és correcte, ja que no hi ha cap desviació superior al 5 %. En el cas d'obtenir desviacions superiors s'haurien d'adoptar mesures correctives.
A continuació, s'estudia l'uniformitat tomogràfica del CT. Per fer-ho, s'utilitzar el terme unitat Hounsfield (UH) que és el número assignat a cada pixel de la imatge i és l'expressió de la densitat de l'objecte irradiat. En els mateixos 5 ROIs que abans es mesura el valor mitja dels números CT, la desviació estàndard i la diferència respecte el centre prenent una tolerància de ±5,00 UH.

- Tall 100:

ROI	Valor mitjà Números CT	SD	Diferència
Centre	-1.10 UH	9.50 UH	
1	-0.90 UH	9.30 UH	0.20 UH
2	-1.50 UH	9.00 UH	-0.40 UH
3	-0.90 UH	9.30 UH	0.20 UH
4	-0.90 UH	8.30 UH	0.20 UH

Valor màx: -1.50 UH	Desv. màx: -0.40 UH
Valor promig: -1.06 UH	Desv. mitjana: 0.05 UH

Repetim aquest anàlisi en el tall 98 i el 102 i obtenim que el valor màxim entre talls és de -1.50 UH i la màxima desviació és de 0.4 UH. És a dir, que aquests valors es troben dins les toleràncies i per tant la calibració és correcte.

4. Conclusions

En aquest estudi s'ha analitzat un equip de tomografia per emissió de positrons (PET/CT) per tal de calibrar-lo i assegurar-ne el funcionament correcte. En aquests aparells, una precisió insuficient pot comportar un greuge en la salut dels pacients i dels treballadors, per això és necessari dur a terme controls de qualitat sovint.

Durant el procediment hem vist que la preparació dels materials per executar la calibració és molt important i que cal prendre bones mesures de seguretat per evitar l'exposició a la radioactivitat, ja que s'ha de manipular constantment un isòtop radioactiu. A més a més, la zona en la qual es treballa està constantment contaminada. Per aquest motiu és necessari que els tècnics d'aquestes àrees tinguin un control mensual de la radiació absorbida pel seu cos. Sobretot és imprescindible protegir més aquelles parts que siguin més sensibles a la radiació, com per exemple els ulls, o aquelles que estiguin més a prop, com serien les mans, tot i que la millor protecció sempre és la de reduir al màxim l'exposició, ja que el contacte constant pot desencadenar greus problemes de salut.

Hem vist que per poder fer un calibratge d'aquest estil és necessari ser curós amb tot el que es fa per intentar aconseguir uns resultats el màxim de bons possibles mentre es manté la seguretat personal.

En referència als resultats de la calibració hem vist que l'equip PET ha demostrat un bon rendiment i que es manté dins dels valors òptims, segurament perquè és un aparell nou que encara manté un molt bon funcionament. Unes proves com aquestes en equips tan nous poden semblar innecessàries, però és important fer-ne cada cert temps per assegurar uns bons resultats que comportaran una bona imatge del cos del pacient i permetrà un millor diagnòstic per actuar de la millor manera possible.

5. Bibliografia

Referencias

[1] Ter-Pogossian, M. M., Raichle, M. E., & Sobel, B. E. (1980). Positron-Emission Tomography. *Scientific American*, *243*(4), 170–181. Recuperat de http://www.jstor.org/stable/24966439

[2] Siemens Healthineers. (2024). *Operator Manual / PETsyngoVG7xx*. [PDF]. Document proporcionat pel professor.

[3] Sociedad Española de Física Médica. (2020). *Protocolo de control de calidad de la instrumentación en medicina nuclear*. [PDF]. Document proporcionat pel professor.

Instrumentació en Radiodiagnòstic. Utilització d'un equip d'adquisició d'imatges: Tomògraf CT. Qualitat de la imatge*

Juliana Blanco, Dina Boujbel, Clàudia Buch, Laura González, Joan Salazar

Instrumentació. Grau en Enginyeria Física. Universitat Politècnica de Catalunya. Campus Nord, 08034 Barcelona

L'ús del PET-CT és clau per garantir un correcte tractament dels pacients. En aquest treball s'explora el funcionament del tomògraf, així com la física que hi ha al darrere. A més, es detallen els resultats obtinguts de la CT duta a terme al *phantom* a l'hospital Quirón-Dexeus.

Paraules clau: PET-CT, *phantom*, tomografia, medicina nuclear, calibratge

I. INTRODUCCIÓ

El PET (*Positron Emission Tomography*) i el TAC o CT (Tomografia Computaritzada) són dues tècniques modernes d'imatge nuclear, indispensables per a una pràctica mèdica d'excel·lència. Aquestes tècniques faciliten tant l'estudi anatòmic com funcional per a la detecció de malalties, tot i que també poden ser utilitzades en el seu tractament i durant diversos procediments mèdics.

El TAC s'utilitza en pràcticament tots els òrgans i, essencialment, consisteix en una radiografia tridimensional. Permet la creació de models 3D de l'interior del cos, facilitant així que els professionals de la salut puguin visualitzar i localitzar anomalies estructurals. D'altra banda, el PET és considerat el mètode més eficaç per a la localització de diversos tipus de càncer, ja que es fonamenta en la detecció de l'activitat metabòlica, la qual és anòmala en els tumors.

En aquest treball s'abordarà l'anàlisi de la física subjacent a aquests dispositius innovadors, així com les mesures de seguretat imprescindibles per prevenir accidents[1]. Posteriorment, s'exposarà el PET-CT i seguidament es detallarà el seu calibratge adequat mitjançant l'ús d'un *phantom*. Finalment, es presentarà la part pràctica realitzada durant la nostra visita a l'hospital.

II. CONCEPTES PREVIS

A. Efecte fotoelèctric

L'efecte fotoelèctric fa referència a la capacitat intrínseca de la llum (radiació electromagnètica) per a provocar l'alliberament d'electrons d'una superfície metàl·lica, la qual absorbeix fotons en el procés. La longitud d'ona de la radiació incident determinarà l'energia dels electrons excitats i conseqüentment emesos, provocant així la ionització dels àtoms de la superfície.

A l'hora de quantificar les energies involucrades en aquest procés s'empra l'equació:

$$E_{\text{fotó}} = h\nu = W + E_{\text{electró}},$$

on W és la funció de treball, particular de cada metall.

B. Aniquilació de positrons en el PET

El PET es basa inherentment en l'aniquilació de positrons. Quan un radiofàrmac n'emet dins l'individu, aquests travessen els teixits fins a trobar electrons. Com a conseqüència d'aquesta interacció hi ha un procés d'aniquilació mútua, la qual provoca la transició de massa a energia. Aquesta es presenta com a dos fotons gamma[2] emesos tot formant un angle de pràcticament 180º. No és un angle perfecte atès que, inicialment, el sistema positró-electró no està en repòs.

Es pot observar aquesta interacció a la Fig. 2.

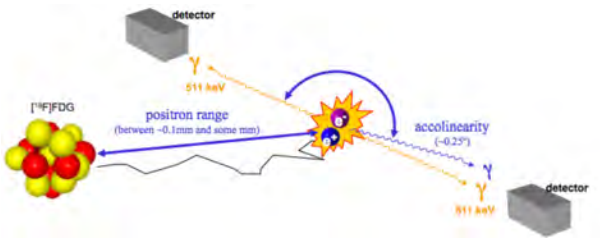

Figura 1. Formació d'un parell de fotons gamma.

III. PROTECCIÓ DAVANT LA RADIACIÓ

Per obrir una secció de Medicina Nuclear, cal la recomanació del Consell de Seguretat Nuclear. Un dels requisits és el control correcte de la irradiació de cada zona.

* en col·laboració amb l'Hospital Universitari Quirón-Dexeus

[1] Del 10 al 20 de desembre del 1990, a Saragossa va haver sobredosi de radiació a causa de recents reparacions. Hi van morir onze pacients, i molts altres van resultar ferits.

[2] Aquests fotons gamma tenen una energia específica de 511 keV cadascun.

Primerament, l'activitat radioactiva correspon a les desintegracions per unitat de temps, mesurades en Becquerels[3]. En ser una magnitud molt petita, se solen emprar els Curies duent a terme la següent conversió d'unitats: $1\ \text{Cu} = 3,7 \cdot 10^{10}$ Bq.

Una altra magnitud que es té en compte és la dosi absorbida, que és l'energia per unitat de massa absorbida degut a la radioactivitat. Es mesura en Greys[4] (en medicina típicament s'empren els mil·ligrays).

Per a una mateixa dosi absorbida, dos feixos de partícules diferents no tenen el mateix efecte biològic. Per a mesurar-ho, s'assigna un factor de qualitat a cada partícula, essent 1 el valor mínim, corresponent als fotons. La dosi equivalent[5] permet entendre com de perjudicial és un feix d'una partícula determinada.

A més, la sensibilitat a la radiació varia per a cada òrgan. La dosi efectiva és la suma ponderada de les dosis equivalents de cada òrgan i és el paràmetre de la legislació. Tant la dosi equivalent com la dosi efectiva utilitzen la mateixa unitat, el sievert (Sv).

Per a l'usuari general, està establerta una dosi efectiva màxima anual de 1 mSv, i pels treballadors exposats, aquesta augmenta fins a 50 mSv. Es classifiquen les àrees on pot haver-hi irradiació segons el perill que suposa per a la salut humana (veure Fig. 2):

(a) *Zona lliure*: sense perill. No li correspon cap senyalització.

(b) *Zona vigilada*: hi ha risc de rebre dosis efectives compreses entre 1 i 6 mSv anuals.

  (i) *De permanència limitada*: es pot rebre una dosi de radiació superior a l'anual permesa.

  (ii) *De permanència reglamentada*: en una sola exposició se superen els límits per a curts períodes de temps.

  (iii) *D'accés prohibit*: en una sola exposició se superen els límits anuals.

Figura 2. Senyalització de les àrees d'irradiació.

Per tal de protegir els treballadors i minimitzar la seva exposició, a més de controlar correctament la radiació generada pels procediments mèdics, l'hospital fa revisions freqüents del nivell de contaminació de l'ambient. Complementàriament, les estructures on hi ha fonts de radiació, com ara on són el PET-CT i la gammacàmera, estan blindades amb plom, a més de les cambres on reposen els pacients abans i després del procediment mèdic. També es disposa de davantals de plom i guants per minimitzar el contacte amb substàncies irradiants, i per norma s'han de dur a terme cursos de protecció radiològica periòdicament.

Per aconseguir el permís del Ministeri, s'ha de controlar el radiofàrmac des que entra fins que surt de l'hospital. Els radiofàrmacs són activats a primera hora per una empresa externa i es porten a l'hospital. Des d'allà es porten a la secció de Medicina Nuclear per un passadís pel qual no hi ha circulació de pacients. Així i tot, per seguretat, s'emmagatzemen en recipients amb un blindatge adient, proporcional a la radiació emesa.

La vida mitjana dels radiofàrmacs és curta, de màxim sis hores. Tanmateix, segueixen emetent radiació durant més temps. Les agulles amb les quals s'injecta el fàrmac al pacient, les gases de cotó i els guants dels infermers, entre d'altres, són també residus radioactius. Consegüentment, tenen el seu contenidor corresponent. En ser de baixa activitat, però, l'hospital simplement els emmagatzema a la sala de residus i se'n desfà quan la seva radiació és menor a vint comptes, la quantitat habitual de fons[6].

IV. DESCRIPCIÓ DEL PET-CT

La PET-CT és una combinació de dues tecnologies d'imatges mèdiques. Una d'elles és la tomografia per emissió de positrons (*Positron Emission Tomography*, PET) i l'altra la tomografia computada (*Computed Tomography*, CT).

El PET utilitza un radiofàrmac dissenyat per a injectar-se al cos amb l'objectiu d'acumular-se als teixits i detectar la seva emissió de positrons, produïda a causa de la desintegració d'aquesta substància.

D'altra banda, la CT projecta les imatges transversals detallades del cos fent servir raigs X. En conjunt, les dues tècniques permeten localitzar i caracteritzar visualment malalties com el càncer. És a dir, permeten l'avaluació més precisa de l'activitat metabòlica junt amb l'anatomia, la qual cosa ajuda en el diagnòstic i en la planificació del tractament.

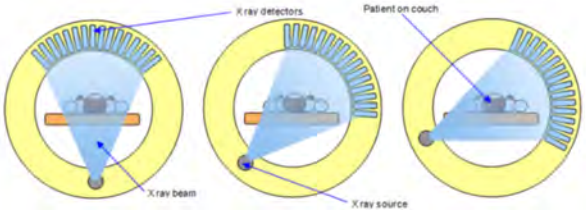

Figura 3. Detectors i emissor de raig X en tres posicions.

[3] Desintegracions per segon.
[4] 1 Gy = 1 J/Kg.
[5] El producte de la dosi absorbida pel factor de qualitat

[6] A Espanya, l'*Empresa Nacional de Residus Radioactius* (Enresa) s'encarrega de l'acondicionament i emmagatzematge final dels residus.

Els escàners PET detecten la radiació emesa per un radiotraçador, com la fluorodesoxiglucosa (FDG), que s'injecta al braç i s'acumula a diferents parts del cos. Es detecten fotons gamma utilitzant una matriu de detectors de material cristal·lí, generalment iodur de cesi (CsI), disposada al voltant del pacient en un arranjament circular o cilíndric. Quan els fotons gamma són detectats, es registren i s'utilitzen per a generar una imatge tridimensional de la distribució de la radioactivitat al cos del pacient. Aquests fotons, com ja s'ha comentat, s'emeten en angles pràcticament oposats degut a la conservació de la quantitat de moviment.

Figura 4. PET-CT.

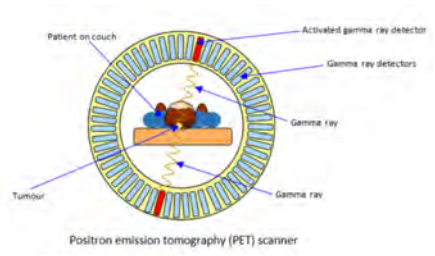

Figura 5. Secció transversal del *Gantry*.

Aquesta tècnica es basa principalment en l'anàlisi d'imatges que proporcionen informació crucial, com ara el nivell de captació de glucosa per òrgan en cada píxel. Aquest paràmetre es regula mitjançant el valor de captació estandarditzat[7] (SUV), el qual ha d'estar calibrat correctament. És responsabilitat fonamental d'un radiofísic certificar i validar que el PET proporcioni un valor estàndard adequat. Per aquesta raó es fa un control de qualitat cada tres mesos.

Quan s'analitzen aquestes acumulacions de glucosa, s'avalua el comportament de les funcions corporals i s'identifiquen possibles anomalies. Per exemple, la concentració de FDG pot revelar cèl·lules canceroses a causa de la seva alta demanda de glucosa. Quan el valor del SUV supera el llindar determinat, indica un excés de captació que alerta el metge, el qual posteriorment investiga possibles malalties. La precisió en el calibratge i el manteniment de l'equip PET són essencials per garantir la fiabilitat dels resultats i una atenció mèdica òptima.

[7] El valor estàndard d'absorció (SUV) és una mesura de l'absorció de radiació en el teixit. Molts factors afecten el SUV, incloent-hi l'exactitud de la dosi, el temps entre la injecció i la imatge (temps de la dosi a l'escaneig), la massa del pacient (variacions de pes són freqüents en pacients oncològics) i els nivells de glucosa en sang.

V. ÚS DEL *PHANTOM* PER AL CALIBRATGE. PROCEDIMENT

L'ús del *phantom*[8] és vital per dur a terme el control de qualitat, ja que cal assegurar-se que tant la imatge com l'alineació dels làsers estiguin en òptimes condicions abans de fer-hi passar el pacient.

Per a no perdre qualitat d'imatge, és important que el pacient quedi centrat correctament, de manera que quedi perfectament alineat amb l'eix z de l'aparell. En el nostre cas el model de *phantom* emprat és el Catphan503, que presenta unes petites marques de referència. Aquestes permeten trobar la posició correcta amb l'ajuda de làsers i d'un anivellador incorporat al tomògraf. Si s'alineen els làsers amb els punts superiors i laterals del *phantom*, aquest queda orientat adequadament, sempre i quan els làsers estiguin ben calibrats (un altre factor que afecta, en darrer terme, a la qualitat d'imatge).

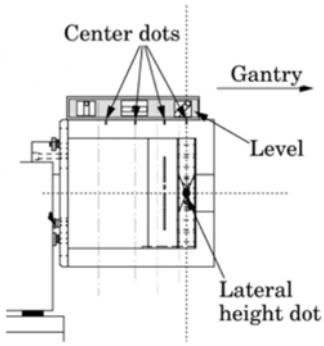

Figura 6. Esquema de posicionament del *phantom*.

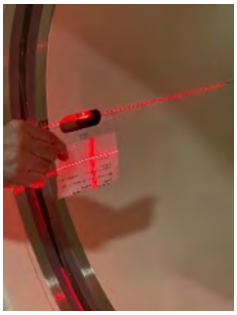

Figura 7. Procés d'alineació amb els làsers.

En aquest model s'hi distingeixen diferents mòduls o zones d'interès en la direcció axial. Cada una està dissenyada amb l'objectiu de verificar certes condicions de cara a l'estudi o d'analitzar diverses propietats del tomògraf.

(a) *Zona de densitats (punt zero):* part del volum situada a l'extrem del *phantom*, la qual es caracteritza per tenir aglomeracions de material de diverses densitats, que en ser sotmeses a una tomografia apareixen en pantalla com a cercles amb diferents tons de gris. Els més foscos corresponen a zones de menor densitat (ja que absorbeixen menys radiació), mentre que els més clars indiquen la presència de materials més densos. Aquesta zona, formalment identificada per CTP404, també mostra un conjunt de línies que permet determinar si s'ha col·locat l'instrument en la posició correcta.

[8] Instrument que s'utilitza com a substitut dels teixits corporals per calibrar el tomògraf i verificar que els mètodes d'imatge funcionen correctament.

(b) *Zona de barres* (I30[9]): en un tall transversal a trenta mil·límetres del punt zero hi ha, situats en cercle, diversos conjunts de línies. El conjunt n té n barres que apareixen progressivament més juntes a mesura que augmenta n. Això proporciona un indicador de la qualitat de la imatge, i es determina fins a quin conjunt n es pot distingir la presència de barres (en el cas de la nostra pràctica, fins al conjunt de 7 barres). El mòdul rep l'identificador CTP528.

(c) *Zona uniforme* (I70 i I110): presenta una distribució homogènia de material, dissenyada per tal de tenir uns números *Hounsfield* dins un 2% de marge al voltant de la densitat de l'aigua (típicament, presenta una variació d'uns cinc o deu valors). Aporta informació sobre el soroll present en les imatges generades en la tomografia, i s'identifica per CTP486.

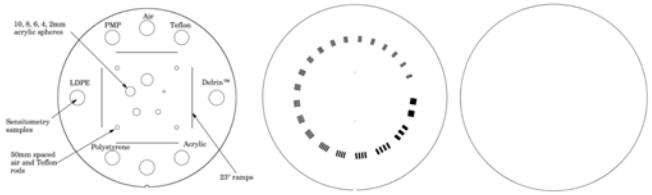

Figura 8. CTP404 (esquerra), CTP528 (centre), CTP486 (dreta)

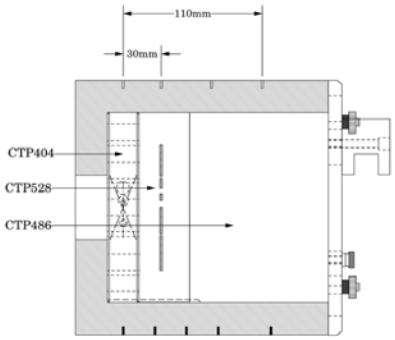

Figura 9. Secció longitudinal del *phantom* (Catphan503).

L'escala de números *Hounsfield* és una mesura quantitativa relativa que s'utilitza per classificar els diversos tipus de teixits segons el seu coeficient d'absorció de la radiació, i així poder generar una imatge en tons de gris. La densitat física del teixit correspon a l'atenuació del feix de raigs X.

La unitat *Hounsfield* (HU) es calcula a partir de la definició de 0 HU a l'aigua destil·lada i de –1000 HU a l'aire (a temperatura i pressió estàndards). Es pot arribar fins a 1000 HU per als ossos, i fins i tot 2000 HU per als ossos densos com ara la còclea. Tal com es veu en la imatge següent, aquests valors s'associen a intensitats diferents en l'escala de grisos, de manera que en les imatges obtingudes per TC podem distingir les diverses zones d'interès per densitat. A major densitat d'un teixit, més quantitat de raigs X s'absorbeix, i per tant més blancs seran els píxels corresponents a la imatge.

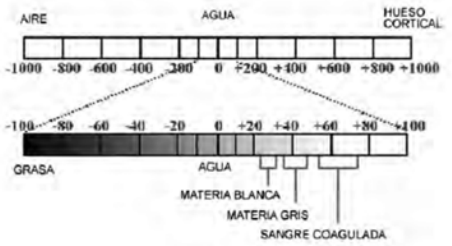

Figura 10. Escala de números *Hounsfield*.

Tanmateix, les imatges encara són processades amb programes d'edició especials per poder interpretar amb més facilitat què apareix en cada zona. Per exemple, s'intenta atenuar el to de la pell, ja que sol aparèixer en tons molt foscos abans de l'edició. Aquest procés es duu a terme via software automàticament.

VI. ANÀLISI DELS RESULTATS

A l'Hospital Universitari Quirón-Dexeus vam dur a terme una CT amb un *phantom*, fet que ens va permetre analitzar en detall cada zona del seu interior.

A. Zona de densitats

A la imatge obtinguda de la zona de densitats del *phantom* s'observa com cada material té un número *Hounsfield* diferent, i per tant una densitat diferent. Si es compara amb l'esquema del mòdul CTP404, es veu que els valors de números *Hounsfield* extrapolats pel *software* d'anàlisi a partir de la imatge obtinguda coincideixen amb els materials especificats pel fabricant. A mode d'exemple, s'aprecia que la zona més fosca de la imatge mostra un mínim de -1001HU i una mitjana d'aproximadament -900HU (a prop del valor esperat de l'aire).

Pel que fa al posicionament del *phantom*, amb aquesta imatge s'aprecia que no es va col·locar adequadament, tot i que amb l'anivellador i els làsers es va intentar alinear de la millor manera possible. El personal va comunicar que encara no s'havia dut a terme el calibratge periòdic dels làsers, de manera que possiblement el mal anivellament sigui degut a aquest fet. Hi ha quatre marques blanques sobre el perímetre a nord, sud, est i oest, de les quals

[9] La I seguida d'un nombre indica la distància en mil·límetres a la qual s'introdueix el *phantom* al tomògraf.

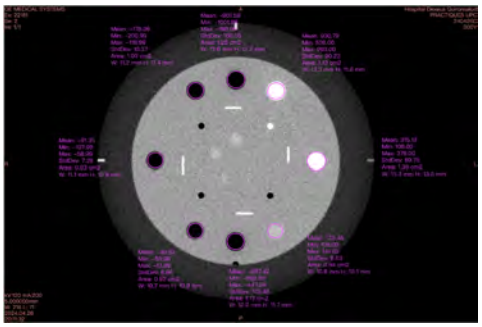

Figura 11. Secció del mòdul CTP404

només se'n veuen tres (la inferior no es distingeix, i la de la banda dreta queda atenuada).

D'altra banda, tal com es veu a la imatge següent, el *phantom* tampoc es va situar correctament en la direcció axial, i hagués fet falta moure'l lleugerament més endins en direcció al Gantry.

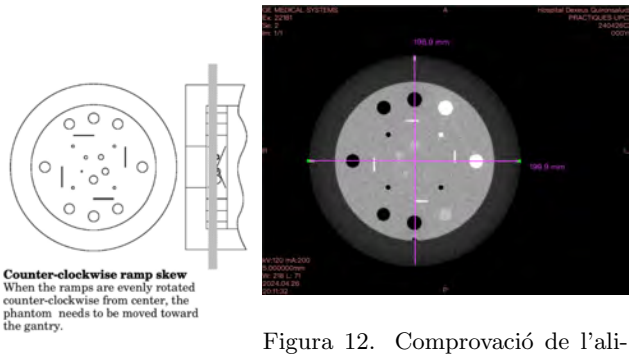

Figura 12. Comprovació de l'alineament del *phantom*

B. Zona de barres

La CT de la zona de barres permet veure fins a quina resolució es pot distingir el detall. Tal com s'aprecia a la Figura 13, es poden discernir fins a set línies. Aquest grup correspon a una resolució de 0.063 cm, tal com indica el manual del fabricant.

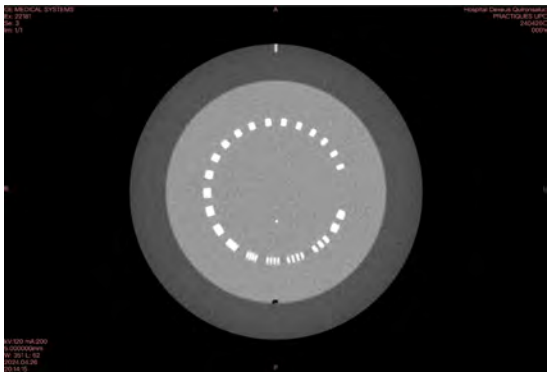

Figura 13. Secció del mòdul CTP528

C. Zona uniforme

La zona uniforme és la que permet detectar el soroll present en les imatges. Idealment, hauria de presentar una desviació d'unes 5 HU. Mitjançant l'eina d'anàlisi de números *Hounsfield* per secció que proporciona el *software*, podem veure que en el nostre cas la desviació és de 6.10, prou correcta.

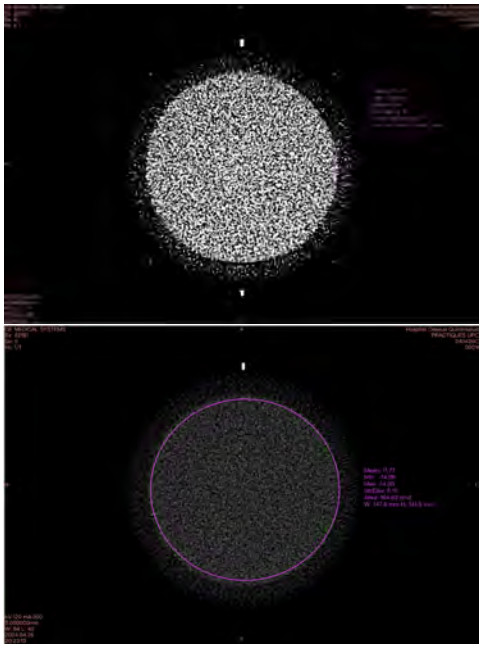

Figura 14. Secció del mòdul CTP486

VII. CONCLUSIÓ I AGRAÏMENTS

L'informe present exposa un estudi exhaustiu sobre la tomografia computada i la tomografia per emissió de positrons. L'anàlisi dels principis físics que regeixen el funcionament d'aquests aparells ha permès comprendre el procés pel qual es detecten i es tracten diverses patologies.

Entendre el funcionament del tomògraf va permetre la realització d'una CT a un *phantom* durant la visita a l'hospital. Tot i que el posicionament del *phantom* no va ser precís, els resultats obtinguts en la part pràctica són coherents i, a més, reflecteixen acuradament la realitat de l'ús clínic de la tomografia computada.

Voldríem aprofitar per agrair enormement els professors de l'assignatura d'Instrumentació d'Enginyeria Física per permetre'ns experimentar de primera mà l'ús d'un tomògraf en la medicina. Especialment, volem expressar el nostre agraïment a l'Antoni Castel Millán, membre de l'equip de Medicina Nuclear de l'hospital, per les seves valuoses indicacions, guia i explicacions.

REFERÈNCIES

[1] T. D. DenOtter and J. Schubert, *Hounsfield unit* (2019).

[2] T. B. Mail, *C atphan® 503 Product Guide* (2017).

[3] Medical imaging, `https://exetermathematicsschool.ac.uk/medical-imaging/`.

[4] C. de Seguridad Nuclear, *La protección radiológica en el medio sanitario* (Consejo de Seguridad Nuclear, 2012).

[5] Sensible solutions for refurbished radiology: Ct scanner components: What does what?, `https://info.atlantisworldwide.com/blog/ct-scanner-components-what-does-what`.

[6] P. A. Bennett, A. Mintz, B. Perry, A. Trout, and P. Vergara-Wentland, *Specialty Imaging: PET-E-Book: Specialty Imaging: PET-E-Book* (Elsevier Health Sciences, 2017).

[7] Tomografía por emisión de positrones (pet/tc), `https://www.radiologyinfo.org/es/info/pet`.

[8] M. Udristioiu and A. Stoian, *HOW TO UNDERSTAND A PHANTOM?*

[9] S. Solanes Casado, *Tecnecio 99m: radiofármaco de diagnóstico utilizado en la actualidad.* (2016).

[10] H. F. Aguinaga, J. A. Rivera, L. J. Tamayo, M. Tobón, and R. C. Osorno Ch, Tomografía axial computarizada y resonancia magnética para la elaboración de un atlas de anatomía segmentaria a partir de criosecciones axiales del perro, Revista Colombiana de Ciencias Pecuarias **19**, 451 (2006).

Instrumentación en Radiodiagnóstico. Utilización de un equipo de adquisición de imágenes: Tomógrafo TC. Calidad de los parámetros del haz de radiación

Leah Benarroch, Lucía Novo, June Kneisz, Eva Prieto
Instrumentació. Grau en Enginyeria Física. Universitat Politècnica de Catalunya.
Campus Nord, 08034 Barcelona

Con este trabajo nuestra intención es desarrollar la práctica que realizamos en el *Centro Médico Teknon* del grupo *QuirónSalud* coordinada por Antoni Castel Millan y Adam Jones, y mostrar la gran importancia del proceso de tomografía computarizada en el mundo de la medicina y el radiodiagnóstico.

Palabras clave: tomografía computarizada (TC), índice de dosis de tomografía computarizada (CTDI), rayos X, *phantom*.

I. INTRODUCCIÓN

A lo largo de los años ha habido grandes avances en la medicina, entre ellos, en 1973 fue inventado el primer tomógrafo comercial. Más adelante, éstos han ido mejorando añadiendo detectores, reduciendo su tiempo de obtención de imágenes y mejorando su resolución, permitiendo así poder conseguir imágenes del cuerpo completo, hasta llegar a los tomógrafos computarizados que conocemos hoy en día que se han convertido en una de las principales herramientas de diagnóstico.
Un tomógrafo computarizado (TC) es un equipo que permite obtener imágenes tridimensionales del interior del cuerpo utilizando rayos X, lo que permite identificar lesiones más fácilmente.

Además de permitirnos adquirir imágenes rápidamente, la tomografía computarizada es un método no invasivo e indoloro. Por estas razones, en muchos casos es el método idóneo para estudiar patologías internas que necesiten tratamiento con urgencia.

No obstante, tampoco se debe abusar de él, ya que no deja de ser un método que emplea radiación ionizante, aunque en pequeña medida. Es por esto por lo que los protocolos de seguridad y las pruebas de control para asegurar que no se sobrepasen los límites de radiación fijados y que todo funcione según lo establecido son esenciales.

Para la realización de esta práctica hemos tenido la suerte de poder acceder al TC que hay en el servicio de Oncología Radioterápica del Centro Médico Teknon. Antoni Castel Milan, jefe de protección radiológica, y Adam Jones nos han compartido sus conocimientos sobre el tema, además de darnos las directrices necesarias para realizar las pruebas que se explicarán a lo largo de este trabajo.

II. PRINCIPIOS FÍSICOS

Para entender bien el funcionamiento de una TC es esencial conocer cuáles son los principios físicos que se esconden detrás de ella.

Los rayos X son radiaciones electromagnéticas ionizantes capaces de atravesar materia (cuanto mayor sea su voltaje más penetración tienen).

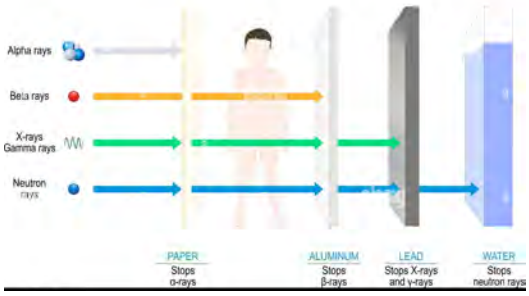

Figura 1. *Comparación de la penetración de diferentes partículas.*

Se diferencian de los rayos gamma, no por su energía, como se podría llegar a pensar, sino por su origen. Los rayos X se producen a partir de electrones de la capa externa, generalmente por su desaceleración, y los gamma son de origen nuclear. En el ámbito de la TC los rayos X de mayor interés son los rayos X de Bremsstrahlung, producidos por la desaceleración (o aceleración) de un electrón que se da al pasar cerca de un núcleo debido a su campo. Siguiendo el principio de conservación de la energía, se emitirá radiación en forma de fotón (radiación de frenado) cuya energía será la misma que la perdida por la del electrón.

El efecto fotoeléctrico se da con mayor proporción con bajas energías.

Al iluminar una superficie metálica con un haz de luz (fotones) con cierta frecuencia mínima idónea (diferente para cada metal), se absorbe el fotón y se emiten electrones libres de la superficie.

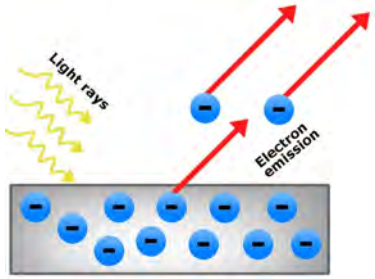

Figura 2. *Efecto fotoeléctrico.*

La ecuación característica que nos permite estudiar este efecto es la siguiente:
$h\nu = W + Ec$, donde h es la constante de Planck, ν la frecuencia del fotón, W la función de trabajo propia de cada metal y Ec la energía cinética del electrón creado.

El hecho de que la radiación dispersada tenga una frecuencia menor a la incidente lo explica el efecto Compton (o *scattering*).

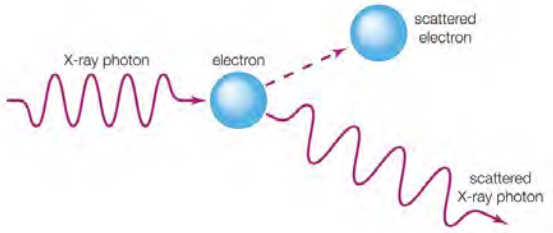

Figura 3. *Efecto Compton.*

Este efecto se basa en la disminución de la frecuencia (que implica también el aumento de la longitud de onda) y la pérdida de parte de la energía de un fotón al chocar con un electrón en reposo (respecto al sistema de referencia del fotón). En este choque el fotón le cede esta energía perdida al electrón y, debido a esto, el electrón sale con un ángulo θ. La fórmula que nos permite estudiar este fenómeno es la siguiente:
$\Delta\lambda = \lambda c\,(1 - cos\theta)$, donde λc es la longitud de onda de Compton y θ el ángulo de dispersión.

Por último, el fenómeno que se da cuando los fotones tienen una muy alta energía, es la creación de pares.
Nos centraremos en concreto en la creación del par electrón-positrón. Si pasa un fotón con suficiente energía (mayor a 1.022 MeV, que es el doble de la energía de un electrón en reposo) cerca de un núcleo, se forma un electrón y su antipartícula, es decir, un positrón.

III. TOMOGRAFÍA COMPUTARIZADA

La tomografía computarizada (TC), como ya hemos explicado, es una técnica de diagnóstico por imágenes. Esta técnica utiliza un ordenador conectado a una máquina de rayos X a fin de crear una serie de imágenes detalladas del interior del cuerpo. Las imágenes se toman desde distintos ángulos y se usan para crear vistas tridimensionales (3D) de la zona escaneada.

A) Estructura del Tomógrafo TC

La estructura del tomógrafo TC incluye los siguientes componentes:

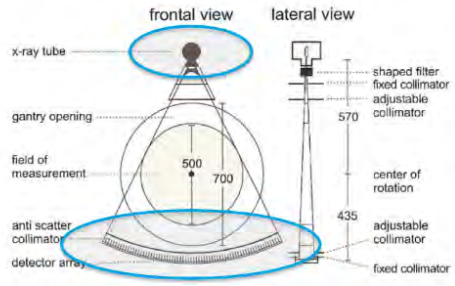

Figura 4. *Equipo Tc*

- El gantry contiene el tubo de rayos X y los detectores, que están dispuestos en lados opuestos. Durante el escaneo, el gantry gira alrededor del paciente, permitiendo que el tubo de rayos X emita haces de rayos X desde diferentes ángulos. Los detectores en el otro lado del gantry recogen la radiación que atraviesa el cuerpo del paciente, convirtiendo esta información en señales eléctricas que se utilizan para generar imágenes transversales detalladas del área escaneada. Dependiendo del tipo de TC, el número de detectores puede variar. En la práctica utilizamos un tomógrafo de una fila con 16 detectores.

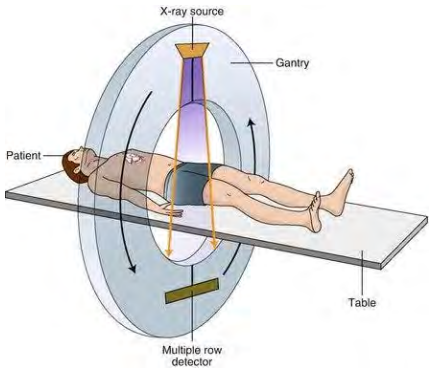

Figura 5. *Mesa TC.*

- En la mesa de exploración móvil se coloca al paciente. La mesa está motorizada y se puede manejar tanto manualmente con los controles que hay a ambos lados del gantry, como de forma remota desde el ordenador. Se puede mover de arriba a abajo, de izquierda a derecha, y hacia delante y hacia atrás.
- El ordenador recoge las señales eléctricas de los detectores. Éstos captan en forma de señal analógica la cantidad de radiación absorbida y la transforman en señal digital. El ordenador utiliza algoritmos matemáticos para convertir estas señales en imágenes detalladas de cortes transversales del cuerpo.

B) Tipos de TC

Existen varios tipos de TC, cada uno diseñado para aplicaciones específicas y ofreciendo diferentes ventajas. Entre ellos encontramos:

- TC Helicoidal (o Espiral): Captura imágenes rápidamente, reduciendo el tiempo de exploración. Consiste en ir moviendo lentamente la mesa del paciente a través del escáner mientras el tubo de rayos X gira de manera continuada alrededor del paciente.
- TC Espectral (o de doble energía): Es una técnica avanzada de TC, que utiliza dos niveles diferentes de energía de rayos X para adquirir datos. Esta tecnología proporciona información adicional sobre la composición y características de los tejidos y materiales dentro del cuerpo, mejorando la precisión diagnóstica.
- TC Multidetector: Se utilizan múltiples filas de detectores para la adquisición de imágenes. Esta técnica ha mejorado tanto la calidad como la velocidad de adquisición de las imágenes.

Y la lista continúa. A lo largo de los años las técnicas del TC han mejorado considerablemente las capacidades de diagnóstico y la planificación de tratamientos.

IV. PARÁMETROS DOSIMÉTRICOS

Debido a los efectos nocivos y riesgos a los que el paciente se expone haciendo uso de pruebas en las que se emplean rayos X, es de suma importancia la correcta proporción de dosis al mismo. Es decir, aquella cantidad de radiación con mejor relación entre la resolución mínima requerida para el diagnóstico y los daños ocasionados al paciente. En este contexto nace el comúnmente conocido Índice de Dosis de Tomografía Computada (CTDI). Es una métrica adaptada que ha dado lugar a nuevos paradigmas con el objetivo de regularizar y estandarizar el sistema y los parámetros a utilizar.

Así pues, el CTDI estima el promedio de dosis efectiva absorbida por el instrumento de medida sobre su centro longitudinal, aludiendo así a la absorción de Rayos X a lo largo de la longitud del barrido. A pesar de que dicho dispositivo puede simplemente colocarse en el aire, se requiere el uso de un *phantom* para una mayor similitud a un cuerpo humano. Un *imaging phantom* o simplemente *phantom* es un objeto especialmente diseñado para la evaluación, análisis y tuneado de dispositivos de *imaging* que está diseñado para simular cabezas y cuerpos pediátricos y adultos. El sistema de medida CTDI suele ir acompañado de un subíndice, $CTDI_{\mathrm{i}}$, donde i corresponde a la medida del instrumento de medida utilizado. Típicamente corresponde a un semiconductor o una cámara de ionización de 100 mm, dispositivos utilizados para medir con precisión la dosis de radiación. Dichas especificaciones dan lugar a la siguiente ecuación:

$$CTDI_{\mathrm{i}} = \frac{1}{(N \times T)} \int_{L/2}^{L/2} D(z)dz,$$

con N: Número de imágenes transversales a lo largo del eje z y T: Grosor de haz de rayos X a lo largo del eje z.

Para una correcta asignación de dosis, se debe realizar distintas mediciones de la dosis para distintos puntos del *phantom*: una desde el centro del mismo y otras cuatro simétricamente distribuidas en la periferia si se trabaja con la cámara de ionización y una central si se trabaja con el semiconductor. La ejecución de este procedimiento da lugar al $CTDI_{\mathrm{W}}$, donde la w indica la ponderación de tal modelo. Así, obtenemos la siguiente fórmula:

$$CTDI_{\mathrm{W}} = \frac{1}{3} CTDI_{\mathrm{i,center}} + \frac{2}{3} CTDI_{\mathrm{i,perif}}$$

Definimos "pitch" como el radio entre el movimiento de la mesa y la anteriormente presentada NxT, quedando así un número menor que uno para un movimiento menor de la mesa que aquel referido a la cobertura total del área del *phantom* durante una exploración de TC, lo que se traduce en una superposición de radiación y por tanto mejor resolución, y viceversa. De esta manera, diferenciamos entre TCs axiales, con pitch=1, helicoidales, para TCs con Pitch<1 y "escaneos con separación" con Pitch<1. Así pues, definimos $CTDI_{\mathrm{vol}} = \frac{CTDIw}{pitch}$.

Por último, obtenemos la denominada dosis de medida del producto (DLP) a través de la siguiente multiplicación, $DLP = CTDI_{\mathrm{vol}} \times L$, donde L: longitud irradiada. Queda así relacionada la dosis con el riesgo de tal radiación, que será determinada, en nuestro caso, según las indicaciones del

Protocolo Español de Control de Calidad en Radiodiagnóstico.

V. EVALUACIÓN DE LA PRUEBA DEL TOMÓGRAFO

A continuación, explicaremos el procedimiento de la TC gracias a la prueba experimental que realizamos en el Centro Médico Teknon.
El tomógrafo utilizado es de la marca Philips, y los programas de ordenador empleados: Brilliance CT y Ocean. Los instrumentos de medida son los siguientes: un semiconductor que mide el parámetro de interés con la mesa en movimiento y una cámara de ionización (tipo lápiz) conectada a un transductor o electrómetro. Estos últimos recogen la señal y están conectados a un PC donde procesarla. El transductor está conectado al PC por bluetooth.
El ordenador está conectado al gantry y le da las instrucciones de cómo se tiene que mover y qué energía e intensidad hay que administrar.
También tenemos a nuestra disposición una consola de mando para regular el disparo, el movimiento de la mesa, etc.

Antes de la realización de pruebas al paciente, cabe llevar a cabo un control de calidad que asegure su correcto funcionamiento e indique los valores y efectos de los parámetros de radiación para así poder decidir la dosis que se le proporcionará a dicho paciente.

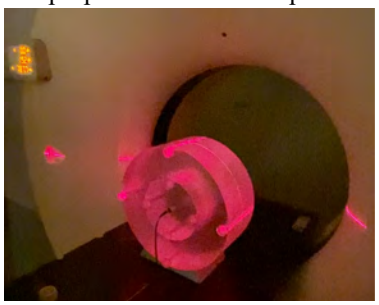

Figura 6. *Phantom en el gantry.*

Para ello, cabe colocar el phantom en el centro del gantry, de tal manera que quede perpendicular al eje z y alineado respecto a los cuatro láseres del TC.
A continuación, se introduce y centra el instrumento de medida de dosis de radiación y se pone en marcha el tomógrafo desde un ordenador del que se ve la sala propiamente acondicionada, sala en la cual se encuentra el personal que inspecciona y da indicaciones al paciente.
En nuestra prueba experimental de TC llevamos a cabo dos pruebas de tomógrafo: una con aire y la otra con un *phantom*.
El perfil no es el mismo en estos dos casos debido al *scattering*. El *phantom* es más representativo de la dosis de un paciente real. Hay dos tipos de *phantoms* de PMMA (polimetilmetacrilato): *body* (d=32cm, L=15cm), y *head* (d=16cm, L=15cm).
Los datos obtenidos tras la práctica se encuentran en el anexo.
En primer lugar, en la prueba con aire, hay que centrar la cámara de ionización tipo lápiz en el gantry gracias a los láseres de manera que se encuentre centrada tanto en el isocentro como en el centro de radiación. A continuación, hay que polarizarla. Para ello, se aplica una diferencia de potencial de ΔV=120 kV. Al usar una cámara de ionización, es necesario realizar varias medidas, desde la periferia y el centro.
Después, realizamos la misma prueba pero esta vez con un *phantom* tipo *body* con exploración Abdomen 3 en modo helicoidal. Es necesario alinear una vez más el *phantom* en el gantry.
Por problemas técnicos no se pudo utilizar el lápiz. Así pues, utilizamos un semiconductor colocado en el centro, y por lo tanto no es necesario polarizar pero sí mover la mesa. Se introduce el phantom hacia adentro en el gantry con la mesa en movimiento (“head first”). El pitch es superior a 1, por lo que la mesa va más rápido que la rotación. Imponemos como tolerancia que la desviación sea inferior al 20%. Al realizar las medidas, se obtiene un CTDIvol con una tolerancia inferior al 20% con respecto al valor teórico.
Finalmente, a través de un algoritmo, el software del ordenador reconstruye las imágenes. Una vez analizado y asegurado el sistema, queda abierto al uso del paciente.
Es importante mencionar la importancia del control de calidad de este proceso, ya que se debe seguir y cumplir un protocolo con un manual de exactamente 326 páginas, por lo que es innegable el cuidado y atención que debemos prestar a todas estas reglas durante el procedimiento.

VI. APLICACIONES

Las aplicaciones son muy amplias, desde el diagnóstico por imagen hasta el tratamiento de patologías oncológicas. El radiodiagnóstico, la medicina nuclear y la oncología radioterápica utilizan radiaciones ionizantes para sus procedimientos. Entre sus aplicaciones más importantes tenemos: la evaluación de fracturas óseas, hemorragias internas… tras un accidente; la detección de tumores y cáncer identificando y caracterizando estas masas tumorales en los distintos órganos del cuerpo; la planificación de cirugías y tratamientos radioterápicos por obtención de imágenes precisas de la anatomía del paciente; el seguimiento de la evolución temporal de un proceso dinámico en un volumen de interés, como puede ser monitorizar la progresión de enfermedades crónicas y evaluar su respuesta frente a tratamientos médicos y quirúrgicos; y un largo etcétera. Por tanto, no podemos negar la gran importancia y versatilidad de la tomografía computarizada dentro de la medicina moderna.

VII. CONCLUSIÓN

La tomografía computarizada ha revolucionado el campo de la medicina diagnóstica al proporcionar con rapidez imágenes detalladas y precisas del interior del cuerpo humano.
En este trabajo hemos explorado los principios físicos en los cuales se apoya este proceso, la estructura del tomógrafo TC, los diferentes tipos que existen, el procedimiento experimental de la prueba de TC apoyándonos en la práctica que realizamos en el Centro Médico Teknon, y por último el amplio abanico de aplicaciones en la detección y monitorización de enfermedades.
Sin embargo, la TC enfrenta desafíos como la exposición a la radiación o la necesidad de mejorar la resolución de las imágenes. Así pues, la investigación en este ámbito continúa y es crucial para resolver estas limitaciones.
Hemos tenido la suerte de presenciar una prueba de TC en el Centro Médico Teknon, donde hemos podido comprender mejor el funcionamiento de la TC así como la importancia de la instrumentación física para el desarrollo de dispositivos que mejoren el mundo.

VIII. AGRADECIMIENTOS

Nos gustaría expresar nuestro agradecimiento a Antoni Castel Millan y Adam Jones, miembros del equipo de Medicina Nuclear del *Centro Médico Teknon* del grupo *QuirónSalud* y coordinadores de la práctica en cuestión. Gracias por brindarnos la oportunidad de conocer un hospital desde el punto de vista de un RFIR (Radiofísico interno residente). También queremos agradecer a los propios profesores de la asignatura de instrumentación de ingeniería física, por ser los responsables de la organización entre ambas entidades y facilitar el contacto.

IX. ANEXO: DATOS

1. Equipo evaluado

Generator

- Name: Brilliance 16
- Model: Brilliance 16
- Type: HF/DC
- Serial number: Sistema: 5330- Generador: 3589
- Manufacturer: PHILIPS

Tube

- Name: CT Tube
- Insert Type: MRC600
- Serial number: 152123
- Manufacturer: PHILIPS

2. Medidas

Maniquí CT: Body Modo: Helicoidal Tensión (kV): 120 Tiempo rotación (s): 0,75 Longitud piranha (cm): 21 Espesor corte (mm): 2 Colimación (mm): 24 Pitch: 0,938 Tiempo total exploración(s): 8,382 CTDIvol equipo (mGY): 18,7 Tiempo medida piranha (s): 15 Tasa dosis medida (mGy/s) (RTI CTDP): 0,697684712901716	Exploración: Abdomen 3 FOV (cm): 35 Intensidad (mA): 331 Carga/slice (mAs): 265 DOM: DDOM Número detectores: 16 Avance/incremento(mm):1 Número imágenes: 209 Velocidad rotación (mm/s): 30,016 DLP equipo (mGycm): 469,8 Dosis medida (mGy) (RTI CTDP): 11,0814391929366 Tiempo medido (ms) (RTI CTDP): 15883,16015625

3. Waveforms

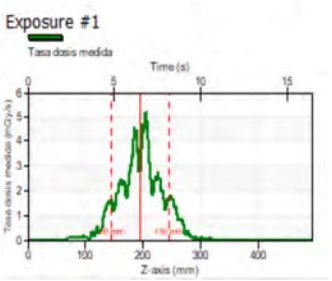

4. Análisis

CTDI (CT Dose Profiler) [Row1] Result: Pass Set kV 120,0 kV CTDI(100,c) 8,344 mGy CTDI(w) 13,56 mGy CTDIvol 14,45 mGy DLP 303,5 mGycm	CTDI (CT Dose Profiler) [Row 2] Result: Pass Set kV 120,0 kV CTDI(100,c) 4,711 mGy CTDI(w) 7,656 mGy CTDIvol 8,162 mGy DLP 171,4 mGycm
CTDI (CT Dose Profiler) [Row 3] Result: Pass Set kV 120,0 kV CTDI(100,c) 7,071 mGy CTDI(w) 11,49 mGy CTDIvol 12,25 mGy DLP 257,3 mGycm	CTDI (CT Dose Profiler) [Row 4] Result: Pass Set kV 90,0 kV CTDI(100,c) 2,398 mGy CTDI(w) 4,281 mGy CTDIvol 3,603 mGy DLP 75,67 mGycm

CTDI (CT Dose Profiler) [Row 5] Result: Pass	
Set kV	120,0 kV
CTDI(100,c)	6,995 mGy
CTDI(w)	11,37 mGy
CTDIvol	12,12 mGy
DLP	254,5 mGycm

CTDI (CT Dose Profiler) [Row 6] Result: Pass	
Set kV	120,0 kV
CTDI(100,c)	11,16 mGy
CTDI(w)	11,83 mGy
CTDIvol	27,01 mGy
DLP	567,2 mGycm

X. REFERENCIAS

[**1**] *Comprehensive Methodology for the Evaluation of Radiation Dose in X-Ray Computed Tomography.* American Association of Physicists in Medicine. 2010. One Physics Ellipse. College Park, MD 20740-3846.

[**2**] Journal of Nuclear Medicine Technology. *Principles of CT: Radiation Dose and Image Quality.* November 15, 2007.

[**3**] *Protocolo español de Control de Calidad en Radiodiagnóstico.* SEFM-SEPR-SERAM. 2011, Madrid, Senda Editorial.

XI. BIBLIOGRAFÍA

- *Diccionario de cáncer del NCI*. (s. f.). Cancer.gov. https://www.cancer.gov/espanol/publicaciones/diccionarios/diccionario-cancer/def/tomografia-computarizada
- Derivetecel, U. (2023, 2 diciembre). *¿Qué es un «Gantry»? En términos de tomografía.* Medical 997).
- *La tomografía computada: principios e historia de su desarrollo – Grupo CT Scanner*. (s. f.). https://grupoctscanner.com/la-tomografia-computada-principios-e-historia-de-su-desarrollo/
- Cassini, A., Levinas, L., & Pringe, H. (2013). Einstein y el efecto Compton. *Scientiae Studia*, *11*(1), 185-209. https://doi.org/10.1590/s1678-31662013000100009
- Connor, N. (2020, 3 julio). *¿Qué es la producción de pares de positrones y electrones? Definición*. Radiation Dosimetry. https://www.radiation-dosimetry.org/es/que-es-la-produccion-de-pares-de-positrones-y-electrones-definicion/
- *Rayos X*. (s. f.). National Institute Of Biomedical Imaging And Bioengineering. https://www.nibib.nih.gov/espanol/temas-cientificos/rayos-x

Radiation Oncology: Experimental Dosimetry Characterization

Elisabet Alzuria De Sancha, Paula Benítez Sesmilo, Júlia Muñoz Torrico, Ruth Mora Soto, Pau Sabater Nácher, Joan Vila i Miñana

Instrumentació. Grau en Enginyeria Física. Universitat Politècnica de Catalunya.
Campus Nord, 08034 Barcelona

In contemporary medical practice, up to 60% of cancer patients will receive radiotherapy at some point during their treatment. The aim of this article is to provide a comprehensive analysis of the operational mechanisms of the accelerators utilized in this therapeutic modality and the procedures used to design and measure the radiation dose administered to the patient.

Keywords: radiotherapy, particle collisions, linear accelerator, radiation dosimetry

I. BACKGROUND

Radiotherapy operates by employing ionizing radiation to disrupt the DNA strands in cancer cells, thereby inhibiting their ability to proliferate. The primary objective is to deliver the maximum radiation dose to the targeted area while preserving as much healthy tissue as possible. It is essential to regulate the radiation doses meticulously to prevent the development of secondary malignancies due to the irradiation of healthy tissues, a condition known as radiation-induced cancer.

In contrast to chemotherapy, which has a systemic impact on the entire body, radiotherapy is localized, targeting a specific area for treatment. This treatment area is precisely delineated to minimize the irradiation of surrounding healthy tissue.

II. INTERACTIONS

1. Interactions of charged particles with matter

Charged particles, interacting through their own electric fields, lose energy when colliding with matter in events known as Coulomb collisions. These collisions occur through three distinct types of interactions:

a. Inelastic Collision: The particle transfers small amounts of energy to electrons, potentially leading to ionization or excitation of the atoms.
b. Elastic Collision: The kinetic energy of the particle is transferred to the medium, causing it to vibrate or move, without any permanent alteration to its atomic or nuclear structure. Elastic collisions are characterized by the conservation of both momentum and kinetic energy.
c. Radiative Collision: During the collision, energy is transferred between the particles, resulting in the emission or absorption of photons. These collisions are crucial in various natural phenomena, including spectroscopy, astrophysics, and plasma physics.

2. Interactions of uncharged particles with matter

The principal mechanisms by which photons interact with matter include:

a. Photoelectric Effect: In this process, a photon interacts with an atom, transferring all its energy to eject an electron. The remaining energy is imparted as kinetic energy to the ejected electron. For the photoelectric effect to occur, the incident photon must possess energy exceeding the binding energy of the electron.
b. Compton Scattering: This interaction is the most probable for gamma rays and high-energy X-rays with atoms in biological tissues. It results in the emission of a scattered photon with reduced energy compared to the incident photon, and an electron, typically from the outer shell, which gains kinetic energy approximately equal to the energy difference between the incident and scattered photons.
c. Pair Production: In this phenomenon, a photon transforms into an electron-positron pair. This process necessitates the presence of a nearby nucleus or electron to conserve linear momentum and energy. Pair production occurs when the photon's energy surpasses the threshold of 1.022 MeV, the combined rest mass energy of the electron and positron.

III. DOSIMETRY DEFINITIONS

Some relevant Magnitudes, Units, and Concepts in Radiation-Matter Interactions are:

1. Gray (Gy): Named after British physicist Louis Harold Gray, the gray (Gy) is the SI unit for measuring the absorbed dose of ionizing radiation. One gray is defined as the absorption of one joule of radiation energy per kilogram of matter: $1\,Gy = 1\,J/kg$
2. Kilovolt Peak (kVp): is a unit of measurement that describes the peak voltage applied across an X-ray tube during the production of X-rays. This peak voltage determines the maximum energy of the X-ray photons generated. Higher kVp settings generally reduce the skin dose because higher energy photons are less likely to be absorbed by the skin, but they increase the overall dose due to greater penetration, affecting the radiation dose received by the patient.
3. Tissue Phantom Ratio (TPR): TPR is a parameter used in radiation therapy to quantify the dose of radiation at a specific depth in tissue-equivalent material relative to a reference depth. It is defined as the ratio of the dose at a given depth d to the dose at a reference depth d_{ref}, typically measured in water:

$$TPR = \frac{D(d)}{D(d_{ref})}$$

where $D(d)$ is the dose at depth d and $D(d_{ref})$ is the dose at the reference depth d_{ref}.

4. Percentage Depth Dose (PDD): is a critical parameter in radiation therapy that provides information on how the radiation dose decreases with increasing depth in tissue or tissue-equivalent material (usually water). It is defined as the ratio (expressed as a percentage) of the dose at a specific depth d to the dose at the reference depth d_{max} along the central axis of the beam:

$$PDD = \left(\frac{D(d)}{D(d_{max})}\right) \times 100\%$$

where $D(d)$ is the dose at depth d and $D(d_{max})$ is the dose at the depth of maximum dose d_{max}

5. Source-to-Skin Distance (SSD): refers to the distance between the radiation source and the patient's skin. In radiation therapy, standard SSDs (e.g., 80 cm or 100 cm) are used to ensure consistency and accuracy in treatment delivery.
6. Penumbra: The penumbra is the transitional region at the edge of a radiation beam where the dose sharply decreases from the fully illuminated (or fully dosed) region to the completely dark (or zero dose) region. This region impacts the precision and effectiveness of radiation therapy treatments.

IV. MEDICAL LINEAR ACCELERATOR

A medical linear accelerator (LINAC) is used to destroy cancerous cells of a tumor through radiation, with as little affectation as possible to the surrounding healthy tissue. A beam is accelerated through the gantry which is pointed towards the isocenter of the tumor. In order to reach the tumor from different angles and ensure better results in its elimination, the gantry is rotated around the patient.

The accelerator has a multileaf collimator that shapes and modulates the intensity of the radiation beam that is being administered to the patient. This modulatory capacity enables the patient to receive high doses of radiation with great precision, hence protecting the colliding healthy tissue and increasing the impact on tumoral cells. The accelerated beam of photons collides with a heavy metal target to produce high energy X-Rays. The leaves of the multileaf collimator are positioned so that the X-Rays passing through take the form of the tumor. [1]

The administration of the treatment requires precision and constant vigilance of the patient and their statistics. Hence the presence of an X-ray imaging system that provides CT images, enabling the technical team to monitor the patient's correct position in real time. There are flat panels (made from silicon) receiving X-Rays from the tube, the information collected is used to create tomographic images. The real-time images are superimposed with the initial CT scan used for the planning of the treatment. There are four variables to take into consideration: position (x, y, z) and time, since the original tomographic scans are static images and the real-time data is dynamic. This task is done in the control room, besides the accelerator's room. It is a crucial part of the process since it ensures that the treatment is going according to plan, with the required precision.

Another fundamental part of the LINAC is the patient table/hospital stretcher, equipped with immobilization

systems to prevent involuntary movements and ensure the maxim stillness of the patient. Previous to the application of the radiation, it is positioned at the coordinates that will provide the safest course of treatment: the isocenter of the lesion. It can be moved rotationally and translationally, adapting its height, position and angle to the surface. It is important that the material from which the stretcher is made of, is such that it does not absorb a high proportion of the dose that is being administered, as it would alter the amount of dose required and could even completely discard the predictions made. Since the gantry is moving while applying the radiation, the length of the intersection between the beam's path and the table is constantly changing, making it very difficult and impractical to calculate the corresponding dose in real time. Hence, the chosen material is carbon fiber.

Every aspect, number, and parameter is monitored in the control room, next to the patient's room where the radiation is taking place. A group of radiophysics and technicians observe the course of the treatment and make the necessary adjustments in order to protect healthy tissue and maximize precision. The control area consists of three zones:

- The recording and computerization system, which controls the treatment parameters in real-time, such as the dose, beam position, and table position. It also records data to ensure everything is functioning correctly and can be reviewed at any point during the treatment.
- The imaging system, to superimpose the CT scan of the patient in real-time with the reference CT scan used for treatment planning.
- The patient monitoring system, along with a communication system to give instructions and interact with the patient if necessary.

This instrument itself and these monitoring techniques have enabled the performance of high precision treatments such as radiosurgery that were unthinkable before. In order to ensure its proper use, a specialized team has to take care of a very important part: the calibration of the accelerator.

V. CALIBRATION

Before any radiation is administered, the accelerator must be calibrated in order to make the necessary adjustments and verify its accuracy. Certain parameters and settings have to be checked, such as the beam energy, beam shape and dose rate. The calibration process requires awater phantom, a calibrated ion chamber and an electrometer. A 10x10 field is used. The tank is filled with water at room temperature, then the dosimeter is situated inside in the position of reference for a beam of photons of 6MV, which is of approximately 1.5-2.5cm. It must be ensured that the dosimeter is aligned with the beam and that its axis is perpendicular with the beam's direction.

Once defined which size of the radiation field is needed for the treatment, the photon beam must be tested to make sure that it covers the interest zone and its focus is then situated at 100 cm from the water's surface (SFD distance). There are very strict rules concerning the materials that have to be put in place during the calibration, according to the procedures set by the International Atomic Energy Agency (IAEA). For instance, a water phantom is always used, that is to avoid any alteration on correction factors and because of the fact that the standard protocol is written based on absorbed dose in water. There is a +/- 2% of tolerance in the readings; nevertheless, many hospitals chose to lower the tolerance, such as Teknon Hospital, that allows a +/- 1%.

VI. PROTOCOL

Apart from the calculations of the dosage and the determination of which type of treatment is required for each patient, it is of great importance that the target is reached with the necessary precision and intensity and within a small range of variation of these values. [2]

There are two ways of ensuring that radiation does not reach any area that isn't the tumor, the first one being taking into account the movement of the patient (voluntary and involuntary). For voluntary movement, in patients such as little kids who are constantly moving or elderly people who have basic necessities more frequently, the beam automatically stops when it detects movement in the periphery of the hospital stretcher. In the case of involuntary movement, a cast of the patient's general area of interest is made, using a thermoplastic sheet previously heated up so that it can be malleable and placed in the needed area of the patient, shaping into the specific form of the person receiving the treatment. Once this is done, a cross is marked in the tumor isocenter.

Once the modeling of the treatment and dosage of the radiation is calculated, a computed tomography scan (CT) must be taken, so that the isocenter of the tumor can be located. Then, when starting the treatment, the patient must

be located in the hospital stretcher and the mold is used to ensure that the radiation is received in the correct place. The hospital stretcher/table in which the patient is positioned to enter the accelerator is made up of carbon fiber, which reduces the attenuation and scattering of the incident radiation. Since there is a cross marked where the tumor is located, with the help of lasers that have the same trajectory as the radiation beam, there is a control protocol to make sure that all the beams are in the correct position and are located towards the right direction.

The beams of the accelerator are adjusted to the patients' anatomy in order to create an additive effect in the distribution of the radiation. That way, the selected area for the treatment receives the totality radiation coming from each beam whereas the surrounding area of the tumor receives an inferior amount of radiation. Moreover, by radiating the tumor using beams positioned in different angles can result in a greater homogeneity of the incident radiation in the tumor. Also, the treatment is often rotational, ensuring that only the affected area is receiving the full radiation at all times, not any other part. [3]

Finally, another important issue to cover is the received dosage. The patient must receive the dose of radiation within the clinical window of 95%-107% of the intended radiation for that area. If it is less than 95% there is the risk of not having the expected effect on the tumor (and therefore it is not eliminated) whereas if the radiation is greater than 107% of the necessary one, there is a chance of over-irradiation and inducing cancer in that particular area. Also, each specific organ or tissue has a corresponding ponderative factor, which is taken into account when calculating the dosage of radiation needed.

On top of that, the radio physicists have a list with the exact steps of the procedure and the parameters that have to be adjusted in the accelerator, to make sure that nothing is forgotten and the treatment goes as smoothly as possible.

VII. EXPERIMENTAL MEASUREMENTS

According to the procedure detailed in IAEA [4] and in the calibration section, the measurement of charge at the different depths of the water tank along different axes was conducted. This enables the characterization of different properties of the beam through the analysis of the data, carried out below. The studied field consisted of a 15cmx15cm 6 MV polychromatic photon be am generated by a WFF (with flattening filter) clinical linear accelerator.

The analysis of the beam includes the dosimetric - PDD -, isodoses- and quality - TPR 20-10 - properties.

1. PDD

The most habitual description of the instrument is the percentage depth dose, defined as the absorbed dose rate (taking as a reference the maximum of absorption) in water as a percentage. Its shape is very characteristic: first, there is a rapid initial increase corresponding to the radiation entering the tissue. There is a maximum in a depth called the depth of maximum dose. Then, the curve starts to decrease gradually with increasing depth; the photon beam loses energy as it penetrates deeper into the tissue.

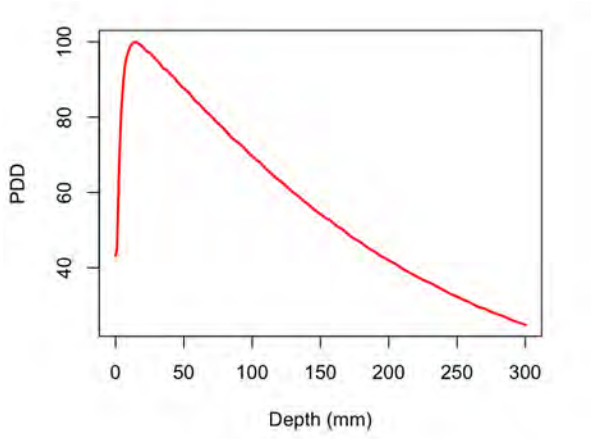

FIG. 1. PDD of the data analyzed.

Examining the beam profiles, it is evident that the measured curves for the X and Y axes coincide, indicating the rotational symmetry of the beam. Moreover, three different regions can be distinguished, corresponding to the central region, the penumbral region, and the umbral region. Ideally, there should only be the central region, meeting flatness and symmetry. However, the impossibility of the beam to fulfill this requirement creates the other two regions, which is manifested as the unintentional irradiation of cells in nearby organs. This extra radiation can be computed with the penumbra region, this region is defined as the separation widens between the dose levels at 80% and 20% on the beam profile, which is standardized to 100% at the central axis (see Figure 2 and Figure 3). The width of the penumbra is relevant to know which organs are gonna be exposed.

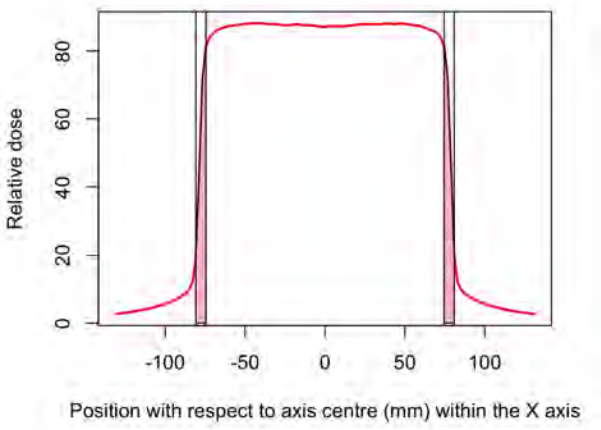

FIG. 2. Beam profile for the X axis.

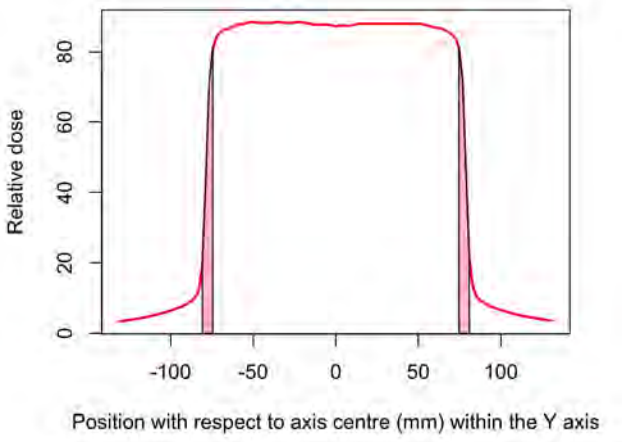

FIG. 3. Beam profile for the Y axis.

2. Isodoses

Additionally, the dose data enables the calculation of isodose curves. Isodose curves are lines connecting points of equal percentage depth dose. They are computed by using the 3D dose matrix, defined from the CT images. It is determined using a specific algorithm depending on the planning system. Once this matrix is obtained, the system normalizes it at a defined point in the matrix and then searches for points with the same value to draw the isodose curves. By studying them, one can note that the more distance between the radiation source and the tissue surface, the worse the shape of the isodose becomes in terms of doses distributed for the patient (less symmetric and uniform). This could be due to greater electron scatter in the air between the applicator and the tissue surface.

3. TPR

Another important definition is the tissue-phantom rate, defined as the ratio in water at depths of 20 g/cm2 and 10 g/cm2, used as the beam quality index for high energy photon radiation.

Despite the nominal beam energy being 6 MV, the dosimetric parameters are damped by a quality factor. For photons produced in WFF accelerators, the quality of the beam is specified through the tissue phantom ratio (TPR), which is determined through the following relation:

$$TPR_{20,10} = 1,2661\, PDD_{20,10} - 0,0595 = 0.704026$$

where $PDD_{20,10}$ is, as defined, the ratio of the PDD at 20 cm and 10 cm depth for a field size of 10 cm × 10 cm defined on the surface of the water dummy with an SSD (Focus Surface Distance) of 100 cm. This empirical equation was fitted from a sample of almost 700 accelerators.

Upon the characterization of the TPR20,10, together with the ionization chamber properties, the k_Q, a crucial factor for the determination of the dose, can be obtained. Using task group 398, yields k_Q = 0.9875. [5]

VIII. CONCLUDING REMARKS

This document summarizes the importance of radiotherapy in cancer treatment and also focuses on how an accurate measurement of the dosage and the location of the tumoral tissue is essential for maximizing the therapeutic effect on tumors (while reducing the harm to healthy cells). Therefore, the calibration, protocol and calculations are of extreme importance, as highlighted in the experimental part in which we are able to determine parameters crucial for the dose calculation. With the information that we learnt in the two practical sessions that we went through in *Centre Mèdic Teknon*, we wanted to emphasize the importance of the Physics that is behind radiotherapy and that plays a big role in improving the chances of overcoming cancer. Finally, we cannot end this article without an acknowledgement to Josep Sànchez Barrachina and Antoni Castel Millán, who taught us about the hospital and their techniques as well as guiding us through the different machinery.

[**1**] https://www.youtube.com/watch?v=vpgWxZAZh-U, retrieved 10/5/2024

[**2**] Notes taken during the practical sessions

[**3**] M. Cruz Lizuaín Arroyo, *Fundamentos de Física Médica. Volumen 3: Radioterapia Externa I. Bases Físicas, Equipos, Determinación de la Dosis Absorbida y Programa de Garantía de Calidad*, SEFM, ADI Ediciones 64, 66 (2012).

[**4**] IAEA. Technical report series, Rev. 1 398, (2024)

[**5**] *AAPM Committee tree AAPM Committee Tree - Task Group No. 398 - Pathways to Leadership in Medical Physics - Cohort C (TG398)*. Available at: https://www.aapm.org/org/structure/?committee_code=TG398 (Accessed: 31 May 2024).